ROLE OF ACROLEIN IN NEUROTRAUMA AND RELATED NEURODEGENERATION

by

Seth Anthony Herr

A Dissertation

Submitted to the Faculty of Purdue University

In Partial Fulfillment of the Requirements for the degree of

Doctor of Philosophy

Department of Basic Medical Sciences

West Lafayette, Indiana

May 2021

THE PURDUE UNIVERSITY GRADUATE SCHOOL
STATEMENT OF COMMITTEE APPROVAL

Dr. Riyi Shi, Chair

Department of Basic Medical Sciences

Dr. Amy Brewster

Department of Psychological Sciences

Dr. Richard Van Rijn

Department of Medicinal Chemistry and Molecular Pharmacology

Dr. Wei Zheng

School of Health Sciences

Approved by:

Dr. Laurie Jaeger

ACKNOWLEDGMENTS

I would like to first thank my thesis research advisor Dr. Riyi Shi who always shared a common excitement for research and encouraged me to take on many projects. I especially appreciate Dr. Shi teaching me the importance of good writing and letting me help him with numerous publications and grant applications. I learned a lot and we made a great team over the years.

Thank you to Dr. Amy Brewster who was the first to encourage me to pursue a PhD, and taught me many of the fundamentals of good science.

Thank you to all of the collaborating labs who made this thesis possible. To all the members of my committee and the Shi lab, past and present, who provided much support to my projects. To lab alumni Dr. Breanne Butler who patiently taught me how to do spinal cord surgeries, and Dr. Glen Acosta, who taught me much about biochemistry and is still a close friend and mentor.

To new lab members Dr. Siyuan Sun and Sunny Zaiyang Zhang, I'm glad you both are excited to continue the projects I started with Dr. Shi. I look forward to seeing all you will accomplish during your time here.

Thank you to Dr. Colleen Gabauer, who always went out of her way to stand up for graduate students. I admire you very much for this. To Drs. Gabauer, James Mohler, and Gregore Koliantz for letting me lead their classes as a TA. Teaching comes with many unique challenges and I learned so much from you all.

Finally thank you to my family. I sacrificed a lot of time to be here and do this, and I truly appreciate your understanding and support.

TABLE OF CONTENTS

LIST OF FIGURES

ABSTRACT

Neurotrauma is a general term describing injury to the central nervous system (CNS); which comprises of the brain and spinal cord. The damage resulting from neurotrauma includes primary injury, which occurs from different sources such as compressed air hitting the brain (bTBI) or an object/bone contusing the spinal cord, resulting in a spinal cord injury (SCI). These various means of primary brain and spinal cord injury are further complicated by the many possible combinations of severity levels and frequencies. However, primary injuries are regarded in many cases as unavoidable with the immediate nerve damage being largely irreversible. Despite all this, primary injuries of the CNS are related by common biochemical pathways in secondary injury. Secondary injury is the cause of declining outcomes after neurotrauma and poor recovery. Secondary injury begins immediately after primary injury and can continue to trigger death of neurons for years later. Given this contribution to poor recovery and its slow progression, secondary injury provides an excellent window of opportunity for therapeutic intervention. A major factor and key link in secondary injury and its perpetuation is reactive aldehyde formation, such as acrolein, from lipid peroxidation. The common formation of acrolein in neurotrauma is attributed to the unique structure of the CNS: with neurons containing a high lipid content from myelin and heavy metabolic activity they are vulnerable to acrolein formation. Thus, acrolein in secondary injury is a point of pathogenic convergence between the various forms of neurotrauma, and may play a role as well in the development of neurotrauma linked disorders and related neurodegeneration. The overall goal of this thesis is to therefore develop better strategies for acrolein removal. We explore here endogenous clearance strategies and targeted drug delivery in SCI, investigate detailed cellular structure changes in bTBI, and acrolein formation and removal in Parkinson's disease. These findings of pathology, and effectiveness of new or existing acrolein removal strategies, will allow us to better employ treatments in future studies.

CHAPTER 1. INTRODUCTION

1.1 Prevalence and impact of spinal cord injury

Spinal cord injury (SCI) is a debilitating condition with a large socioeconomic impact. The National Spinal Cord Injury Statistical Center claims there are approximately 12,500 new cases of SCI each year in North America costing $2.35 million per patient (1). The primary causes of SCI (over 90%) result from traffic accidents, violence, sports or falls (2). The most common groups who receive a SCI include young males and the elderly, and the male-to-female ratio for SCI is 2:1 for adults (2). The stages of life in which men or women receive SCI are similar, with men affected during their early and late adulthood (3rd and 8th decades of life), and women during their adolescence (15–19 years) and late adulthood (7th decade of life) (2). Adolescents and young adults have much better chances, and speeds, of successful recovery than adults over 60. This could be due to many factors, including the increased mobility of youth and thus better rehab abilities, or the difference in ways the SCI occurs; where people over 60, for instance, injuries result from different factors such as osteoporosis or falls (1).

1.2 Clinical outcomes of spinal cord injury

Symptoms from primary injury to the spinal cord are dependent on location of the injury. Injury to the thoracic area and below causes paraplegia while injury at higher regions (closer to the neck) including the cervical level result in quadriplegia (also known as tetraplegia) (3). The instance of primary injury to these cord regions differs. The C5 region is the most commonly affected (50%), followed by the thoracic level (35%) and lumbar region (11%) (2). Symptoms resulting from these injuries include an abundance of complications in addition to paralysis. Obesity is a major issue, primarily attributed to the lack of movement (4). This lack of movement and disconnected signaling from the CNS also results in muscle degeneration, causing cardiovascular issues and hypotension (5). Muscle deterioration can also cause difficulty breathing and increased risk for pneumonia, bowel and bladder dysfunction, and loss of sensation or pain (6). Neuropathic pain is a common complication of SCI and can be lifelong (7). These complications all contribute to lower survival rates, with the survival rate of individuals with tetraplegia and paraplegia from 1955 – 2006 was 47 and 62%, respectively (8). Other studies also show a strong relation between injury

location/severity and survivability, with those who require a wheelchair (high severity) have an estimated 75% of a normal life expectancy, while other can have a life expectancy up to 90% of a healthy individuals (9).

1.3 Etiology of spinal cord primary injury

Impacts to the spine that fracture or severely dislocate vertebrae and damage the cord tissue is known as primary injury. Most injuries do not cut the spinal cord, but cause contusion or compression (10). Hyperextension injuries mostly from whiplash are common, as well as distraction injuries which occur when vertebrae are pulled apart, stretching the spinal cord (11). Finally, although not as common, laceration and transection injuries are possible. Relevantly, and a newer phenomenon with the development of modern warfare, compressed air from explosives result in blast waves causing blast injury: the most common cause of SCI in war (12). Blast SCI also results in higher severity scores and is associated with longer hospital stays compared with SCI in the civilian population (13). It's currently unclear how much of the spinal injury is due to the blast wave, or from other events after the blast (whiplash, being thrown from a vehicle, etc.). Recently, to study this further, researchers have begun developing controlled models of rodent blast injury, with results indicating the wave alone can damage cord tissue (14). Regardless, these primary SCI injuries cause acute damage to neuronal axons, break blood vessels, and kill cord tissue cells. While this acute damage is regarded as unavoidable, secondary injuries provide a long timeframe for intervention to lower clinical severity levels and improve the quality of life after SCI.

1.4 Etiology of secondary injury

Central Nervous System (CNS) trauma is characterized by an immediate, primary (physical) injury and delayed, secondary (chemical) injury. Primary injury leads to acute clinical signs of neurotrauma such as loss of motor control, loss of consciousness and memory, confusion, and irritability, depending on the location and severity of trauma in the CNS. On a cellular level, primary injury results in complex combinations of mechanical and shear stress to the cellular structure, and can directly destroy cells by crushing, cutting, or stretching. In the white matter many neurons that are impacted by a primary injury may be left with cell bodies intact, but have

damage to axons. These and other damaged but surviving cells will likely die over time. However, while cell death immediately following physical insults is largely inevitable (due to the lack of time for applying treatment), the cellular damage occurring during the delayed secondary injury period is potentially preventable, given its long therapeutic window for intervention (15). Many established mechanisms for secondary injuries exist. For instance, secondary injuries to white matter results in neurons with diffuse axonal injuries having disrupted axonal transport and axonal swelling, eventually leading to Wallerian degeneration (16, 17). Impacts to the blood brain barrier (BBB) is also an important mechanism in secondary injury. Damage to blood vessels and microvasculature can cause ischemia and starve neurons of nutrients. Neurons starved of blood release excess amounts of glutamate, and recipient neurons often die from this exposure in glutamate excitotoxicity (18). Although much more debated, inflammation plays a role in secondary injury and neuronal cell death. Immune cells undergo chemotaxis and division, responding to the cell death, BBB disruption, and excitotoxic signals from neurons. While immune cells such as microglia and macrophages provide many benefits after neurotrauma such as axonal ensheathing and removal of debris, many act aggressively as in response to an infection (19, 20). Even though they provide benefits, their abundance and unwanted behaviors leads to issues such as excess levels of neurotoxic chemicals, including acrolein. Acrolein (detailed in the next segment) is a known neurotoxin that is a byproduct of myeloperoxidase in activated microglia/macrophages (21). While acrolein also has other generative sources, its production by immune cells is an example of how abundant immune cells can lead to further secondary injury.

Relevantly, these mechanisms of secondary injury in neurotrauma are heavily implicated in long term neurodegenerative disorders such as Parkinson's disease (PD). Traumatic brain injury (TBI), even if it's an isolated life event, significantly increases the likelihood of developing PD (22). Brain tissue from PD patients is hallmarked by slow neuronal and axonal degeneration, chronic inflammation and BBB permeability, and reactive aldehyde production such as acrolein (23-25). In fact, evidence from our lab suggests acrolein plays a role in the aggregation of hallmark PD protein alpha-synuclein (26, 27).

Primary injury not only can physically damage the CNS tissue and cause instantaneous cell death, it also triggers a cascade of secondary injury resulting in additional and amplified neuronal degeneration and tissue damage. Secondary injury is therefore an important target for therapeutics and a major factor in sustained death of neurons.

1.5 Acrolein is a critical component of secondary injury

As mentioned above, secondary injury is an important target in neurotrauma and neurotrauma related neurodegenerative disorders such as PD. If a key mechanistic instigator of secondary injury is found its correction could not only benefit various forms of neurotrauma, but also such linked disorders. Already, oxidative stress has received much attention for its role in perpetuating secondary injury and capability of instigating and sustaining long-lasting cellular damage (28). Specifically, a key element of neuronal oxidative stress is lipid peroxidation (LPO) and the generation of radical aldehydes such as acrolein (29). Acrolein is a proven neurotoxin in the CNS, capable of reacting with proteins, lipids, and DNA, causing significant cellular damage and death (29). Acrolein is an α,β-unsaturated aldehyde that is highly reactive. It has been used commercially for making acrylic acid and DL-methionine, for water treatment, and as a tissue fixative. Given its chemical structure, acrolein is highly volatile and unstable, and its reactivity makes it challenging to detect in an experimental or in-vivo environment (30). Interestingly, acrolein has a variety of common sources, both endogenous and exogenous.

1.6 Exogenous sources of acrolein

Exogenously, acrolein exposure occurs primarily as a form of pollution, and is categorized as an environmental toxin. Apart from its intentional industrial manufacturing, acrolein is generated when lipid rich organic compounds reach high temperatures, such as burning of cooking oils, wood, and certain gas (30). Cigarette smoke generates a concerning amount of acrolein. Acceptable levels of acrolein exposure are below 30 ppb as established by the EPA. However, cigarette smoke far exceeds this standard, producing roughly 1-5 ppm of acrolein (31-33). While exogenous sources are not the primary generative sources in neurotrauma, they none-the-less pose a concerning risk for human health when considering, for example, neurotrauma patients may be smokers. In fact, urine levels of the acrolein-glutathione metabolite 3-HPMA, are more than 3-fold higher in people who smoke (34). Furthermore, studies show that acrolein is capable of diffusing through tissues. Therefore, these exogenous acrolein exposures could further impact CNS health.

1.7 Endogenous sources of acrolein

Endogenously, acrolein is produced from reactive oxygen species and resulting attacks on lipids, causing LPO. Oxidative stress and LPO are well established as playing a role in the pathology of many major diseases (cancer, cardiovascular disease, arthritis, diabetes, Alzheimer's and Parkinson's disease etc.) (29). Apart from LPO and ROS, acrolein production can also result from mechanisms involving inflammation or oxidative phosphorylation during mitochondrial function, metabolism of arachidonic acid by lipoxygenases, and other enzymes as well (35, 36).

Inflammation is abundant in neurotrauma. An initial influx of neutrophils peaks 1 - 2 days post SCI, which is followed by a peak in macrophage/microglia cells around 1 week post SCI (37). This surge of inflammation can take months, or years in some instances, before returning to baseline values (37). While inflammation has many beneficial aspects, such as removal of debris and dead cells, the surge of inflammation in SCI will also contribute to the surge of acrolein and ROS. Immune cells possess high levels of myeloperoxidase (MPO), an enzyme that contributes to their bactericidal abilities (38). MPO generates hypochlorous acid, also found in bleach and chlorine products, as well as other damaging anti-microbial products including acrolein (21, 38). However, given the development of antibiotics and sterile environment of hospitals, this bactericidal ability is unnecessary in SCI. Yet, after SCI immune cells expressing acrolein generating MPO are significantly elevated and thus a cause of concern.

1.8 How acrolein formation impacts health

Acrolein remains significantly elevated for up to two weeks in rats given severe spinal cord injuries, despite its reactivity (50). This persistent elevation may be due to the fact that LPO can be initiated by both ROS and acrolein, creating a vicious cycle of self-perpetuation and positive feedback (39). Additionally, the half-life of acrolein is considerably longer than that of other reactive aldehydes or ROS, which further explains the ability of acrolein to maintain such high levels over extended periods of time in tissues (40). The threat of acrolein perpetuation extends beyond lipids, to degradation of proteins and even DNA when at high enough concentrations (41). Acrolein is also capable of attacking the nucleophilic bases of DNA to produce exocyclic products and can modify histones (42). When adducting to proteins, acrolein can inhibit their function thus promoting their degradation (31, 43). Further, acrolein interaction with nucleophilic amino acids

such as lysine, histidine, and cysteine to form acrolein-protein adducts. The most stable of which is acrolein-bound lysine, or FDP lysine, that is used in the generation of antibodies for indirectly measuring acrolein levels in tissue biochemistry (44). Given the reactivity, multiple generative sources, and effects on a range of biological processes, acrolein poses a major concern for human health.

1.9 Strategies for combating acrolein

Acrolein is both a product and initiator of LPO, a detrimental process of lipid (fatty acid) degradation when attacked by free radicals, thereby perpetuating oxidative stress and continued damage to neuronal tissue for extended periods of time. As such, LPO and acrolein are of particular concern to the CNS, with neurons containing many lipid rich mitochondria and myelin sheaths. Additionally, acrolein can further deplete the endogenous antioxidant system which is already overwhelmed in neurotrauma. Endogenous systems remove acrolein either through binding to glutathione to form 3-HPMA or to Keap1 in the Nrf2 regulation system (45, 46). However, the production of endogenous glutathione is limited and is not readily bioavailable when administered orally. On the other hand, while drugs improving the Keap1/Nrf2 system show some promising results, they remain in the early stages of development and additional research is required to effectively boost this slow-to-respond pathway (47). To this end, aldehyde scavengers have been employed to target acrolein with much success. In SCI acrolein peaks after injury in 48 hours and remains significantly elevated for at least 2 weeks post injury (48). Removing acrolein in SCI results in significant benefits to motor function and neuropathic pain, as well as cell survivability and injured tissue structure (49, 50). Acrolein scavengers such as hydralazine are also FDA approved and therefore safe for use. However, these FDA approved medications have side effects, making their use in neurotrauma patients challenging, despite the benefits of acrolein removal. Therefore, a search for alternatives is necessary.

Reducing acrolein as an effective and feasible neuroprotective strategy in neurotrauma also provides the opportunity to benefit other disorders hallmarked by oxidative stress. While the benefits of acrolein removal are largely known, many limitations exist with the current clearance strategies, or remain unexplored. To this end, we investigate novel means for the removal of acrolein in SCI (see chapters 3 and 5) and set the groundwork for investigating acrolein mediated BBB damage in bTBI (chapter 3). Provided the strong link of neurotrauma and long term

degenerative disorders such as PD, we investigate the role of acrolein in PD (chapter 2). By identifying acrolein as a common link to secondary injury, and employing effective acrolein removal tools, we can benefit many forms of neurotrauma such as bTBI and SCI, as well as neurotrauma linked neurodegenerative diseases such as PD.

1.10 References

1. Hachem LD, Ahuja CS, Fehlings MG. Assessment and management of acute spinal cord injury: From point of injury to rehabilitation. The journal of spinal cord medicine. 2017;40(6):665-75.

2. Alizadeh A, Dyck SM, Karimi-Abdolrezaee S. Traumatic Spinal Cord Injury: An Overview of Pathophysiology, Models and Acute Injury Mechanisms. Frontiers in Neurology. 2019;10(282).

3. Wilson JR, Cadotte DW, Fehlings MG. Clinical predictors of neurological outcome, functional status, and survival after traumatic spinal cord injury: a systematic review. Journal of neurosurgery Spine. 2012;17(1 Suppl):11-26.

4. Shojaei MH, Alavinia SM, Craven BC. Management of obesity after spinal cord injury: a systematic review. The journal of spinal cord medicine. 2017;40(6):783-94.

5. Claydon VE, Steeves JD, Krassioukov A. Orthostatic hypotension following spinal cord injury: understanding clinical pathophysiology. Spinal Cord. 2006;44(6):341-51.

6. Association of Pneumonia, Wound Infection, and Sepsis with Clinical Outcomes after Acute Traumatic Spinal Cord Injury. Journal of Neurotrauma. 2019;36(21):3044-50.

7. Shiao R, Lee-Kubli CA. Neuropathic Pain After Spinal Cord Injury: Challenges and Research Perspectives. Neurotherapeutics. 2018;15(3):635-53.

8. Middleton JW, Dayton A, Walsh J, Rutkowski SB, Leong G, Duong S. Life expectancy after spinal cord injury: a 50-year study. Spinal Cord. 2012;50(11):803-11.

9. Shavelle RM, Paculdo DR, Tran LM, Strauss DJ, Brooks JC, DeVivo MJ. Mobility, continence, and life expectancy in persons with Asia Impairment Scale Grade D spinal cord injuries. American journal of physical medicine & rehabilitation. 2015;94(3):180-91.

10. Sekhon LH, Fehlings MG. Epidemiology, demographics, and pathophysiology of acute spinal cord injury. Spine. 2001;26(24 Suppl):S2-12.

11. Choo AM-T, Liu J, Liu Z, Dvorak M, Tetzlaff W, Oxland TR. Modeling spinal cord contusion, dislocation, and distraction: Characterization of vertebral clamps, injury severities, and node of Ranvier deformations. Journal of Neuroscience Methods. 2009;181(1):6-17.

12. Szuflita NS, Neal CJ, Rosner MK, Frankowski RF, Grossman RG. Spine Injuries Sustained by U.S. Military Personnel in Combat are Different From Non-Combat Spine Injuries. Military medicine. 2016;181(10):1314-23.

13. Blair JA, Patzkowski JC, Schoenfeld AJ, Cross Rivera JD, Grenier ES, Lehman RA, et al. Are spine injuries sustained in battle truly different? The spine journal : official journal of the North American Spine Society. 2012;12(9):824-9.

14. del Mar N, von Buttlar X, Yu AS, Guley NH, Reiner A, Honig MG. A novel closed-body model of spinal cord injury caused by high-pressure air blasts produces extensive axonal injury and motor impairments. Experimental neurology. 2015;271:53-71.

15. Lipinski MM, Wu J, Faden AI, Sarkar C. Function and Mechanisms of Autophagy in Brain and Spinal Cord Trauma. Antioxid Redox Signal. 2015;23(6):565-77.

16. Johnson VE, Stewart W, Smith DH. Axonal pathology in traumatic brain injury. Experimental neurology. 2012.

17. Hemphill MA, Dauth S, Yu CJ, Dabiri BE, Parker KK. Traumatic brain injury and the neuronal microenvironment: a potential role for neuropathological mechanotransduction. Neuron. 2015;85(6):1177-92.

18. Belov Kirdajova D, Kriska J, Tureckova J, Anderova M. Ischemia-Triggered Glutamate Excitotoxicity From the Perspective of Glial Cells. Front Cell Neurosci. 2020;14:51.

19. Kato G, Inada H, Wake H, Akiyoshi R, Miyamoto A, Eto K, et al. Microglial Contact Prevents Excess Depolarization and Rescues Neurons from Excitotoxicity. eNeuro. 2016;3(3).

20. Greenhalgh AD, Zarruk JG, Healy LM, Baskar Jesudasan SJ, Jhelum P, Salmon CK, et al. Peripherally derived macrophages modulate microglial function to reduce inflammation after CNS injury. PLoS Biol. 2018;16(10):e2005264.

21. Melissa M. Anderson, Stanley L. Hazen, Fong F. Hsu, Heinecke JW. Human Neutrophils Employ the Myeloperoxidase–Hydrogen Peroxide–Chloride System to Convert Hydroxy-amino Acids into Glycolaldehyde, 2-Hydroxypropanal, and Acrolein. J Clin Invest. 1996;99(3).

22. Jafari S, Etminan M, Aminzadeh F, Samii A. Head injury and risk of Parkinson disease: a systematic review and meta-analysis. Movement disorders : official journal of the Movement Disorder Society. 2013;28(9):1222-9.

23. McGeer PL, McGeer EG. Glial reactions in Parkinson's disease. Movement disorders : official journal of the Movement Disorder Society. 2008;23(4):474-83.

24. D. T. Dexter, C. J. Carter, F. R. Wells, F. Javoy-Agid, Y. Agid, A. Lees, et al. Basal Lipid Peroxidation in Substantia Nigra Is Increased in Parkinson's Disease. J Neurochem. 1989;52(2).

25. Gray MT, Woulfe JM. Striatal blood-brain barrier permeability in Parkinson's disease. J Cereb Blood Flow Metab. 2015;35(5):747-50.

26. Ambaw A, Zheng L, Tambe MA, Strathearn KE, Acosta G, Hubers SA, et al. Acrolein-mediated neuronal cell death and alpha-synuclein aggregation: Implications for Parkinson's disease. Mol Cell Neurosci. 2018;88:70-82.

27. Acosta SA, Tajiri N, de la Pena I, Bastawrous M, Sanberg PR, Kaneko Y, et al. Alpha-synuclein as a pathological link between chronic traumatic brain injury and Parkinson's disease. J Cell Physiol. 2015;230(5):1024-32.

28. Chen CH, Ferreira JC, Gross ER, Mochly-Rosen D. Targeting aldehyde dehydrogenase 2: new therapeutic opportunities. Physiol Rev. 2014;94(1):1-34.

29. Burcham PC. Acrolein and Human Disease: Untangling the Knotty Exposure Scenarios Accompanying Several Diverse Disorders. Chem Res Toxicol. 2017;30(1):145-61.

30. Ghilarducci DP, Tjeerdema RS. Fate and effects of acrolein. Reviews of environmental contamination and toxicology. 1995;144:95-146.

31. Kirkham PA, Spooner G, Ffoulkes-Jones C, Calvez R. Cigarette smoke triggers macrophage adhesion and activation: role of lipid peroxidation products and scavenger receptor. Free Radic Biol Med. 2003;35(7):697-710.

32. Dong JZ, Moldoveanu SC. Gas chromatography-mass spectrometry of carbonyl compounds in cigarette mainstream smoke after derivatization with 2,4-dinitrophenylhydrazine. Journal of chromatography A. 2004;1027(1-2):25-35.

33. Roemer E, Schramke H, Weiler H, Buettner A, Kausche S, Weber S, et al. Mainstream Smoke Chemistry and and Toxicity of the Reference Cigarettes 3R4F and 2R4F. Beiträge zur Tabakforschung International/Contributions to Tobacco Research. 2014;25(1):316-35.

34. Carmella SG, Chen M, Zhang Y, Zhang S, Hatsukami DK, Hecht SS. Quantitation of acrolein-derived (3-hydroxypropyl)mercapturic acid in human urine by liquid chromatography-atmospheric pressure chemical ionization tandem mass spectrometry: effects of cigarette smoking. Chem Res Toxicol. 2007;20(7):986-90.

35. Adibhatla RM, Hatcher JF. Lipid oxidation and peroxidation in CNS health and disease: from molecular mechanisms to therapeutic opportunities. Antioxid Redox Signal. 2010;12(1):125-69.

36. Adibhatla RM, Hatcher JF. Role of Lipids in Brain Injury and Diseases. Future lipidology. 2007;2(4):403-22.

37. Beck KD, Nguyen HX, Galvan MD, Salazar DL, Woodruff TM, Anderson AJ. Quantitative analysis of cellular inflammation after traumatic spinal cord injury: evidence for a multiphasic inflammatory response in the acute to chronic environment. Brain : a journal of neurology. 2010;133(Pt 2):433-47.

38. Kubota K, Saiwai H, Kumamaru H, Maeda T, Ohkawa Y, Aratani Y, et al. Myeloperoxidase exacerbates secondary injury by generating highly reactive oxygen species and mediating neutrophil recruitment in experimental spinal cord injury. Spine. 2012;37(16):1363-9.

39. Liu-Snyder P, McNally H, Shi R, Borgens RB. Acrolein-mediated mechanisms of neuronal death. Journal of neuroscience research. 2006;84(1):209-18.

40. Borgens RB, Liu-Snyder P. Understanding secondary injury. The Quarterly review of biology. 2012;87(2):89-127.

41. Moghe A, Ghare S, Lamoreau B, Mohammad M, Barve S, McClain C, et al. Molecular mechanisms of acrolein toxicity: relevance to human disease. Toxicological sciences : an official journal of the Society of Toxicology. 2015;143(2):242-55.

42. Chen D, Fang L, Li H, Tang MS, Jin C. Cigarette smoke component acrolein modulates chromatin assembly by inhibiting histone acetylation. J Biol Chem. 2013;288(30):21678-87.

43. Deshmukh HS, Shaver C, Case LM, Dietsch M, Wesselkamper SC, Hardie WD, et al. Acrolein-activated matrix metalloproteinase 9 contributes to persistent mucin production. American journal of respiratory cell and molecular biology. 2008;38(4):446-54.

44. Kaminskas LM, Pyke SM, Burcham PC. Strong Protein Adduct Trapping Accompanies Abolition of Acrolein-Mediated Hepatotoxicity by Hydralazine in Mice. Journal of Pharmacology and Experimental Therapeutics. 2004;310(3):1003-10.

45. Ma Q. Role of nrf2 in oxidative stress and toxicity. Annu Rev Pharmacol Toxicol. 2013;53:401-26.

46. Zheng L, Park J, Walls M, Tully M, Jannasch A, Cooper B, et al. Determination of urine 3-HPMA, a stable acrolein metabolite in a rat model of spinal cord injury. J Neurotrauma. 2013;30(15):1334-41.

47. Miller DM, Singh IN, Wang JA, Hall ED. Nrf2-ARE activator carnosic acid decreases mitochondrial dysfunction, oxidative damage and neuronal cytoskeletal degradation following traumatic brain injury in mice. Experimental neurology. 2015;264:103-10.

48. Luo J, Shi R. Acrolein induces axolemmal disruption, oxidative stress, and mitochondrial impairment in spinal cord tissue. Neurochem Int. 2004;44(7):475-86.

49. Gianaris A, Liu NK, Wang XF, Oakes E, Brenia J, Gianaris T, et al. Unilateral microinjection of acrolein into thoracic spinal cord produces acute and chronic injury and functional deficits. Neuroscience. 2016;326:84-94.

50. Park J, Zheng L, Marquis A, Walls M, Duerstock B, Pond A, et al. Neuroprotective role of hydralazine in rat spinal cord injury-attenuation of acrolein-mediated damage. J Neurochem. 2014;129(2):339-49.

CHAPTER 2. NEUROPROTECTION OF ACROLEIN SCAVENGERS HYDRALAZINE AND DIMERCAPROL IN A MODEL OF PARKINSON'S DISEASE.

2.1 Introduction

Parkinson's disease (PD) is a common neurodegenerative disease associated with a severe movement disorder (1). PD results from dopamine (DA) deficiency due to degeneration of nigral DA neurons. Although the exact cause is unknown, oxidative stress has been implicated as one of the most important contributors to nigral cell death in PD (2-4). However, despite decades of efforts, treatments that target free radicals have been largely ineffective in reducing dopaminergic cell death and delaying or alleviating motor deficits in PD (2). Therefore, further understanding of the mechanisms of oxidative stress and identification of a novel and more effective target is highly warranted and desirable. We have demonstrated that acrolein, an aldehyde produced by lipid peroxidation, is capable of directly damaging nerve cells and generating free radicals (5, 6). In addition, acrolein has a much longer half-life than better known reactive oxygen species such as the superoxide anion (O2−) and hydroxyl radical (%OH) (7). Furthermore, evidence from our lab and others has indicated that acrolein plays a significant role in secondary oxidative stress related to spinal cord trauma (8, 9) and multiple sclerosis (10, 11). These findings have led us to postulate that acrolein plays a particularly damaging role through the perpetuation of oxidative stress, enhancing cellular degeneration and functional loss. Oxidative stress is a well-established pathology in PD, and therefore we hypothesize that acrolein plays a vital role in facilitating DA neuronal cell death. Furthermore, acrolein may present a novel and effective target for therapeutic interventions aimed at suppressing oxidative stress, reducing DA cell death, and alleviating motor deficits.

2.2 Materials and Methods

2.2.1 Animals and Injury model

Animals that underwent surgery were anaesthetized with a combination of ketamine (100 mg/kg) and xylazine (10 mg/kg) and placed in a Kopf stereotaxic frame. With the head held firmly in place by the frame, a 2 cm mid-sagittal skin incision was made on the scalp to expose the skull.

A dermal drill was used to drill a hole in the skull to expose the dura mater. For animals treated with 6-OHDA (Sigma, Cas. No. 28094-15-7), a solution of the toxin (8μg/2μL) was administered via a unilateral injection to the left side of the brain into the region of substantia nigra at coordinates AP: -5.4, ML: -3 lateral and -8.2 DV from bregma using a 10μL Hamilton syringe at a rate of 1μL/min for a 4 min duration. Sham-operated animals received the vehicle (saline) and were used as injured controls. Following the infusion of 6-OHDA, or vehicle, the infusion needle was allowed to sit in place for 5 min and then slowly withdrawn, and the skin incision closed with stainless steel wound clips.

2.2.2 Treatments

Dimercaprol (Alfa aesar) was dissolved in saline and administered to the lesioned animals through a daily 5mg/kg of IP injections for 5 weeks, starting immediately (within 5 min) after 6-OHDA injection. The same dose of saline was administered daily in the same way to the sham group and 6-OHDA group for 5 weeks.

Depending on the group, acrolein scavengers hydralazine or dimercaprol were used. Hydralazine (Sigma) at 5mg/kg in saline was injected to the lesioned animal through intraperitoneal (IP) injections every day for 15 days and every other day for the rest of the experiment, up to 30 days. An equivalent dose of saline was administered daily in the same way.

2.2.3 Immunohistochemistry

Animals were deeply anaesthetized with a ketamine/ and xylazine cocktail and perfused transcardially with Krebs solution. Brains fixed in 4% paraformaldehyde were cryoprotected with 15–30% sucrose, frozen with optimal cutting temperature OCT compound, and then cut in 25 μm sections on a cryostat and stored in PBS containing 0.01% Sodium azide in 4ºC until use. Serial coronal sections were made from the rostral-to-caudal direction. Sections for the striatum or SN were processed for anti-TH immunohistochemistry staining. These sections were washed in 0.01M PBS then placed in 3% H2O2/water to quench endogenous peroxidase activity. After washing three times in PBS, sections were incubated in 5% normal goat serum for 30 min at room temperature, and then sections were reacted with primary antibodies (TH: RRID: AB 2564816, 1:1000, Biolegend) over night at 4ºC. After several washing steps, the sections were incubated

with the second antibody (anti-mouse antiserum IgG) for 2 h at room temperature, then processed by the ABC method (1:100, Vector, Cat.No.PK-4000) with one drop of solution A and one drop of solution B in 5 mL of PBS for 30 min. After three washing steps, sections were incubated in peroxidase substrate solution before mounting on slides. The TH+ staining density was analyzed by Image J densitometric analysis, and expressed as a percentage of the control.

Standard immunofluorescence for acrolein was carried out as previously reported (12).

2.2.4 Open field test

For dimercaprol rats, every week (day 7, 14, 21, 27, 35, in the morning) after injury, animals were placed in a Plexiglas activity box (100 cm x 100 cm x 20 cm) in a darkened room. A red light and a camera were placed on top of the box to record the activity of the animal. Each rat was placed in the box and activity was recorded for 15 minutes. The box was thoroughly cleaned with 70% ethanol and water between each animal to discourage the rat from engaging in thigmotaxic behavior. The area covered and distance traveled per animal were quantified using an automated video tracking system (ANY-maze) to obtain motor behavior.

For hydralazine rats, twelve hours after injury or sham surgery, animals were placed in a Plexiglas activity box (100 cm×100 cm×20 cm) in a darkened room. Food was placed over the center of the box, and the box was thoroughly cleaned with water between experiments to discourage the rat from engaging in thigmotaxic behavior. Eight infrared beams were arranged in an X–Y matrix, 20 cm apart and 4.5 cm off the ground, and beam interruptions (breakages) resulting from movements of the rat in the matrix were counted using a Veeder-Root Series 7999 Mite Totalizer (ID# 79998D-110, Gurnee, IL). The lag time between counts was 14 ms. At 30 min, the total number of beam breaks was tabulated. Custom-designed in-house software recorded the state of the infrared beams at 200 ms intervals (Koob et al., 2006). With this data, the experimenter could determine the rat's position in space and time over the course of the experiment and detect the animal's movement in real time.

2.2.5 Rotarod test

For dimercaprol rats, the rotarod test was performed on day 7, 14, 21, 27, and 35 (in the afternoon) after the surgery. Performance was measured by the duration that an animal stays on

the rod as a function of drum speed. Animals were allowed first to remain stationary for 10s. The drum begins turning at the lowest speed and takes five minutes to steadily reach the highest speed. The ability of the rat to remain on the rotating rod was recorded. The trial was ended if the rat completely falls off the rungs, or grips the device and spins around twice without actually walking on the rungs. Each animal received 4 to 7 training sessions before surgery to ensure that it did not fall off and remained for 30 seconds after drum reaches the highest speed. Animals were subjected to rotarod test weekly after injury.

For hydralazine rats, animals were allowed first to remain stationary for 10s. The speed was then gradually increased by 3 rpm per 10s until a rotational speed of 30 rpm (at which naïve, uninjured rat will not fall off during 2 min test interval) was reached. The animal must remain on the apparatus for the remainder of the 2 min test interval at this 30 rpm speed. The trial ends if the rat completely falls off the rungs, or grips the device and spins around twice without actually walking on the rungs.

2.2.6 Cell culture

The SK-N-SH dopaminergic cell line (purchased from ATCC, USA) was used in this study. The cells were routinely cultured in DMEM supplemented with 10% FBS and 1% penicillin/ streptomycin, and maintained at 37ºC in a humidified atmosphere of 5% CO2. Twenty-four hours after plating or when the cell density was 60%-70%, the cells were treated with different concentrations (0, 10, 25, 50, 100, 200, 500, 1000μM) of acrolein for 4 hours. Some of them were treated with additional different concentrations (0, 10, 50, 100, 200, 500μM) of dimercaprol after 15 min of acrolein exposure. After various treatments, cell viability was measured by 3-[4,5-Dimethylthiazol-2-yl]-2,5-diphenyl tetrazolium bromide (MTT). Briefly, MTT (Sigma, Cas.No.57360-67-9) solution reconstituted in DMEM (0.5mg/mL, 100μL of medium in each well) was added in each well, and the plates were then incubated at 37ºC for 1 h. After removing the medium, an equal volume of Dimethyl sulfoxide was added to each well to dissolve the remaining formazan crystals. The absorbance of each well was measured spectrophotometrically (molecular device, Spectra) at 570 nm, and the background absorbance at 660 nm was subtracted from these values. Each experiment was repeated four times.

For hydralazine experiments, a similar dopaminergic cell line was used: MES23.5 cell line. The cells were routinely propagated in Sato's N1 medium (87.5% (v/v) DMEM, glutamine (4 mM),

newborn calf serum (2%, v/v), fetal bovine serum (5%, v/v), penicillin/streptomycin (1%, v/v), 15mM HEPES (pH 7.4), and 1× SATO (50× SATO: insulin, 0.25 mg/mL; human transferrin, 0.25 mg/mL; pyruvic acid, 2.43 mg/mL; putrescine, 0.2 mg/mL; sodium selenite, 0.25 μg/mL; progesterone, 0.315 μg/mL). MES23.5 cells were used to test the effects of hydralazine on 6-OHDA-mediated cytotoxicity. One group of cells were incubated with 400 μM 6-OHDA for 2 h (6-OHDA group). In the other group, cells were treated with 500 μM hydralazine after a 15-min delay following 6-OHDA exposure (6-OHDA/HZA). Cell viability was determined using the MTT test and expressed as percent of control.

2.2.7 Statistics

Statistical analysis of multiple comparison was carried out by oneway ANOVA followed by either Tukey or (where specified) the Newman-Keuls post hoc test (Prism 6, GraphPad, La Jolla, CA, or IBMSPSS, SPSS Inc., an IBM company, Chicago, IL, USA). In analyzing percentage primary cell viability data by ANOVA, square root transformations were carried out to conform to ANOVA assumptions. The Student's t-test was used when comparing only two groups. $p < 0.05$ was considered statistically significant, and the results were expressed as the mean ± SEM.

2.3 Results

2.3.1 Increased levels of Acrolein in the brains of 6-OHDA-injected rats and subsequent reduction via dimercaprol

We found that the injection of 6-OHDA into the substantia nigra (SN) also significantly increased the level of protein-bound acrolein in both the SN and striatum. Specifically, anti-acrolein immunofluorescence staining revealed significantly increased levels of acrolein in both the SN and striatum of 6-OHDA injected rats compared with sham rats when examined at 5 weeks post injection ($P<0.01$). In addition, the increased levels of acrolein in 6-OHDA rats could be significantly alleviated by a daily injection of dimercaprol (DP) ($P<0.05$) (Figure 2.1A,B,C).

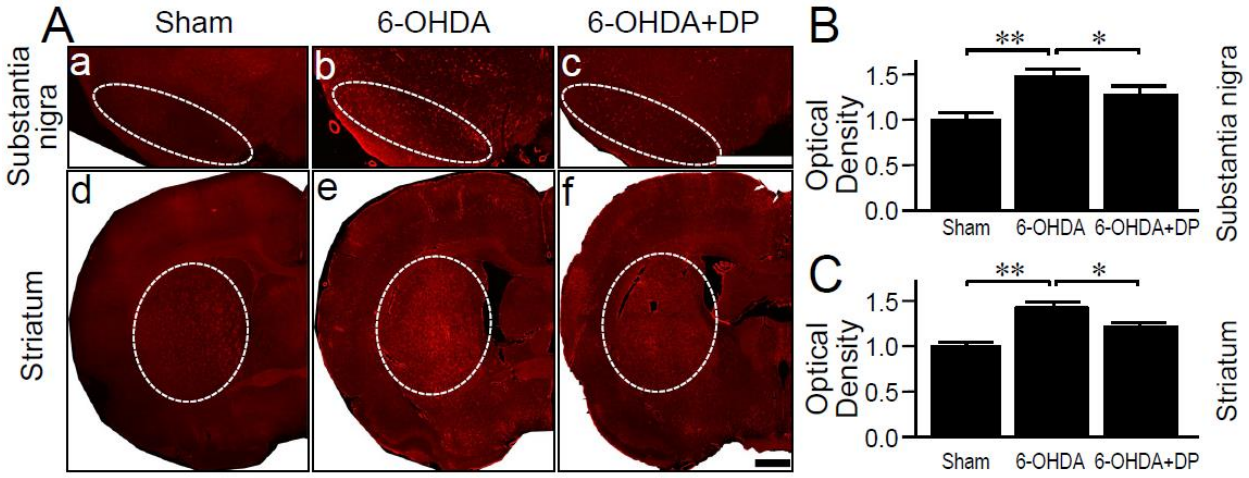

Figure 2.1. Acrolein and alpha-syn expression tested by Immunofluorescence in rats resulting from 6-OHDA lesion and the treatment of DP. A: Note the significant increase of acrolein immunoreactivity in both substantia nigra and striatum of the 6-OHDA-injected group compared to the sham group when examined 5 weeks post injection. However, this 6-OHDA-mediated increase in acrolein immunoreactivity was alleviated with a daily IP injection of DP. Quantitative analysis reveals a significant increase of acrolein staining following 6-OHDA injection (compared to sham rats), as well as decreases of optic density (OD) values of acrolein staining in the SNpc (B) and striatum (C) when 6-OHDA animals were treated with 5 mg/kg DP (compared to 6-OHDA rats), N = 5 in each group.

2.3.2 Dimercaprol and hydralazine alleviate the loss of striatal dopaminergic nerve terminals in 6-OHDA-lesioned rats

We found that 6-OHDA injections resulted in a 58.3% reduction of TH+ cells in the SN (Fig. 2.2A,B) and a 82.8% reduction of TH immunoreactivity in the striatum compared to sham injury group when examined at 5 week post injection (Fig. 2.2A,C). Daily IP treatment of dimercaprol (DP) at 5mg/kg limited the loss of TH+ cells to 39.4 % in the SN, and the reduction of TH immunoreactivity to 58.5 % in the striatum (Fig. 2.2A,B,C).

In hydralazine rat groups, we found that 6-OHDA injection resulted in a 93.75% reduction of TH immunoreactivity in the striatum in a brain coronal section (Fig. 2.3B,D) compared to control rats (Fig. 2.3A, D). However, systemic treatment with 5 mg/kg hydralazine increased TH immunoreactivity by 4-fold in 6-OHDA-treated rats (Fig. 2.3C, D).

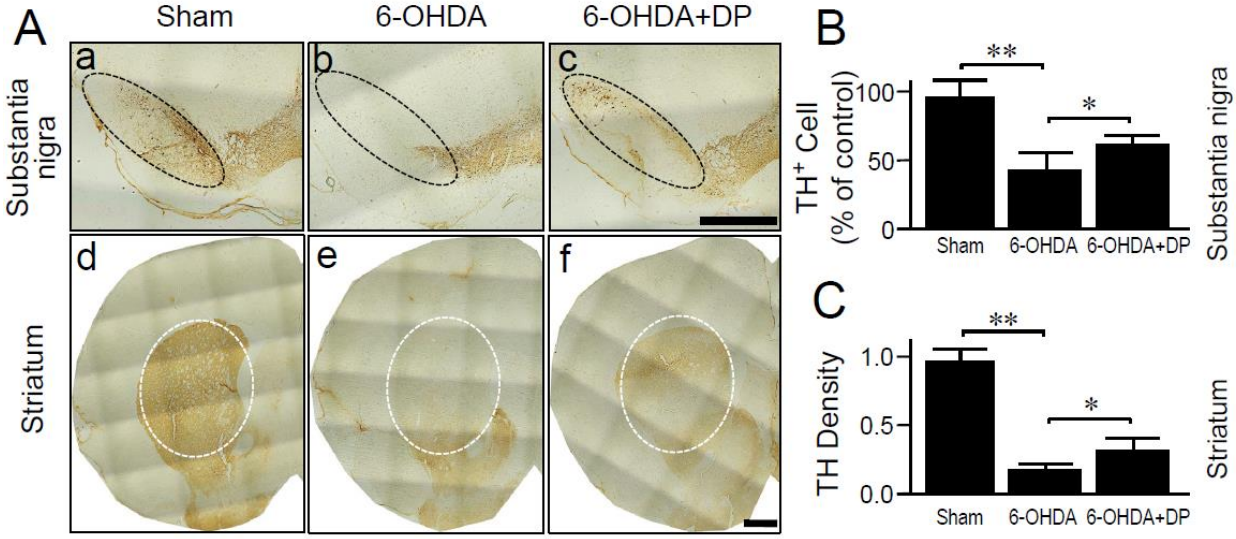

Figure 2.2. Histological analysis of the changes of tyrosine hydroxylase (TH) staining in rats in response to 6-OHDA lesion and the treatment of DP. Note the marked reduction of TH immunoreactivity in both substantia nigra and striatum in the 6-OHDA-injected group compared to the sham group when examined 5 weeks post injection. However, this 6-OHDA-mediated reduction in TH immunoreactivity was significantly alleviated with a daily IP injection of DP (A). Quantitative analysis shows a significant decreases of TH+ cells in 6-OHDA rats when compared to that in sham, as well as an increase of TH+ cells) for 6-OHDA animals treated with 5mg/kg DP in the SNpc (B) and TH density in the striatum (C). (*P<0.05, **P<0.01, ANOVA). Data were expressed as mean ± SD. N = 5 in each group. Scale bar = 1 mm (for Aa-Ac, or Ad-Af).

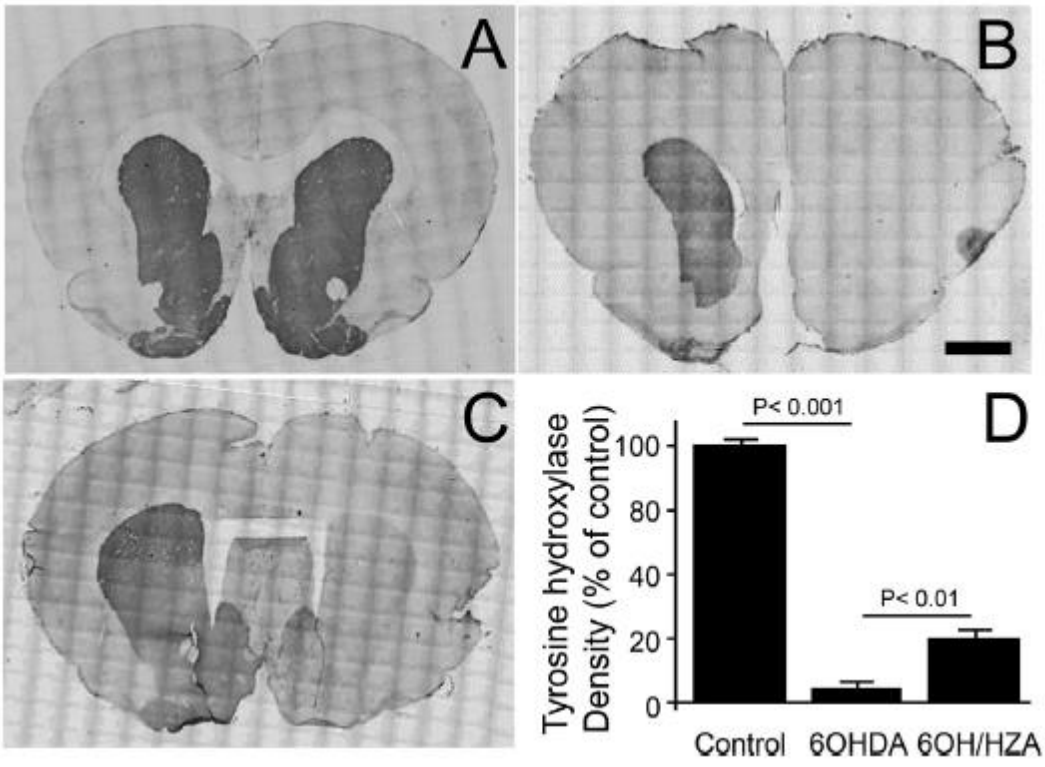

Figure 2.3. Histological analysis of tyrosine hydroxylase (TH) staining in the rat striatum following injection of 6-OHDA in the MFB. Photomicrograph of 25 μm coronal brain section showing TH immunolabeling in the striatum of control (A), 6-OHDA-lesioned (B), and 6 OHDA-lesioned and hydralazine- treated groups (C). Note the marked reduction of TH immunoreactivity in the 6-OHDA-injected group compared to the sham group. However, this 6-OHDA-mediated reduction in TH immunoreactivity was significantly alleviated with IP injection of hydralazine. In quantitative analysis of TH staining intensity (D), 6-OHDA injection caused a>90% reduction inTH immunolabeling ($p < 0.001$, ANOVA). However, systemic injection of hydralazine (HZA) resulted in a significant increase in TH immunolabeling compared to the 6-OHDA group ($p < 0.01$, ANOVA). All data are expressed as the mean ± SEM, N=4. Scale bar: 2mm for A–C.

2.3.3 Motor deficits of 6-OHDA-lesioned animals examined using an activity box were alleviated by dimercaprol and hydralazine

For DP rat groups, to measure the general locomotor activity of the rats and their willingness to explore, open field test was carried out before and after surgeries (weekly). 6-OHDA-lesioned rats showed a significant reduction in activity beginning in the 3rd week, when the total distance traveled was 51 ± 13.3 m, when compared with the sham group ($p < 0.01$)(88 ± 2.2 m). However, systemic treatment with DP significantly increased motor activity at the 4th ($p < 0.05$) and 5th week ($p < 0.01$), when the total distances traveled were 72 ±11.1 m and 53 ± 5.3 m, while the total distance traveled in 6-OHDA-lesioned rats were 44 ± 13.5 m and 33 ± 6.5 m,

for the same time points (Fig. 2.4A). In Fig. 2.4B, the 6-OHDA-lesioned rats were much less active after injections, and explored less area, staying mostly in one corner of the box and showing little interest in exploring when compared with sham at 5 weeks post injection. However, rats that received both 6-OHDA and DP showed an increase in both distance traveled and area explored when compared to 6-OHDA-lesioned rats (Figure 2.4B).

For hydralazine groups, 6-OHDA-lesioned rats showed a typical reduction of activity assessed by activity box method. There was a reduction of >50% in the distance traveled by 6-OHDA-treated rats compared to uninjured control (no surgery) or sham-operated animals during 1 h of recording (Fig. 2.5A). Specifically, uninjured control rats traveled an average of 223 ± 67m within an hour. Rats in the sham group (surgery but no 6-OHDA) traveled a similar distance, 246 ± 71m ($p > 0.05$ when compared to control). In 6-OHDA-injected rats, the traveling distance was reduced to 97 ± 32 m, a significant decrease compared to the control or sham group ($p < 0.01$). However, the 6-OHDA-induced reduction in the distance traveled was significantly alleviated by a daily injection of hydralazine. The hydralazine application partially restored the distance traveled to 193.2 ± 19.5, a significant increase compared to the 6-OHDA group ($p < 0.01$) (Fig. 2.5A). When assessed by the area the rat covered within one hour, similar results as those assessed by the distance traveled were obtained (Fig. 2.5B). Specifically, 6-OHDA produced a significant decrease in the area covered compared to the control or sham group (43.3 ± 18.5 vs. 94.0 ± 10.1 or 97.8 ± 2.1, $p < 0.01$). However, the 6-OHDA-mediated reduction in the area covered was significantly reversed when hydralazine was applied daily for two weeks ($p < 0.01$ comparison between 6-OHDA and 6-OHDA plus hydralazine, 43.3 ± 18.5 vs 80.0 ± 5.6).

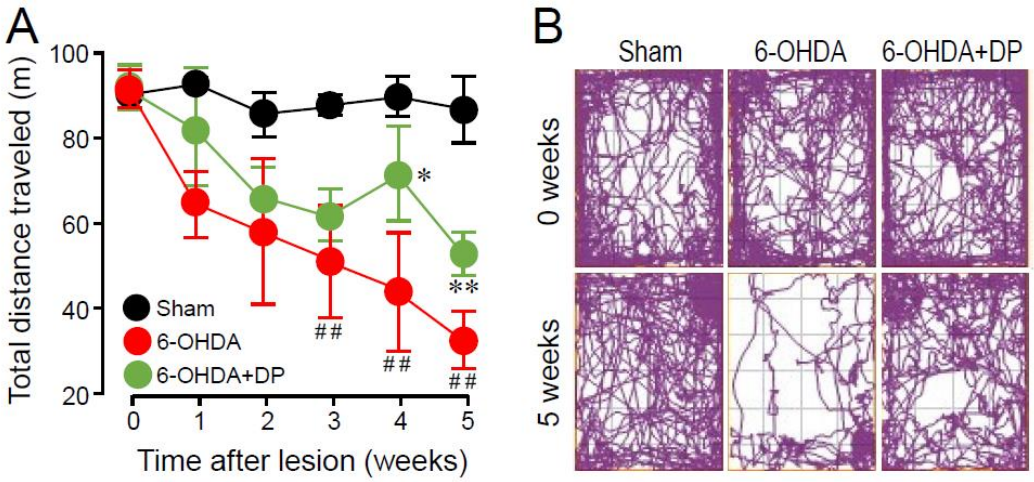

Figure 2.4. Quantitative motor behavioral analysis based on the open field test. As shown the rats in sham group were significantly more active, walked a greater distance, compared to the 6-OHDA-injected animals (A,B). However, compared to 6-OHDA rats, a significant improvement in motor function was observed when 6-OHDA-injured rats were treated with 5 mg/kg DP, which was observed in quantitate analysis of total distance (A) and can be visualized in track plot (B), at 4 to 5 weeks after injury. DP was applied through daily IP injection at a dosage of 5mg/kg for 5 weeks after injury. (*P<0.05, **P<0.01, compared to 6-OHDA group. ##P<0.01, compared sham group. ANOVA). Data were expressed as mean ± SD. N = 5 in each group.

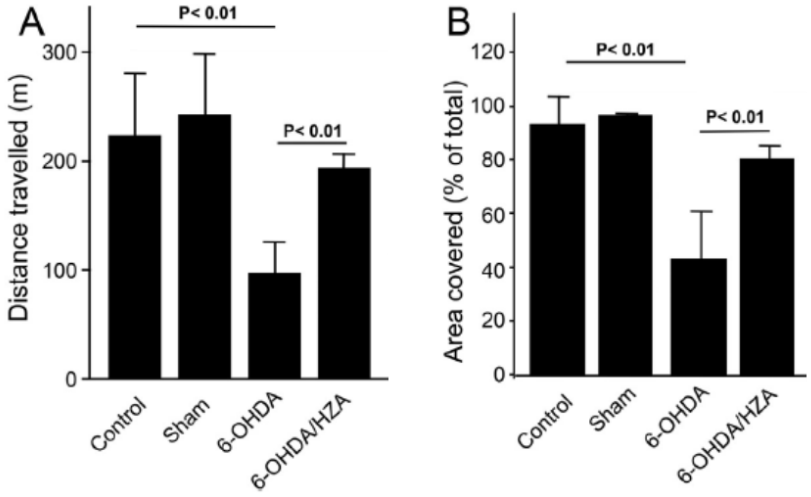

Figure 2.5. Quantitative behavioral analysis based on the openfield test. The data for the mean distance traveled (A) and the mean area covered (B) in the exploration open-field box were quantified for control, sham, 6-OHDA-injected, and 6-OHDA-injected/hydralazine-treated. As shown, control animals were significantly more active, traversed a greater distance, and covered more area compared to the 6-OHDA animals. The sham animals did not differ from the uninjured control rats with respect to mean distance traveled or mean area covered, whereas the 6-OHDA-injured groups showed a clear reduction in both parameters ($p < 0.01$). This reduction was partially restored by hydralazine treatment ($p < 0.01$). ANOVA was used in all statistical comparisons. All data are expressed as the mean ± SEM, N=4–6.

2.3.4 6-OHDA-induced motor deficits and their alleviation by dimercaprol and hydralazine based on rotarod activity

For DP groups, the rotarod tests were carried out before and after surgery each week. We found that 6-OHDA injections reduced the maximal time that a rat could walk on a moving rotarod. Specifically, the maximal time for the rats (sham injury group, 6-OHDA, 6-OHDA+DP) before the surgery was 330 s. 6-OHDA injection gradually reduced the maximal time on the rotarod, with a significant reduction (compared to sham injury) starting at week 3 ($p < 0.05$), when the maximal time was 198 ± 67.7 s, which was significantly lower than 327 ± 5.8 s in the sham injury group for the same time point. However, systemic treatment of DP gradually mitigated such reduction of the maximal time, and significantly at weeks 4 and 5 ($p < 0.01$), when the maximal times were 318 ± 23.5 s and 300 ± 40.1 s, respectively. Such values are significantly higher than that of the 6-OHDA group for the same time points ($p < 0.01$), which were 174 ± 65.0 s and 167 ± 24.3 s, respectively (Figure 2.6A).

Similar results were also obtained when motor ability was measured using the maximal speed that a rat could sustain on the rotarod. The maximal speed for rats of all the groups before surgery was 35 rpm. 6-OHDA injections resulted in a steady reduction of the maximal speed on the rotarod (examined weekly). A significant reduction was measured at the 4th and 5th week post injection, when the maximal speeds were 22 ± 6.8 s and 21 ± 2.6 rpm, which were significantly lower than in the sham injury group ($p < 0.01$)(35 rpm). Similarly, IP injections of DP allowed rats to remain at significantly increased speeds at weeks 4 and 5 post injury, when compared with 6-OHDA injection only group ($p < 0.01$) (Figure 2.6B).

For hydralazine groups, we found that 6-OHDA produced a reduction in the maximal speed that a rat could sustain on the rotarod (Fig. 2.7). Specifically, the maximal speed for control and sham-treated animals was 29.7 and 28.9 rpm respectively. 6-OHDA significantly reduced this value to 13.6 ± 3.0 ($p < 0.001$). Hydralazine injection in 6-OHDA-treated rats resulted in a maximal speed of 20.1 ± 2.1, which is significantly higher than the effect of 6-OHDA alone (13.6 ± 3.0, $p < 0.01$) (Fig. 2.7A). When the maximal time that a rat could hang on to a moving rotarod at a speed of 30 rpm was used as the indicator, similar results were obtained. Specifically, the maximal time for control and sham treated animals was 174.9 ± 8.3 and 165 ± 13.4 s respectively. 6-OHDA administration reduced this value to 70.9 ± 10.7 s ($p < 0.001$). Hydralazine injection in 6-OHDA

treated rats resulted in a maximal time of 93.1 ± 17.9 s, which is significantly higher than the effect of 6-OHDA alone ($p < 0.05$) (Fig. 2.7B).

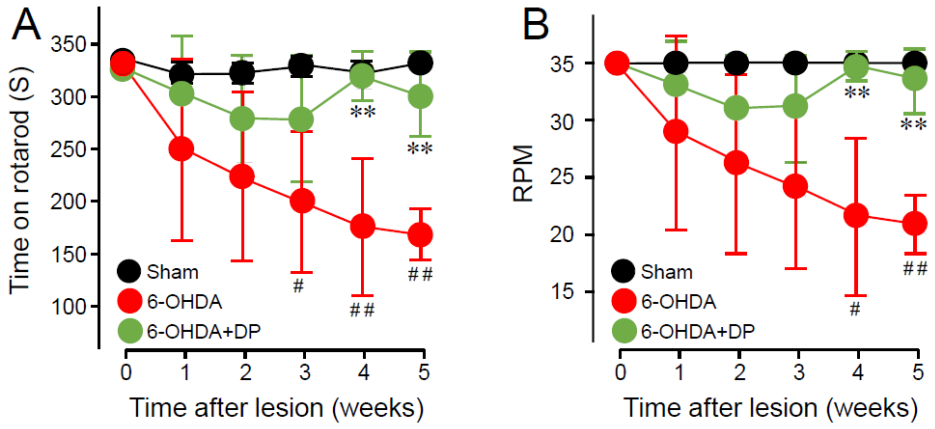

Figure 2.6. Mitigation of 6-OHDA-induced motor deficits by DP. The maximum time (A) and top speed (B) on the rotarod were examined every week for all groups. As shown, 6-OHDA-injured rats displayed a clear reduction of both measures when compared with sham rats. However, compared to 6-OHDA rats, a significant improvement in motor function was observed in 6-OHDA animals treated with DP, which was observed in both time (A) and RPM (B) on rotarod at 4 to 5 weeks after injury. DP was applied through daily IP injection at the dosage of 5 mg/kg for 5 weeks after injury. (*P<0.05, **P<0.01, compared to 6-OHDA group. #P<0.05, ##P<0.01, compared to sham group. ANOVA). Data were expressed as mean ± SD. N = 5 in all groups.

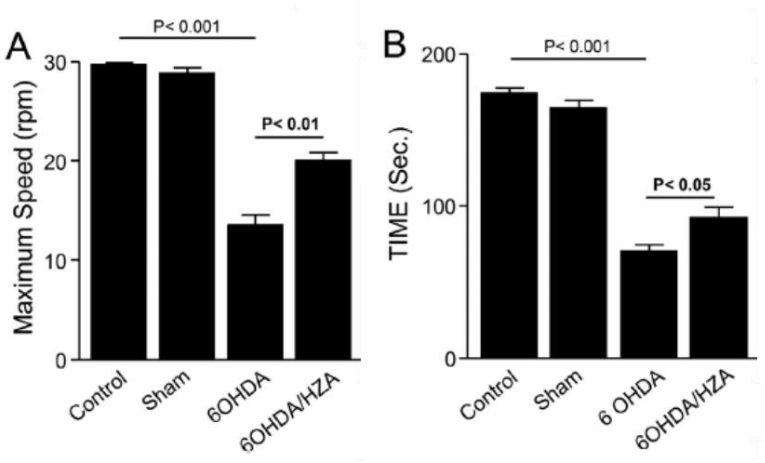

Figure 2.7. Quantitative behavioral analysis based on the rotarod test. The top speed (A) and maximum time (B) on the rotarod were examined for control, sham, 6-OHDA-injected, and 6-OHDA-injected/hydralazine-treated (HZA) groups. The sham animals did not differ from the uninjured control rats with respect to top speed and maximum time. 6-OHDA injection caused a significant decrease in performance on the rotarod test, both in terms of top speed (A, $p < 0.001$) and maximum time (B, $p < 0.001$). However, this impairment was partially restored by hydralazine treatment ($p < 0.01$ and $p < 0.05$ in A and B, respectively). ANOVA was used in all statistical comparisons. All data are expressed as the mean ± SEM, N=4–6.

2.3.5 In-Vitro validation of increased cell survival after acrolein exposure when co-treated with dimercaprol or hydralazine

We examined the potential neuroprotective effects of DP on acrolein-mediated cell death at a concentration of 100 μM. The administration of DP, applied 15 min after initial acrolein exposure, at concentrations of 10, 50, 100, 200μM, increased the cell viability to 55 ± 5.5% ($P>0.05$), 76 ± 2.8% ($P<0.01$), 94 ± 17.6% ($P<0.05$), 90 ± 17.7% ($P<0.05$) when compared to acrolein only. But likely due to the DP toxicity, 500 μM of DP only increased the cell viability to 57 ± 4.2% ($P>0.05$), which is not significant compared to acrolein only (Fig. 2.8A).

Alternatively, using hydralazine and the MES23.5 dopaminergic cell line, we have found that 6-OHDA reduced cell survival (48 ± 6%) which was significant compared to control (100%, $p < 0.001$) (Fig. 2.9A). The addition of hydralazine (applied 15 min after the incubation of 6-OHDA) can enhance cell viability to 71 ± 1% ($p < 0.01$, n=9 in all conditions).

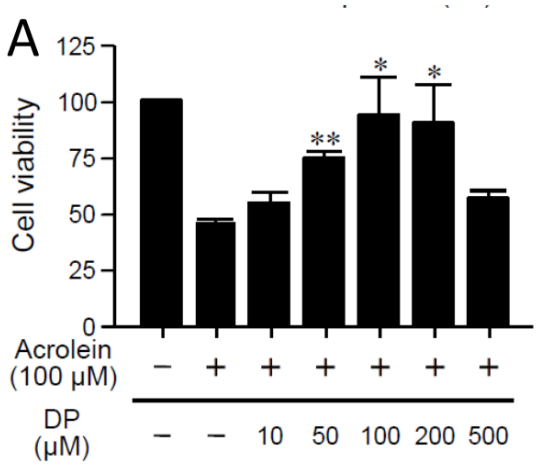

Figure 2.8. Alleviation of acrolein-induced SK-N-SH cell death by DP. SK-N-SH cells were exposed to different concentrations of acrolein for 4hrs which induced a dose dependent cell viability death, based on MTT test (A). When acrolein was used at a concentration of 100 μM, the addition of DP at various concentrations could result in significant reduction of acrolein mediated cell death. *p<0.05, **p<0.01, mean ± SEM. n = 4 each group.

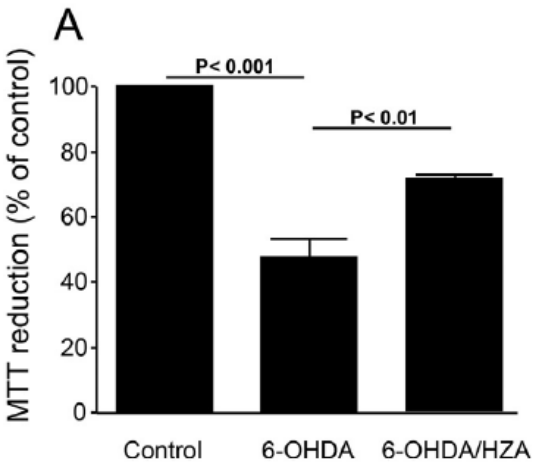

Figure 2.9. Mitigation of 6-OHDA-mediated MES23.5 dopaminergic cell death by hydralazine. Cells were incubated with 400 μM 6-OHDA for 2 h (6-OHDA group), and some cells were treated with 500 μM hydralazine after a 15-min delay (6-OHDA/HZA). Cell viability was determined by absorbance of the MTT reduction product at 550 nm and expressed as percent of control (A). ($p < 0.01$and $p < 0.001$, ANOVA). All data are expressed as the mean ± SEM, N=9–14.

2.4 Discussion

Parkinson's disease (PD) is hallmarked by oxidative stress, acrolein increase, and cell death of critical dopaminergic cells (13, 14). Here, we used two FDA approved medications for heavy metal toxicity (Dimercaprol, DP), or for hypertension (Hydralazine, HZA). Interestingly, these medications are both shown to be effective acrolein scavengers (9, 15). DP and HZA are safe for use in humans and could therefore have and accelerated path to use in other conditions, such as PD.

Here we look at these drugs in a 6-OHDA injection model of PD. First, and importantly, we find that acrolein is significantly increased in this model in both striatum and substantia nigra (Fig. 2.1). Next we administered through IP injection, in two separate experiments, either DP or HZA and examined benefits on cellular survival *in vivo* and *in vitro*, as well as any benefits to behavioral outcome (locomotor). Specifically, we found that DP and HZA significantly raise levels of TH+ cells, a marker for dopaminergic cells, in 6-OHDA rats (Figs. 2.2 & 2.3). Next, both DP and HZA improved locomotor, in both activity box and rotarod tests (Figs. 2.4 – 2.7). Finally, as an additional mechanistic validation, we tested DP or HZA using dopaminergic cell lines. We have seen prior that aldehyde scavengers can protect PC12 cells from acrolein exposure (9, 15, 16), and here show that similar strategies also protect dopaminergic cells (Fig. 2.8).

6-OHDA is a receptor mediated toxin, binding selectively to TH+ cells. In our *in-vivo* and *in-vitro* experiments, some cell death and development of PD symptoms will not be prevented in this model by aldehyde scavengers. However, because PD development and 6-OHDA generates a significant amount of neurotoxic acrolein, we hypothesize that acrolein may exacerbate the pathologies of PD. By alleviating the secondary injury progression in PD, we show significant cell survival and behavioral recovery by using HZA or DP. Another major hallmark of PD is accumulation of alpha-synuclein. Although not detailed here, our lab has demonstrated that acrolein can directly alpha-synuclein aggregation. When combined with acrolein *in-vitro*, purified alpha-synuclein proteins will aggregate (12, 16). Further, direct injection of acrolein into the rat brain significantly increases alpha-synuclein protein levels (16). Other groups report similar findings of acrolein injection and alpha-synuclein aggregation/increased concentrations in the rat brain (14, 17). Limitations of the study include the use of traditional dimercaprol instead of newer modified version Dimercaptosuccinic acid. Further, the use of 6-OHDA provides limitations as this model mimics an early-to-mid stage of PD, but not later stages when Lewy bodies are present.

Acrolein clearance is a growing strategy for prevention of alpha-synuclein aggregation. We detail here the benefits of acrolein scavenging in a model of PD. Future studies will examine the effects of alternative acrolein scavengers, which may have enhanced benefits. Furthermore, neurotrauma causes increased acrolein and alpha-synuclein aggregation, which is a likely link to the development of PD after neurotrauma (12, 18). Therefore, future studies will also investigate if similar acrolein removal strategies can prevent the development of PD after CNS injury.

2.5 Acknowledgments

Much of this work is published with permission to reprint. Seth Herr is a co-author and contributed collaboratively to data collection, study design, and manuscript writing. This work was supported by the Indiana State Department of Health (Grant # 204200 to RS), National Institutes of Health (R01 grant #NS073636 to RS, and R01 grant # NS049221 to J.-C. R.). This publication was also made possible by the Stark Neurosciences Research Institute, Eli Lilly and Company, and by the Indiana Clinical and Translational Sciences Institute, funded in part by grant #UL1TR001108 from the National Institutes of Health, National Center for Advancing Translational Sciences.

2.6 References

1. Przedborski S. Pathogenesis of nigral cell death in Parkinson's disease. Parkinsonism Relat Disord. 2005;11 Suppl 1:S3-7.

2. Henchcliffe C, Beal MF. Mitochondrial biology and oxidative stress in Parkinson disease pathogenesis. Nature Clinical Practice Neurology. 2008;4(11).

3. Jenner P. Oxidative stress in Parkinson's disease. Annals of neurology. 2003;53(S3):S26-S38.

4. Imam SZ, Trickler W, Kimura S, Binienda ZK, Paule MG, Slikker W, Jr., et al. Neuroprotective efficacy of a new brain-penetrating C-Abl inhibitor in a murine Parkinson's disease model. PLoS One. 2013;8(5):e65129.

5. Luo J, Shi R. Acrolein induces axolemmal disruption, oxidative stress, and mitochondrial impairment in spinal cord tissue. Neurochem Int. 2004;44(7):475-86.

6. Luo J, Shi R. Acrolein induces oxidative stress in brain mitochondria. Neurochem Int. 2005;46(3):243-52.

7. Esterbauer H, Schaur RJ, Zollner H. Chemistry and biochemistry of 4-hydroxynonenal, malonaldehyde and related aldehydes. Free Radical Biology & Medicine. 1991;11(1):81-128.

8. Hamann K, Durkes A, Ouyang H, Uchida K, Pond A, Shi R. Critical role of acrolein in secondary injury following ex vivo spinal cord trauma. J Neurochem. 2008;107(3):712-21.

9. Park J, Zheng L, Marquis A, Walls M, Duerstock B, Pond A, et al. Neuroprotective role of hydralazine in rat spinal cord injury-attenuation of acrolein-mediated damage. J Neurochem. 2014;129(2):339-49.

10. Leung G, Sun W, Zheng L, Brookes S, Tully M, Shi R. Anti-acrolein treatment improves behavioral outcome and alleviates myelin damage in experimental autoimmune enchephalomyelitis mouse. Neuroscience. 2011;173:150-5.

11. Tully M, Tang J, Zheng L, Acosta G, Tian R, Hayward L, et al. Systemic Acrolein Elevations in Mice With Experimental Autoimmune Encephalomyelitis and Patients With Multiple Sclerosis. Front Neurol. 2018;9:420.

12. Acosta SA, Tajiri N, de la Pena I, Bastawrous M, Sanberg PR, Kaneko Y, et al. Alpha-synuclein as a pathological link between chronic traumatic brain injury and Parkinson's disease. J Cell Physiol. 2015;230(5):1024-32.

13. D. T. Dexter, C. J. Carter, F. R. Wells, F. Javoy-Agid, Y. Agid, A. Lees, et al. Basal Lipid Peroxidation in Substantia Nigra Is Increased in Parkinson’s Disease. J Neurochem. 1989;52(2).

14. Wang YT, Lin HC, Zhao WZ, Huang HJ, Lo YL, Wang HT, et al. Acrolein acts as a neurotoxin in the nigrostriatal dopaminergic system of rat: involvement of alpha-synuclein aggregation and programmed cell death. Sci Rep. 2017;7:45741.

15. Tian R, Shi R. Dimercaprol is an acrolein scavenger that mitigates acrolein-mediated PC-12 cells toxicity and reduces acrolein in rat following spinal cord injury. J Neurochem. 2017;141(5):708-20.

16. Ambaw A, Zheng L, Tambe MA, Strathearn KE, Acosta G, Hubers SA, et al. Acrolein-mediated neuronal cell death and alpha-synuclein aggregation: Implications for Parkinson's disease. Mol Cell Neurosci. 2018;88:70-82.

17. Shamoto-Nagai M, Maruyama W, Hashizume Y, Yoshida M, Osawa T, Riederer P, et al. In parkinsonian substantia nigra, alpha-synuclein is modified by acrolein, a lipid-peroxidation product, and accumulates in the dopamine neurons with inhibition of proteasome activity. J Neural Transm (Vienna). 2007;114(12):1559-67.

18. Uryu K, Giasson BI, Longhi L, Martinez D, Murray I, Conte V, et al. Age-dependent synuclein pathology following traumatic brain injury in mice. Experimental neurology. 2003;184(1):214-24.

CHAPTER 3. CRITICAL ROLE OF MITOCHONDRIAL ALDEHYDE DEHYDROGENASE 2 (ALDH2) IN ACROLEIN SEQUESTERING IN RAT SPINAL CORD INJURY

3.1 Introduction

It is well-established that the most severe damage resulting from spinal cord injury (SCI) does not occur immediately after physical impact. Rather, mechanical insult induces a cascade of secondary biochemical reactions that exacerbate the initial effects of trauma and spread throughout the cord. Oxidative stress and lipid peroxidation-derived aldehydes have emerged as key culprits in sustaining such secondary injury, and contributing significantly to the pathological outcomes (1-5). Aldehydes, represented by acrolein as the most reactive aldehyde, are capable of directly adducting proteins, lipids, and DNA, and are known to cause significant damage to key cellular organelles (6-9).

We have provided extensive evidence that acrolein plays a particularly damaging role in perpetuating oxidative stress, causing cellular degeneration and functional loss in SCI (1-5). We have also shown that, as both a product and catalyst for lipid peroxidation, acrolein induces a vicious cycle of oxidative stress, amplifying and continuously propagating degeneration in SCI (1-5). Further, while acrolein reduction can effectively mitigate neuronal damage, injecting acrolein produced pathologies reflecting those observed in SCI (10). These studies support the notion that acrolein is not only sufficient, but necessary to instigate neurodegeneration post-SCI. As such, lowering acrolein has emerged as a novel and effective therapeutic strategy in SCI (4). However, while the application of exogenous aldehyde scavengers has led to significant benefits, many have unwanted side effects as they are FDA approved for other conditions (5, 11). Therefore, a need remains for exploring alternatives with minimal side effects, before further clinical application is considered.

Mitochondrial aldehyde dehydrogenase-2 (ALDH2) is an oxidoreductase, effective at removing aldehydes in the brain and spinal cord (12-14). Despite its well-recognized role in aldehyde removal, ALDH2 remains largely under-studied in SCI. Relevantly, recently discovered ALDH2-selective activator, Alda-1, can catalyze ALDH2 enzymatic activities by multiple folds in rodents and *in vitro* (15, 16). This offers a uniquely promising opportunity to test our hypothesis,

solidifying this enzyme as a therapeutic target to suppress aldehydes while also further illuminating the role of ALDH2 in SCI.

Here we demonstrate that the expression of ALDH2 was indeed suppressed in the event of SCI, and that SCI caused increased ALDH2-acrolein adduct formation, suggesting augmented acrolein binding to ALDH2 due to acrolein accumulation. In addition, Alda-1 application worked to significantly lower acrolein and preserve SCI tissue. Finally, *in vitro* data suggests that an ALDH2 inhibitor, disulfiram, can worsen acrolein-induced cell death while Alda-1 can mitigate it (17). These data provide the initial evidence that ALDH2 is a key enzyme critical to post-SCI acrolein accumulation and related tissue damage, as well as a potential therapeutic target.

3.2 Materials and Methods

3.2.1 Animals and Injury model

Young male Sprague Dawley rats weighing 200-240grams were purchased from Envigo (Indianapolis, IN). They were kept on standard light/dark cycles and fed with chow diet. Rats were fully anesthetized before spinal cord surgery. For all the surgeries, a laminectomy was first conducted at T10. Following the exposure of spinal cord tissue, rats were given a contusion injury, using a New York University (NYU) weight drop impact device at a moderate setting (height of 25mm and weight of 10g). Rats health was carefully monitored post-surgery. The general procedures used this study are well-established and are similar to prior publications from this group (5, 11).

3.2.2 Treatments

Aged matched healthy rats were used as controls. Alda-1 was purchased from ApexBio (Houston, TX) and dissolved in 50% DMSO, 50% peg400 as described by others (13). Injury rats were given either a vehicle with no Alda-1 (vehicle control), or Alda-1 at 15mg/kg, administered by intraperitoneal injection (IP). Alda-1 has been shown to effectively enter the central nervous system through this administration technique (13, 18). Treatment was administered every two hours post-surgery for a total of 2 doses, twice on the following day (morning and evening), and once in the morning on day 2 and once an hour before sacrifice (48hour acute timepoint, 6 total doses of Alda-1). Rats were sacrificed by intracardial perfusion with chilled phosphate-buffered

saline (PBS). All animal work was done in accordance with approved protocol by Purdue Animal Care and Use Committee.

3.2.3 Co-Immunoprecipitation

Immunoprecipitation of the spinal cord for each experimental group was done according to instructions from the Pierce Classic IP Kit (ThermoFisher, #26146), and as described previously by our group (19). In short, 2mg/mL protein lysate from each sample group was pre-cleared using the control agarose resin. The lysate (2 mg protein) was incubated with anti-ALDH2 (50 kDa, Santa Cruz) or anti-acrolein-lysine (Abcam) at 4°C overnight to form the immune complex. 20 μL of Pierce A/G Agarose was added into the mixture to capture the immune complex and incubated at 4°C for 1 hour. The elution of the immune complex was carried out using the 2x non-reducing lane marker sample buffer and DTT. The collection tubes were boiled in a water bath for 5 min and eluates were applied to 15% SDS-PAGE for immunoblotting with anti-ALDH2 and imaged using Azure c300 Western blot imaging system (Azure Biosystems, Dublin, CA).

3.2.4 Western blot

After sacrifice, spinal cord tissue was dissected and frozen -80°C. Tissue was homogenized with 1xRIPA buffer and Protease inhibitor cocktail, then centrifuged at 14,000RPM for 30minutes. Supernatant was collected, and protein concentrations were measured using the Bicinochoninic Acid protein assay kit (Pierce, Rockford, IL, USA) and SPECTRAmax plate reader (Molecular Devices, Sunnyvale, CA). Thirty micrograms of protein with 20% Sodium dodecyl sulfate, β-mercaptoethanol, and 2x Laemmli buffer were loaded to a 15% Tris-HCL gels and electrophoresed at 80 volts for 2-3 hours. Proteins were then transferred to a nitrocellulose membrane by electro blotting on ice in 70 volts for 1 hour in 1x transfer buffer with 20% methanol (Tris-Glycine buffer from BioRad, Hercules). The membrane was blocked in 1x casein (Vector, #SP-5020) at room temperature for 10 minutes, and immunolabeled overnight at 4°C with one of these primary antibodies, anti-acrolein-lysine (Abcam), anti-ALDH2 (50kDa, ThermoFisher), anti-Beta-Actin (45kDa, BioLegend). After overnight incubation, the membranes were further incubated with either biotinylated anti-mouse or anti-rabbit secondary antibody (Vector, #BA-2000, #BA-1000) at room temperature for 45 minutes, and signal amplified with an ABC-AmP kit for 10 minutes

(Vector, AK-6000). All washes were done with 1x casein. The DuoLux substrate (Vector, #SK-6605) immunodetection kit was used for chemiluminescent signal acquisition and the Azure c300 Western blot imaging system (Azure Biosystems, Dublin, CA) was used to image the membrane. The AlphaView software (Protein Simple, San Jose, CA) was used to quantify the relative signal for each band. Data is normalized with Beta-Actin.

3.2.5 Immunohistochemistry

Cord tissue was collected after perfusion and immediately fixed in cold 4% formaldehyde in 1xPBS, for a maximum of 48 hours. Tissue was then cryoprotected in 30% sucrose, and frozen in OTC using acetone and dry ice slurry and sliced into transverse sections with a cryotome (Leica) at 25 uM thickness. Sections were stored in 0.01% Sodium Azide and PBS at 4℃, until staining of T10 epicenter tissue. Staining was done using separate techniques for revealing acrolein, or tissue structure. For acrolein, sections were immunostained with anti-acrolein-lysine (Abcam) followed by biotinylated secondary antibodies (Vector Laboratories), incubated in ABC avidin/biotin complex solution (Thermo Scientific™, #32020) and developed using the DAB Peroxidase (HRP) Substrate Kit, 3,3′-diaminobenzidine (Pierce™ DAB Substrate Kit). Images were taken using a standard light microscope. For revealing tissue structure, Crystal Violet (Nissl) and Eosin Y counterstains were done, as previously described by our group (10). Quantification was done using standard techniques for area measurement on ImageJ software. Cyst is expressed as a percentage of total slice area.

3.2.6 Cell viability assay

PC12 cells were obtained from American Type Culture Collection (ATCC) and grown in Dulbecco's modified Eagle's medium (DMEM; Invitrogen, La Jolla, CA) supplemented with 12.5% horse serum, 2.5% fetal bovine serum, and 1% penicillin. The incubator was set at 5% CO2 at 37°C. Culture media were changed every other day, and cells were split every week.

Acrolein was prepared at 50mM in PBS as stock solution and diluted to the final concentration (100 μM) in medium upon use. Alda-1 was dissolved at 20 mM in DMSO as stock solutions and diluted to the desired concentration in medium. ALDH2 inhibitor disulfiram was dissolved in cell medium to predetermined concentrations. PC12 cells were plated in 96-well plates.

After incubating for 24 hours, acrolein (500 μM) was added into each well of acrolein group and treatment groups. Equal volumes of medium were added into wells of the negative control group. After incubation for 15 minutes, alda-1 (25 μM) or Disulfiram (1 or 5 μM) was added at the desired final concentrations into wells and equal volume of medium was added into other wells. After incubating 2hr, cell viability was measured by Cell Counting Kit-8 (CCK-8) system according to the instruction provided by the manufacturer (Dojindo, Japan). Briefly, CCK-8 solution (10μL per 100μL of medium in each well) was added, and the plates were then incubated at 37℃ for 2 hours. The absorbance of each well was read at 450 nm using a microplate reader SPECTRAmax (Molecular Devices, Sunnyvale, CA).

3.2.7 LC/MS/MS

T10 spinal cord sections were dissected after a final dose of Alda-1, 48 hours after injury. Cords were sonicated and centrifuged as described in *western blot* section. For LC/MS/MS, 30 μL were taken from representative samples, and processed for LC/MS/MS as described by (20), with a few modifications: here an XBridge (C8, 3.5 μm, 2.1 x 100 mm) column was used, and analyzed on an Agilent 6460 QQQ. Further, retention times were slightly modified to complement our experimental settings, with software set to look specifically for peaks at 134.9 and 77.1, and a retention time of approximately 2 minutes. Peak area integration was done by manually selecting the peak using the integration tool on Agilent software.

3.2.8 Transgenic mice and injury model

Male transgenic mice breeders, homozygous for knock-in human mutant nonfunctioning ALDH2 (*ALDH2**2), were donated from Dr. Che-Hong Chen at Stanford University. Upon arrival mice were rederived by the Purdue Transgenic and Genome Editing Facility, in order to comply with University pathogen standards. Rederiving was done by pairing *ALDH2*2* studs with WT females, and transplanting the embryos to pathogen free, surrogate WT mothers. After rederiving, new mice generations were self-crossed until the desired homozygous *ALDH2*2* genotype was found. Genotyping was done by tail snip and samples sent to *Transnetyx Inc* for automated PCR sequencing. Using this strategy, homozygous mice were selected and again self-crossed until only

homozygous progeny are born. After final confirmation of desired genotypes, mice will be tested annually to ensure desired genotypes are still present.

For SCI experiments, comparable C57BL/6 WT mice are purchased from *Envigo*. Because the NYU impactor is only suitable for rats, for the mice, an Infinite Horizon Impactor (Precision Systems and Instrumentation, LLC) was used and set to 75 kDyne impact force (moderate contusion injury). Injury was done similarly at T10 cord region, after anesthesia by half dose of ketamine/xylazine cocktail and constant 4% isoflurane/O2. After surgery and sacrifice at either 48 hour or 7 day timepoint, tissue was processed using the Immunohistochemistry protocol described above.

3.2.9 Statistics

All data are presented as mean ± standard error of the mean (SEM). One way ANOVA with Tukey or Fisher post hoc and Student's t test were used for statistical assessment where necessary (JMP 13 Software). Two way ANOVA was done in PRISM. The statistical significance threshold was set at $p < 0.05$.

3.3 Results

3.3.1 Evaluation of ALDH2 expression levels

We first tested the hypothesis that the protein expression level of ALDH2 is reduced in SCI, a situation known to have elevated levels of acrolein. As shown in Fig. 3.1, Western blot analysis shows a significant decrease in ALDH2 expression when examined 2 days following a contusive spinal cord injury (76% of control). Such reduction is significant when compared with control ($p < 0.05$, ANOVA). Treatment of Alda-1, an ALDH2 stimulator, resulted in a trend of recovery of ALDH2 (84% of control) when compared to that in SCI (Fig. 3.1). Representative IHC images are shown on the right side of figure 3.1.

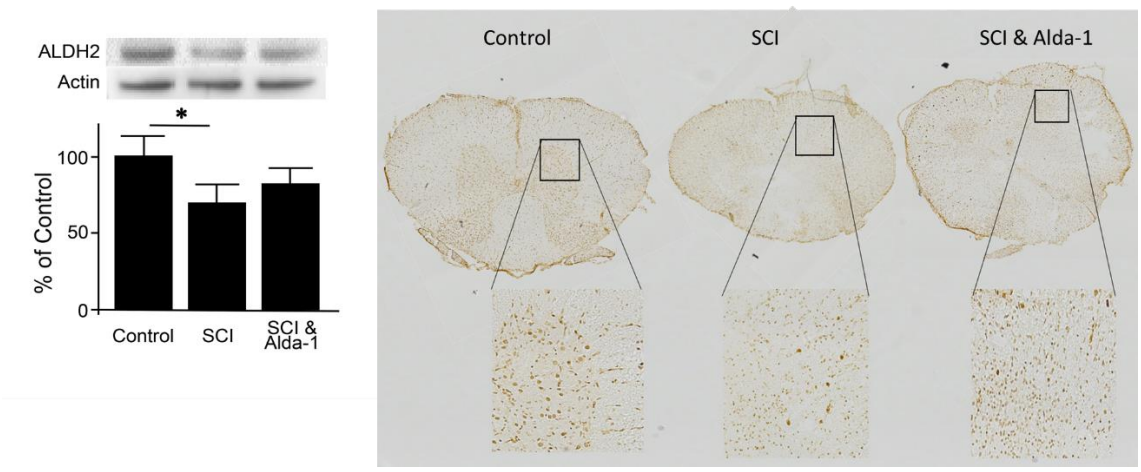

Figure 3.1. Reduction of ALDH2 levels post SCI and its influence by Alda-1. The expression levels of ALDH2 were analyzed by western blot in three groups. Groups were divided into "Control" for uninjured rats, "SCI" for injured rats given vehicle injection, or "SCI & Alda-1," injured rats given 15mg/kg doses of Alda-1 until sacrifice at 48 hours acute timepoint (total 6 doses). Top: representative ALDH2 bands (50kDa) are shown above corresponding Actin bands (45kDa). Bottom: Data is normalized to Actin and graphed below, showing change as a percent of control. Note the ALDH2 level was suppressed post-SCI (76% of control) which is significantly lower than control ($P < 0.05$). However, in the group of "SCI+Alda-1", the application of Alda-1 resulted in a trend of recovery of ALDH2 (84% of control) when compared to that in SCI. n = 8-9 for "Control", "SCI", and "SCI+Alda-1". *$p < 0.05$. Representative ALDH2 histology images are shown on the right, with zoom in box showing staining in white and grey matter. Histology was done using DAB and ALDH2 is shown by brown color.

3.3.2 Acrolein adduct formation with ALDH2

Aldehydes are highly reactive compounds and capable of adducting to proteins, such as ALDH2. In fact, at high concentrations, aldehydes are known to inhibit ALDH2, likely by this mechanism (21-25). As such, we then examined the possibility that the binding of acrolein to ALDH2, a likely step of acrolein-induced ALDH2 inhibition, is elevated in SCI, using a co-immunoprecipitation (Co-IP) technique. As indicated in Fig. 3.2, we performed a Co-IP using spinal cord tissue in three conditions, Control, SCI, and SCI & Alda-1. Anti-ALDH2 was used to stain all lanes. Indicated in Fig. 3.2, ALDH2 precipitated at 50kDa as expected (ALDH2 IP lane). Arrows indicate that acrolein-bound ALDH2 is present in both injury and Alda-1 treated groups. Some background from beads was observed but does not interfere with the 50kDa ALDH2 bands. Confirmation of successful acrolein IP is further shown in supplementary information (Supp. Fig. 3.1).

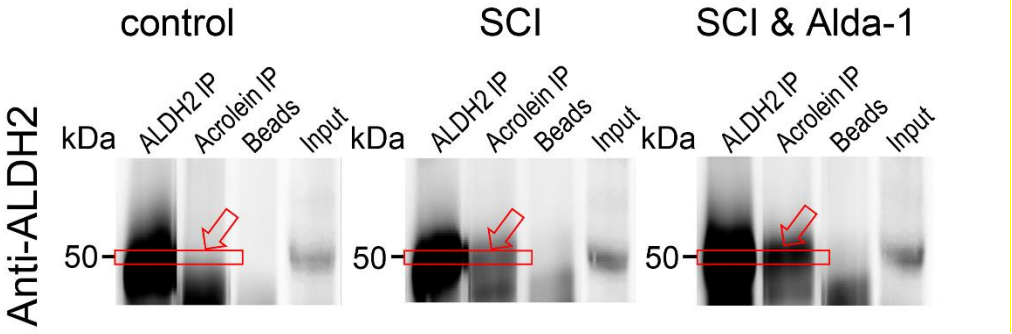

Figure 3.2. Co-Immunoprecipitation indicating Acrolein-bound-ALDH2 in vivo after SCI. Figure is imaged using Anti-ALDH2 antibody. All lanes are consistent for sham "Control" uninjured rats, "SCI" for injured rats given vehicle injection, or "SCI+Alda-1," injured rats given 15mg/kg doses of Alda-1 until sacrifice at 48 hours acute timepoint (total 6 doses). Spinal cord lysates from control, SCI, and SCI+Alda-1 rats were homogenized and immunoprecipitated with ALDH2 or acrolein-lysine antibodies. Then, samples were subjected to SDS-PAGE and immunoblotting detection using anti-ALDH2 to complete the co-immunoprecipitation procedure. "ALDH2 IP" lane shows successful precipitation of the enzyme in all conditions. "Acrolein IP" indicates whether or not ALDH2 positive staining is observed in the Acrolein IP pulldown using anti-acrolein-lysine adduct antibody. Staining indicates acrolein-bound-ALDH2 at 50kDa, outlined by red boxes, with arrows highlighting ALDH2 staining in the acrolein pulldown lane, indicating binding of acrolein to ALDH2. Note that the anti-ALDH2 staining in Acrolein IP lane is mild in control condition. However, such staining is intensified in both SCI and SCI & Alda-1 condition, suggested an augmented binding of acrolein and ALDH2 (arrows). "Beads" lane shows some background from IP beads, but at an irrelevant kDa. "Input" shows presence of ALDH2 in each sample, without immunoprecipitation.

3.3.3 Evaluation of acrolein expression levels

Since acrolein is known to increase in SCI, and ALDH2 can metabolize acrolein to lesser toxic metabolites, we then tested the hypothesis that post-SCI elevated acrolein can be mitigated by the application of Alda-1 using both Western blot and immunohistochemical (IHC) analysis. In Fig. 3.3A, Western blot analysis demonstrates a significant increase in acrolein after SCI (152% of control) when compared to control ($p < 0.05$). However, such elevated acrolein levels can be significantly suppressed to 118% of control when injured animals were treated with Alda-1, which is significant when compared to SCI only ($p < 0.05$). Consistent with Western blot analysis, representative sections of spinal cord with DAB staining from Control, SCI, and SCI+Alda-1 groups reflect these findings. Specifically, acrolein level (brown color) is elevated following SCI, while Alda-1 could suppress post-SCI acrolein elevation. As such, the findings from both Western

blot and IHC staining suggest that ALDH2 enhancement could lower the post-SCI acrolein surge, indicative of a critical role of ALDH2 in post-SCI acrolein elevation (Fig. 3.3A-D).

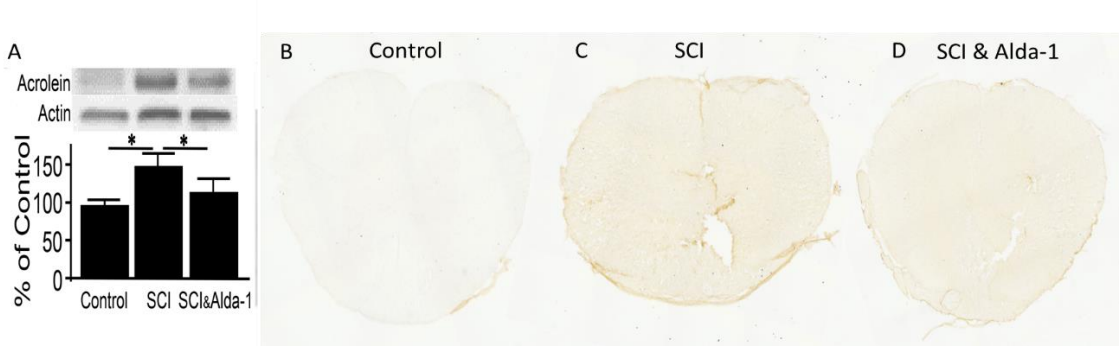

Figure 3.3. Analysis of Acrolein levels post SCI. Acrolein levels were analyzed by Western blot (A), with additional confirmation shown by IHC images (B-D). Groups were divided into "Control" for uninjured rats, "SCI" for injured rats given vehicle injection, or "SCI+Alda-1," injured rats given 15mg/kg doses of Alda-1 until sacrifice at 48 hours acute timepoint (total 6 doses). A) top: Acrolein bands (50kDa) are shown above corresponding Actin bands (45kDa). A) bottom: Data is normalized to Actin and graphed, showing change as a percent of control. Compared to control, the level of Acrolein-lysine adducts is significantly increased in the SCI group (100% vs 152%, $p < 0.05$). However, the application of Alda-1 significantly mitigated such increase shown in SCI & Alda-1 group when compared to SCI only group (118% vs 152%, $P < 0.05$). B-D): immunohistochemistry (IHC) images are from representative transverse spinal cord sections, using anti-acrolein-lysine antibody and DAB staining shows acrolein as a brown color. IHC groups are as follows: Control (B), SCI (C), and SCI+Alda-1 (D). Note the modest staining in control (B), while more acrolein staining is observed in SCI (C). Consistent with western blot analysis, Alda-1 treatment has resulted in lighter staining than that in the SCI-induced elevation of acrolein (D vs C). Western Blot: n=8 for "Control", "SCI", and "SCI+Alda-1" groups. IHC: n = 3-4 for "Control", "SCI", and "SCI+Alda-1" groups. *$p < 0.05$.

3.3.4 Evaluation of cyst formation

Acrolein is an established secondary injury mechanism known to cause severe structure damages. Furthermore, lowering the acrolein using acrolein scavengers could reduce spinal cord cyst, a common pathology observed after contusion injury, resulting from widespread cell death, and a key indication of post-SCI tissue destruction (5, 10). Therefore, we predicted that more effective ALDH2 could reduce acrolein and lead to reduced cyst area. As indicated in Fig. 3.4, no clear cyst is visible in control cord (Fig. 3.4A). However, SCI has resulted in conspicuous cyst formation in the injury site (Fig. 3.4B). Again, the application of Alda-1 significantly reduced the size of the cyst (Fig. 3.4C). Quantitative analysis revealed a significant decrease in cyst size with Alda-1 treatment when compared with SCI (Fig. 3.4D), ($p < 0.05$).

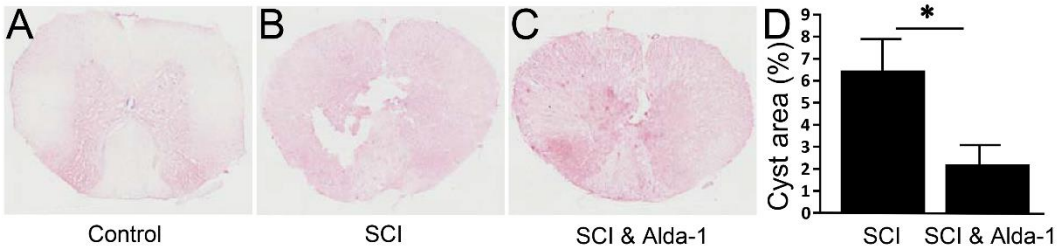

Figure 3.4. Alda-1 treatment reduces cyst formation in the spinal cord post injury. (A-C) Representative images of Crystal violet and Eosin co-staining of spinal cord tissue, with transverse sections indicating cyst formation, 48hours after injury, with or without Alda-1 treatment (total 6 doses). Control sections show no cyst formation (A), while large cysts could be discerned after injury (B). However, the treatment of Alda-1 in injured animals significantly reduced the size of the cyst (C). When the cyst size is expressed as the % of the total area of the transverse section, it is revealed that the cyst in SCI is significantly reduced with the treatment of Alda-1 (D) ($p < 0.05$). n = 3-4 for "Control", "SCI", and "SCI+Alda-1". *$p < 0.05$.

3.3.5 In Vitro analysis

Next, in order to further test the role of ALDH2 in influencing acrolein-mediated cell death, we used neuro-like PC-12 cell culture system to test the hypothesis that enhancing or suppressing ALDH2 activity is accompanied by intensification or reduction of cell survival in the presence of acrolein. As indicated in Fig. 3.5, while acrolein (500 µM) can lead to a significant reduction of cell viability (44% of control, $p < 0.01$), Alda-1 (25 µM) could significantly mitigate acrolein-mediated reduction of cell survival (65% of control, $p < 0.01$ when compared to acrolein only). Interestingly, while Disulfram, an ALDH2 inhibitor, had no significant effect on acrolein-mediated cell death at 1 µM, it can significantly worsen acrolein-mediated reduction of survival at 5 µM (10%) when compared to acrolein only ($p < 0.01$).

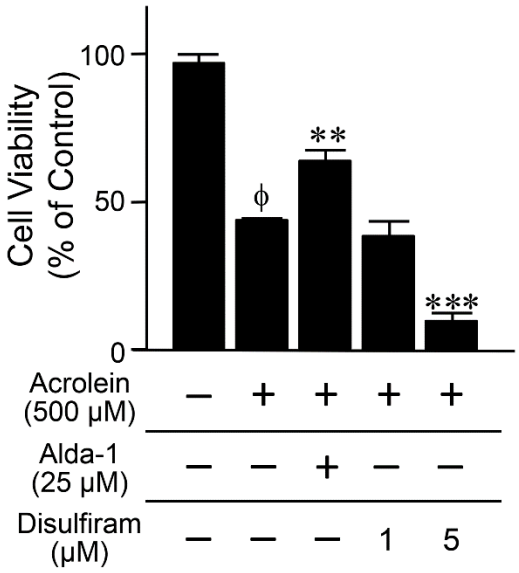

Figure 3.5. Role of ALDH2 in protecting PC12 cells from acrolein toxicity in vitro. Bar graph illustrates the cell viability of PC-12 cells in various conditions related to acrolein toxicity and its influence by the function of ALDH2. Cell viability is expressed as the % of the control. Note acrolein (500 μM) induced a significant reduction of cell viability (44%) when compared to control ($^{\phi}p < 0.001$). However, the application of Alda-1 (25 μM), an ALDH2 stimulator, resulted in an increase of cell viability in SCI to 65%, a significant increase from SCI only (**$p < 0.01$). Interestingly, disulfiram, an ALDH2 inhibitor, when applied at 5 μM, but not at 1 μM, significantly decreased the cell viability (10%), which is significant when compared to SCI only (***$p < 0.001$). Cell viability was determined 2 hours after incubation with various treatment conditions, involved with acrolein, disulfiram, or Alda-1. While Acrolein was applied in the beginning of the experiment, Alda-1 or Disulfiram was administered 15 minutes after the start of acrolein incubation.

3.3.6 Acrolein analysis in transgenic mice

Transgenic mice expressing nonfunctional ALDH2 (*ALDH2*2*), were used to further assess the role of ALDH2 in SCI. In Fig. 3.6, the expression of acrolein was measured by immunohistochemistry. In Fig. 3.6A, Transgenic ALDH2*2 mice (TG) did not show a significant increase when compared with wild type (WT), at two days post injury. Although not significant, there is a trend of higher acrolein in the TG mice. In Fig. 3.6B, acrolein levels are further evaluated in both the white matter and grey matter region of the spinal cords, at 7 days post injury. Dashed line represents control, and data graphed as average fold change from controls. Here, acrolein levels are significantly increased in both grey and white matter regions of the TG mice, when

compared with WT (***p < 0.001 and **p < 0.01, respectively), indicating an enhanced vulnerability of injured ALDH2*2 mice to acrolein surge.

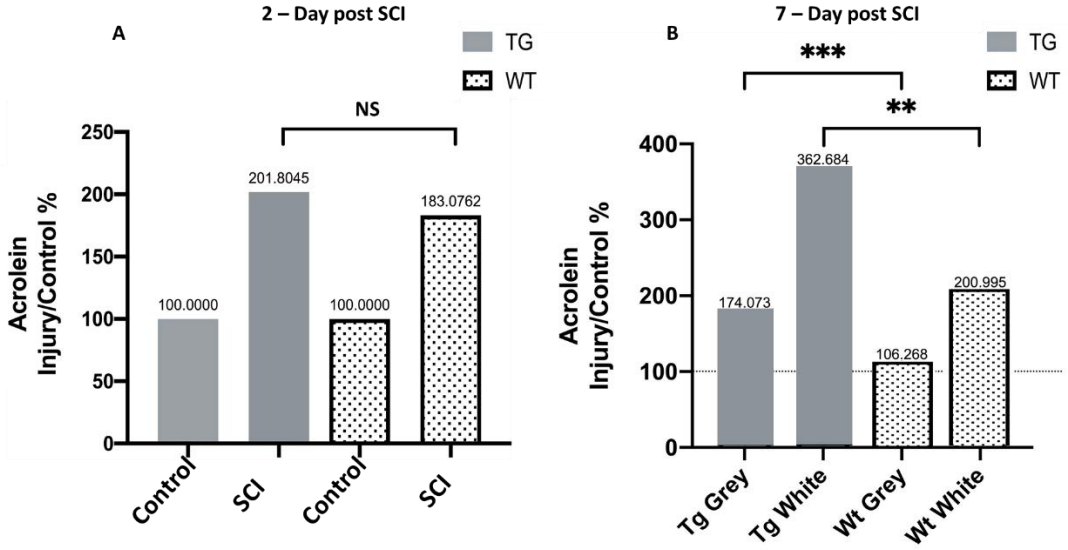

Figure 3.6. Effects of nonfunctional ALDH2 on acrolein levels post SCI in mice. Acrolein levels were determined by DAB immunohistochemistry. A) 2 days post spinal cord injury (SCI), there is a trend of higher acrolein in transgenic mice (TG, Grey bars) when compared to wild type (WT, spotted bars). However, the trend is not significant (NS). B), dashed line represents the baseline acrolein levels, and data graphed as average fold change for each group at 7 days post injury timepoint. Analysis examined both grey and white matter regions of the cord. A significant difference was found between TG Grey and WT Grey (***p < 0.001), and between TG White and WT White (***p < 0.001).

3.4 Discussion

There is strong evidence that acrolein, both a product and an instigator of oxidative stress, plays a critical pathogenic role in spinal cord injury (1-5). Furthermore, anti-acrolein measures have been demonstrated as effective neuroprotective strategies to benefit both motor and sensory functional recovery following SCI. While the utilization of acrolein scavengers as means to reduce acrolein and mitigate related pathologies have been investigated in great detail, other alternative anti-acrolein approaches have not attracted much attention in SCI (12). Aiming to broaden the spectrum of the acrolein sequestering strategy, and improve the effectives and potentially mitigate the inherent short falls of the existing acrolein scavengers, we have initiated an effort in searching for other methods of reducing acrolein. Specifically, in this investigation we have presented the initial evidence that ALDH2, an endogenous mitochondrial aldehyde metabolizing enzyme, is a

critical part of acrolein-mediated pathology and more importantly, a potential target for anti-acrolein pharmaceutical intervention in SCI.

We have shown that, while acrolein is elevated significantly, Alda-1, an enhancer of ALDH2, can significantly reduce acrolein accumulation post-SCI (Fig. 3.3), and enter the injury site of the spinal cord (supp. Fig. 3.2). As Alda-1 is not known to scavenge acrolein directly, but known to catalyze ALDH2 enzymatic activities, we attribute its acrolein reduction ability is by increased ALDH2 detoxification activity (15, 16). This finding not only underscores the importance of ALDH2 in acrolein removal, but suggests ALDH2 is an effective target to reduce acrolein. To further support such supposition, Alda-1 instigated acrolein reduction is associated with spinal cord damage reduction and tissue sparing post-SCI. These findings mirror the neuroprotective effects resulting from acrolein sequestering through externally applied aldehyde scavengers, such as hydralazine and phenelzine (3, 5, 6, 11).

It is well documented that acrolein is elevated significantly following SCI. So far, such elevation has mainly been attributed to the production of acrolein due to injury-induced oxidative stress and lipid peroxidation (26, 27). In the current study, however, we have also found that the expression of ALDH2 is significantly reduced in SCI. It is known that ALDH2 plays a critical role in preventing aldehyde accumulation and disease onset (12). Therefore, a significant reduction of ALDH2 will inevitably lead to an elevation of acrolein in SCI (14). Our findings suggest that in the event of SCI and acrolein elevation, the degradation of ALDH2 further contributes to the accumulation of acrolein.

It is known that acrolein is capable of inhibiting ALDH2, particularly when acrolein concentrations are high (21-25). Although we did not examine the catalytic activity of ALDH2 in the current study, the likelihood of ALDH2 inhibition by acrolein post-SCI is high, as acrolein is known to surge overwhelmingly post-SCI. It is possible that such inhibition also leads to the reduction of ALDH2 expression seen in this study, resulting from heightened degradation of ALDH2. This is based on the evidence that Alda-1, known to disinhibit ALDH2, induced a tendency of augmenting expression of ALDH2 in the presence of acrolein (Fig. 3.1). Taken together, we propose that while both the reduction of ALDH2 expression and functional inhibition contributes to acrolein surge, the application of Alda-1 can enhance the function of ALDH2 by mitigating both deficits, and thus reducing acrolein.

The exact mechanism of acrolein-mediated ALDH2 inhibition is not clear. However, it is generally believed that the inhibitory site (through acrolein binding) and activation side (through Alda-1 binding) are two separate, yet related structures of ALDH2. Interestingly, structural analysis revealed that the binding of Alda-1 to the active site not only facilitates the aldehyde detoxifying, but also hinders aldehydes' access to the inhibitory site and protects ALDH2 from adduct formation (15). This again is consistent with our hypothesis that Alda-1-mediated ALDH2 activity enhancement is likely through at least two mechanisms, enhancing its catalytic acrolein-detoxification activity, and protecting the enzyme from acrolein.

Another interesting phenomenon is the dynamics of acrolein binding to the lysine residue of ALDH2 in various conditions we observed through immunoprecipitation, using antibodies against ALDH2 and acrolein-lysine adducts. Specifically, we have observed that the binding of acrolein to the lysine residue of ALDH2 is elevated in SCI which is expected due to acrolein elevation. However, such binding level appeared to be further augmented when Alda-1 was applied post-SCI (Figure 2 SCI+Alda-1). The exact mechanism of such enhanced level of acrolein-lysine binding in this situation is not clear. One possible explanation for this is that Alda-1-mediated disinhibition of ALDH2 leads to lesser degradation (Fig. 3.1), and thereby higher expression of ALDH2, leading to elevated levels of acrolein-lysine adduct in the co-IP.

In addition to in vivo examination, we also tested the ability of ALDH2 to mitigate acrolein-mediated cell death directly in PC-12 cells which are known to express ALDH2 (28). Specifically, we demonstrated the anti-acrolein ability of ALDH2 in PC12 cells by turning up or turning down the activity of ALDH2 and observing the subsequent cell viability changes in the presence of acrolein. As expected, enhancement of ALDH2 by Alda-1 mitigated cell death while suppressing ALDH2 worsened cell death in the presence of acrolein. This finding is consistent with a previous study where a genetically induced deficiency in ALDH2 in PC-12 cells increased the vulnerability to 4-hydroxy-2-nonenal (HNE), a reactive aldehyde similar to acrolein. These in vitro data from ours and others, have provided strong evidence which supports and complements the in vivo date to indicate that ALDH2 functions as a protector against aldehydes and oxidative stress (29).

In addition to serving as a critical agent to demonstrate the key role of ALDH2 in acrolein removal, Alda-1 may also be a strong candidate for translational purposes. For example, Alda-1 is readily bioavailable when given systemically, and is capable of crossing the blood brain barrier

with no obvious side effects, as observed in animal studies, and confirmed here (18, 30-34)(supp. Fig. 3.2). Therefore, Alda-1 may have the potential to be developed for clinical usage.

Interestingly, individuals with ALDH2 mutations (ALDH2**2*) that nullifies its aldehyde detoxification capabilities, have a significantly higher risk of developing of certain cancers (35, 36), cardiovascular diseases (37, 38), and neurodegenerative diseases such as Alzheimer's and Parkinson's (39-42), all shown to be attributed to higher aldehyde accumulation. This evidence suggests that ALDH2 is likely important for protecting neurons from aldehydes, especially during situations of aldehyde upregulation such as SCI. Not only will compromised ALDH2 lead to more aldehydes (43), but high concentrations of aldehydes can inhibit ALDH2 (25, 44), leading to a vicious cycle of escalating aldehyde accumulation (12). Despite the demonstrated burden of aldehydes, the role of ALDH2 has never been investigated in SCI injury. A recently established ALDH2**2* transgenic (TG) mouse line has enabled us to not only illuminate the critical role of this enzyme in rodent SCI, but also do so in a clinically relevant situation as this is a mutation most common in Asians and found in nearly 8% of the world's population (12, 45). Here, we use such clinically relevant TG mice to further examine the role of ALDH2 after SCI. While the levels of acrolein in TG injured mice were not significantly elevated at 2-days post injury (dpi) compared to WT injured mice, there was a trend of increased acrolein in these mice. Interestingly, this could be due to the low levels of ALDH2 or likely ALDH2 inhibition by acrolein in WT animals (Figs. 3.1 & 3.2). In other words, the low levels of ALDH2, along with potential inhibition by acrolein, leads to increased acrolein concentrations in WT, as if the enzyme is nonfunctional (no significant difference from injured TG vs. injured WT at 2-dpi). Looking further, at 7-dpi acrolein levels are significantly elevated in both white and grey matter of the TG compared to WT. This suggests that in the WT mice, the remaining ALDH2 after injury, over the course of 7 days is likely able to slowly remove acrolein, or, increase the production of more functioning ALDH2. Alternatively, in the TG any increased production of ALDH2**2 or any ALDH2**2 that remains after injury, will have no beneficial effect, and at 7-dpi acrolein levels thus remain elevated. Further experiments examining the expression levels/activity of ALDH2 over the course of 7 days are warranted further confirm theory. However, the surge of acrolein in the WT mice, low levels of ALDH2, and persistence of acrolein surges in TG mice further highlights the need for enhancing ALDH2 after SCI. Remarkably, Alda-1 is capable of restoring ALDH2**2 back to WT activity levels, which will also be examined in future studies with these TG mice.

Despite the probable effectiveness and translational potential of Alda-1, the primary purpose and significance of our finding is to demonstrate the utility of ALDH2 activator and protector as a new and effective strategy to combat acrolein toxicity. This would establish a novel pharmacophore, guiding the development of a new class of ALDH2-focused anti-acrolein drugs for treating SCI with high efficacy. Once established, ALDH2-targated anti-acrolein therapies may not just be treating SCI victims, but could also benefit patients with other conditions where acrolein is implicated, such as traumatic brain injury, Parkinson's diseases, Alzheimer's diseases, multiple sclerosis, Neuropathic pain, cardiovascular diseases, and even cancer (12, 19, 46). Acrolein has also been linked to effects of aging, pollution, and smoking, which further expands the potential value of anti-acrolein therapies (47, 48). Taken together, ALDH2-targeted acrolein sequestration may have broad benefits that potentially have extensive impact on human health.

3.5 Supplemental figures

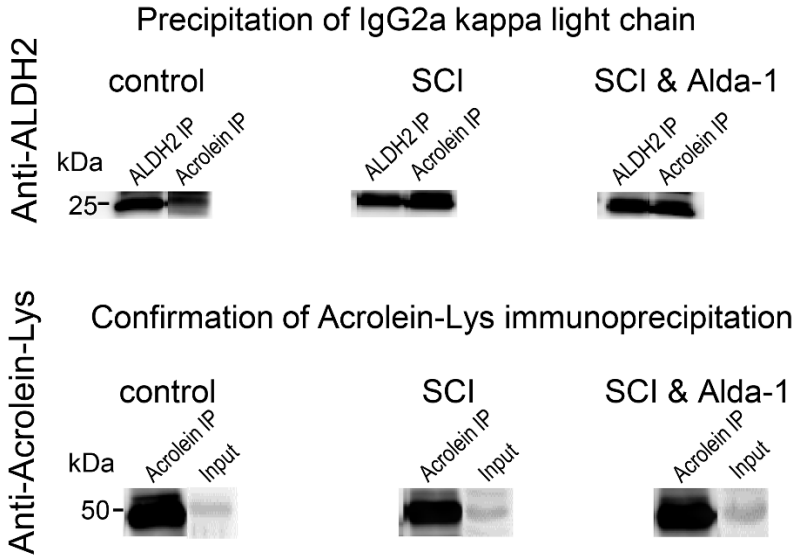

Supplemental Figure 3.1. Supporting co-IP data. To confirm the precipitated primary anti-ALDH2 or anti-acrolein-lysine antibodies are not interfering with the staining, kappa light chain primary antibodies were used. As expected, secondary antibodies stained the light chain of the primary antibodies, showing presence in both anti-ALDH2 and anti-acrolein-lysine pulldown lanes at 25 kDa (top portion of figure). In the bottom half of the figure, confirmation of successful acrolein precipitation is shown, using anti-acrolein-lysine to stain the acrolein IP lane, with relevant input lanes also included. Compared to input, heavy staining was shown, indicating successful precipitation of acrolein at 50 kDa.

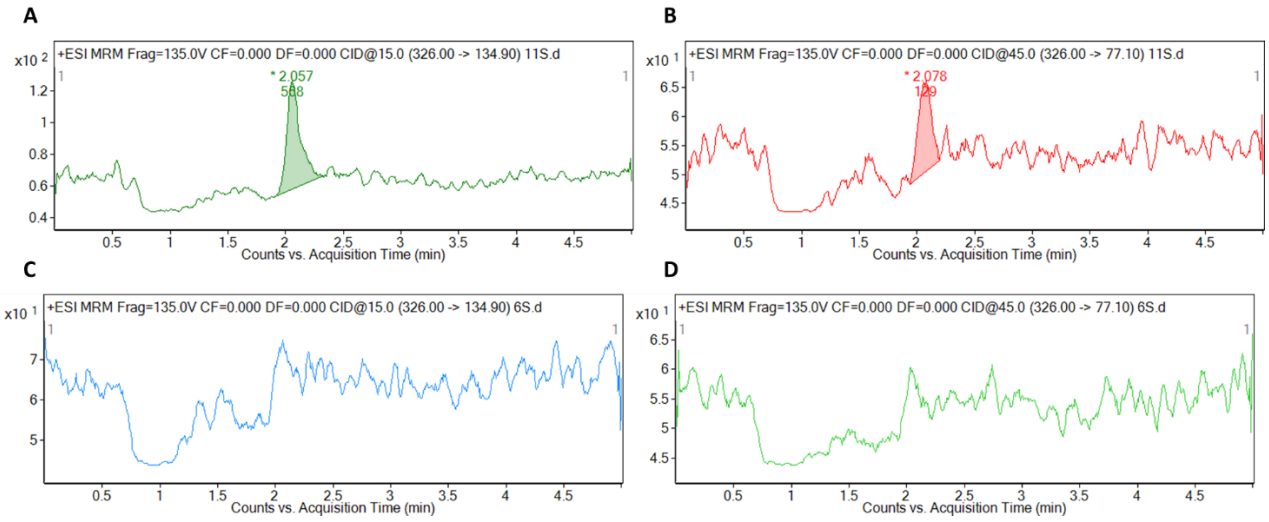

Supplemental Figure 3.2. LC/MS/MS detection of Alda-1 in injured spinal cord tissue. A & C) Detection of the more abundantly produced 139.9 *m/z* fragment. B & D) Additional confirmation of Alda-1 production by detection of the 77.1 *m/z* fragments. A & B) SCI rats were given six total doses of Alda-1 at 15mg/kg over the course of 2 days, and fragments analyzed. A) 2.057 retention time and 588 peak area integration, note y-Axis is 10^2 scale. B) 2.078 retention time and 129 peak area integration. C & D) No detection of Alda-1 in an injured rat cord tissue, who did not receive IP of Alda-1. Data not shown for blanks or positive control.

3.6 Acknowledgments

Funding: NIH R21. Project Number: 1R21NS115094-01.

3.7 References

1. Due MR, Park J, Zheng L, Walls M, Allette YM, White FA, et al. Acrolein involvement in sensory and behavioral hypersensitivity following spinal cord injury in the rat. J Neurochem. 2014;128(5):776-86.

2. Hamann K, Durkes A, Ouyang H, Uchida K, Pond A, Shi R. Critical role of acrolein in secondary injury following ex vivo spinal cord trauma. J Neurochem. 2008;107(3):712-21.

3. Hamann K, Nehrt G, Ouyang H, Duerstock B, Shi R. Hydralazine inhibits compression and acrolein-mediated injuries in ex vivo spinal cord. J Neurochem. 2008;104(3):708-18.

4. Hamann K, Shi R. Acrolein scavenging: a potential novel mechanism of attenuating oxidative stress following spinal cord injury. J Neurochem. 2009;111(6):1348-56.

5. Park J, Zheng L, Marquis A, Walls M, Duerstock B, Pond A, et al. Neuroprotective role of hydralazine in rat spinal cord injury-attenuation of acrolein-mediated damage. J Neurochem. 2014;129(2):339-49.

6. Liu-Snyder P, Borgens RB, Shi R. Hydralazine rescues PC12 cells from acrolein-mediated death. J Neurosci Res. 2006;84(1):219-27.

7. Luo J, Shi R. Acrolein induces oxidative stress in brain mitochondria. Neurochem Int. 2005;46(3):243-52.

8. Shi Y, Sun W, McBride JJ, Cheng JX, Shi R. Acrolein induces myelin damage in mammalian spinal cord. J Neurochem. 2011;117(3):554-64.

9. Wang YT, Lin HC, Zhao WZ, Huang HJ, Lo YL, Wang HT, et al. Acrolein acts as a neurotoxin in the nigrostriatal dopaminergic system of rat: involvement of alpha-synuclein aggregation and programmed cell death. Sci Rep. 2017;7:45741.

10. Gianaris A, Liu NK, Wang XF, Oakes E, Brenia J, Gianaris T, et al. Unilateral microinjection of acrolein into thoracic spinal cord produces acute and chronic injury and functional deficits. Neuroscience. 2016;326:84-94.

11. Chen Z, Park J, Butler B, Acosta G, Vega-Alvarez S, Zheng L, et al. Mitigation of sensory and motor deficits by acrolein scavenger phenelzine in a rat model of spinal cord contusive injury. J Neurochem. 2016;138(2):328-38.

12. Chen CH, Ferreira JC, Gross ER, Mochly-Rosen D. Targeting aldehyde dehydrogenase 2: new therapeutic opportunities. Physiol Rev. 2014;94(1):1-34.

13. Zambelli VO, Gross ER, Chen C-H, Gutierrez VP, Cury Y, Mochly-Rosen D. Aldehyde dehydrogenase-2 regulates nociception in rodent models of acute inflammatory pain. Science Translational Medicine. 2014;6(251):251ra118-251ra118.

14. Liu XZ, Sun X, Shen KP, Jin WJ, Fu ZY, Tao HR, et al. Aldehyde dehydrogenase 2 overexpression inhibits neuronal apoptosis after spinal cord ischemia/reperfusion injury. Neural Regen Res. 2017;12(7):1166-71.

15. Perez-Miller S, Younus H, Vanam R, Chen CH, Mochly-Rosen D, Hurley TD. Alda-1 is an agonist and chemical chaperone for the common human aldehyde dehydrogenase 2 variant. Nat Struct Mol Biol. 2010;17(2):159-64.

16. Che-Hong Chen, Grant R. Budas, Eric N. Churchill, Marie-Hélène Disatnik, Thomas D. Hurley, Mochly-Rosen1 D. Activation of Aldehyde Dehydrogenase-2 Reduces Ischemic Damage to the Heart. Science 2008;321:1493-5.

17. Dennis C. Mays, Patricia Ortiz-Bermudez, Jennifer P. Lam, Ik H. Tong, Abdul H. Fauq, Lipsky JJ. Inhibition of Recombinant Human Mitochondrial Aldehyde Dehydrogenase by Two Intermediate Metabolites of Disulfiram. Biochemical Pharmacology. 1998;55:1099–103.

18. Stachowicz A, Glombik K, Olszanecki R, Basta-Kaim A, Suski M, Lason W, et al. The impact of mitochondrial aldehyde dehydrogenase (ALDH2) activation by Alda-1 on the behavioral and biochemical disturbances in animal model of depression. Brain Behav Immun. 2016;51:144-53.

19. Acosta G, Race N, Herr S, Fernandez J, Tang J, Rogers E, et al. Acrolein-mediated alpha-synuclein pathology involvement in the early post-injury pathogenesis of mild blast-induced Parkinsonian neurodegeneration. Mol Cell Neurosci. 2019;98:140-54.

20. Taneja I, Raju KSR, Mittal M, Dev K, Khan MF, Maurya R, et al. Bioavailability, plasma protein binding and metabolic stability studies of a ALDH2 activator, alda-1, using a validated LC-ESI-MS/MS method in rat plasma. RSC Advances. 2015;5(67):54395-402.

21. David Mitchell, Petersen D. Inhibition of rat liver aldehyde dehydrogenases by acrolein. Drug Metabolism and disposition 1988;16(1):37-42.

22. SONG REN, THOMAS F. KALHORN, SLATTERY JT. Inhibition of human aldehyde dehydrogenase 1 by the 4-hydroxycyclophosphamide degradation product acrolien Drug Metabolism and disposition. 1998;27(1).

23. Jonathan A. Doorn, Thomas D. Hurley, Petersen DR. Inhibition of Human Mitochondrial Aldehyde Dehydrogenase by 4-Hydroxynon-2-enal and 4-Oxonon-2-enal. Chem Res Toxicol. 2006;19:102-10.

24. Katalin Ferencz-Biro, Regina Pietruszko. Inhibition of Human Aldehyde Dehydrogenase Isozymes by Propiolaldehyde. Alcoholism: clinical and experimental research 1984;8(302-307).

25. Yoval-Sanchez B, Rodriguez-Zavala JS. Differences in susceptibility to inactivation of human aldehyde dehydrogenases by lipid peroxidation byproducts. Chem Res Toxicol. 2012;25(3):722-9.

26. Koji Uchida, Masamichi Kanematsu, Yasujiro Morimitsu, Toshihiko Osawa, Noriko Noguchi, Niki E. Acrolein Is a Product of Lipid Peroxidation Reaction. Journal of biological chemistry. 1998;273(26):16058–66.

27. Shi R, Rickett T, Sun W. Acrolein-mediated injury in nervous system trauma and diseases. Mol Nutr Food Res. 2011;55(9):1320-31.

28. Kong D, Kotraiah V. Modulation of aldehyde dehydrogenase activity affects (+/-)-4-hydroxy-2E-nonenal (HNE) toxicity and HNE-protein adduct levels in PC12 cells. J Mol Neurosci. 2012;47(3):595-603.

29. Ohsawa I, Nishimaki K, Yasuda C, Kamino K, Ohta S. Deficiency in a mitochondrial aldehyde dehydrogenase increases vulnerability to oxidative stress in PC12 cells. J Neurochem. 2003;84(5):1110-7.

30. Zhu Q, He G, Wang J, Wang Y, Chen W. Pretreatment with the ALDH2 agonist Alda-1 reduces intestinal injury induced by ischaemia and reperfusion in mice. Clin Sci (Lond). 2017;131(11):1123-36.

31. Rivera-Meza M, Vasquez D, Quintanilla ME, Lagos D, Rojas B, Herrera-Marschitz M, et al. Activation of mitochondrial aldehyde dehydrogenase (ALDH2) by ALDA-1 reduces both the acquisition and maintenance of ethanol intake in rats: A dual mechanism? Neuropharmacology. 2019;146:175-83.

32. Ikeda T, Takahashi T, Tsujita M, Kanazawa M, Toriyabe M, Koyama M, et al. Effects of Alda-1, an Aldehyde Dehydrogenase-2 Agonist, on Hypoglycemic Neuronal Death. PLoS One. 2015;10(6):e0128844.

33. Guo JM, Liu AJ, Zang P, Dong WZ, Ying L, Wang W, et al. ALDH2 protects against stroke by clearing 4-HNE. Cell Res. 2013;23(7):915-30.

34. Fu SH, Zhang HF, Yang ZB, Li TB, Liu B, Lou Z, et al. Alda-1 reduces cerebral ischemia/reperfusion injury in rat through clearance of reactive aldehydes. Naunyn Schmiedebergs Arch Pharmacol. 2014;387(1):87-94.

35. Yokoyama A, Kato H, Yokoyama T, Tsujinaka T, Muto M, Omori T, et al. Genetic polymorphisms of alcohol and aldehyde dehydrogenases and glutathione S-transferase M1 and drinking, smoking, and diet in Japanese men with esophageal squamous cell carcinoma. Carcinogenesis. 2002;23(11):1851-9.

36. Brooks PJ, Enoch MA, Goldman D, Li TK, Yokoyama A. The alcohol flushing response: an unrecognized risk factor for esophageal cancer from alcohol consumption. PLoS medicine. 2009;6(3):e50.

37. Bian Y, Chen YG, Xu F, Xue L, Ji WQ, Zhang Y. The polymorphism in aldehyde dehydrogenase-2 gene is associated with elevated plasma levels of high-sensitivity C-reactive protein in the early phase of myocardial infarction. The Tohoku journal of experimental medicine. 2010;221(2):107-12.

38. Chang YC, Chiu YF, Lee IT, Ho LT, Hung YJ, Hsiung CA, et al. Common ALDH2 genetic variants predict development of hypertension in the SAPPHIRe prospective cohort: gene-environmental interaction with alcohol consumption. BMC cardiovascular disorders. 2012;12:58.

39. Fitzmaurice AG, Rhodes SL, Lulla A, Murphy NP, Lam HA, O'Donnell KC, et al. Aldehyde dehydrogenase inhibition as a pathogenic mechanism in Parkinson disease. Proc Natl Acad Sci U S A. 2013;110(2):636-41.

40. Zhang X, Ye YL, Wang YN, Liu FF, Liu XX, Hu BL, et al. Aldehyde dehydrogenase 2 genetic variations may increase susceptibility to Parkinson's disease in Han Chinese population. Neurobiol Aging. 2015;36(9):2660 e9-13.

41. Hao PP, Chen YG, Wang JL, Wang XL, Zhang Y. Meta-analysis of aldehyde dehydrogenase 2 gene polymorphism and Alzheimer's disease in East Asians. The Canadian journal of neurological sciences Le journal canadien des sciences neurologiques. 2011;38(3):500-6.

42. Kamino K, Nagasaka K, Imagawa M, Yamamoto H, Yoneda H, Ueki A, et al. Deficiency in mitochondrial aldehyde dehydrogenase increases the risk for late-onset Alzheimer's disease in the Japanese population. Biochemical and biophysical research communications. 2000;273(1):192-6.

43. Ohsawa I, Kamino K, Nagasaka K, Ando F, Niino N, Shimokata H, et al. Genetic deficiency of a mitochondrial aldehyde dehydrogenase increases serum lipid peroxides in community-dwelling females. Journal of human genetics. 2003;48(8):404-9.

44. Oelze M, Knorr M, Schell R, Kamuf J, Pautz A, Art J, et al. Regulation of human mitochondrial aldehyde dehydrogenase (ALDH-2) activity by electrophiles in vitro. The Journal of biological chemistry. 2011;286(11):8893-900.

45. Chen CH, Budas GR, Churchill EN, Disatnik MH, Hurley TD, Mochly-Rosen D. Activation of aldehyde dehydrogenase-2 reduces ischemic damage to the heart. Science. 2008;321(5895):1493-5.

46. Ambaw A, Zheng L, Tambe MA, Strathearn KE, Acosta G, Hubers SA, et al. Acrolein-mediated neuronal cell death and alpha-synuclein aggregation: Implications for Parkinson's disease. Mol Cell Neurosci. 2018;88:70-82.

47. Chen D, Fang L, Li H, Tang MS, Jin C. Cigarette smoke component acrolein modulates chromatin assembly by inhibiting histone acetylation. J Biol Chem. 2013;288(30):21678-87.

48. Burcham PC. Acrolein and Human Disease: Untangling the Knotty Exposure Scenarios Accompanying Several Diverse Disorders. Chem Res Toxicol. 2017;30(1):145-61.

CHAPTER 4. STRUCTURAL DISRUPTION OF THE BLOOD-BRAIN BARRIER IN REPETITIVE PRIMARY BLAST INJURY

4.1 Introduction

There has been a surge in blast-induced traumatic brain injury (bTBI) among veterans due to the frequent use of low-cost improvised explosive devices (IEDs) in modern warfare. Approximately 1 in 5 soldiers have suffered from traumatic brain injury, and of these, 52% are due to blast initiated by IEDs (1). Thus, bTBI is often called the signature injury of modern warfare, as it is the most common form of head trauma. Recent evidence highlights that brain injury is directly associated with blast shock waves, shown to play a significant role in both morbidity and mortality (2, 3). Often in warfare, soldiers exposed to bTBI pass medical evaluations because of transient or mild behavioral symptoms, and they return to duty without adequate recovery time and can be exposed to additional mild blast waves. Studies have shown that blast injuries, especially repetitive blast injuries, lead to the progression of neuropathology in both animal models and human patients (4, 5). Among wounded soldiers, bTBI has been linked to numerous neurodegenerative diseases and neurologic comorbidities such as post-traumatic stress disorder (PTSD), depression, Parkinson's disease (PD), and Alzheimer's disease (AD) (1, 6, 7). Unfortunately, while it is well established that bTBI can lead to neurodegenerative diseases, the mechanism is unclear. This is mainly due to the poor understanding of the bTBI pathologies, which are critical to developing effective diagnostic and treatment strategies to intervene and deter post-bTBI neurodegeneration. While a detailed mechanism of bTBI damage is not clear, strong evidence has emerged to support a key pathological role of the blood–brain barrier (BBB). The BBB is the tightest and most robust barrier in the body. This impermeable barrier limits macromolecule entry into the brain to maintain the physiological environment for brain function. BBB damage associated with bTBI contributes to cerebrovascular injuries such as hemorrhage, hematoma, vasospasm, and brain edema (6). In addition, BBB disruption may allow an influx of blood-derived neurotoxins, including unwanted cells or microbial pathogens, leading to chronic inflammatory and immune responses (8).

It is well established that BBB damage has been implicated and well recognized to play a critical pathological role in leading neurodegenerative diseases. In the case of AD, persistent vascular permeability and inflammation in the brain have been correlated with rapid disease onset

and severity (9). Similarly, BBB damage has been found in the striatum of PD patients, a brain region critical to PD pathology.

Although post-bTBI BBB damage has been examined, previous studies have concentrated on functional leakage (size permeability), and not investigated the potential cellular or structural pathology in the BBB that leads to or causes such permeability. Consequently, little is known about the cellular and structural components of BBB damage post-bTBI. Therefore, it is critically important to elucidate the details of the underlying pathology and the possible mechanism of post-TBI BBB damage.

Our lab has an established model of mild blast injury that recapitulates the clinical phenomenon of mild bTBI. Specifically, rats subjected to mild bTBI displayed no clear acute motor deficits, which is in agreement with clinical observations. Despite the lack of behavioral changes, our model shows conspicuous BBB leakage on the ventral region of the brain after a single mild bTBI (10). Furthermore, we have noted initial PD-like pathologies in the brain basal ganglia following mild bTBI (11). Taken together, we have established a clinically relevant bTBI model that is suitable for our current investigation of BBB alterations. We aimed to utilize this model to elucidate the details of BBB damage through structural analysis. These efforts will enhance our ability to diagnose, and more importantly, to establish reparative strategies to delay or even prevent post-bTBI neurodegenerative diseases.

4.2 Materials and methods

4.2.1 Primary blast-induced traumatic brain injury animal model

In vivo experiments were carried out with adult male Sprague Dawley rats weighing approximately 300 g. Rats were maintained with ad libitum access to water and feed in a 12–12 h light–dark cycle. All in vivo experiments were approved by the Purdue University Animal Care and Use Committee.

Animals were anesthetized with a ketamine (30 mg/kg) and xylazine (10 mg/kg) cocktail and the toe-withdrawal reflex was monitored for anesthetic depth. Rats were secured in an open-ended shock wave blast apparatus with a transparent plastic body covering to prevent blast exposure to the lower body. Mild bTBI was produced by a blast wave generator, which delivered a global blast pressure wave in a laboratory setting. The blast chamber consisted of a custom-built

stainless-steel loading chamber and chute bolted together with a polyethylene terephthalate membrane (McMaster-Carr) sealed with an O-ring. Blast generation was achieved when pressure built up in a reservoir until it exceeded the burst strength of the diaphragm. Compressed nitrogen was used as the driver gas and was delivered to the chamber via a custom-built pneumatic switch control. The blast wave was directed downward at a distance of 54 mm from the nozzle of the blast generator to the head of the animal, with a peak pressure of 150 kPa. Further details of the physical characteristics of the blast wave have been previously described (10). Sham animals (n = 4) were anesthetized accordingly and placed in the same room of the blast set-up but outside the blast wave range. Rat brains received either one blast exposure (single blast group) (n = 4) or three consecutive blast exposures (triple blast and triple blast day 3 groups) (n = 4). Rats were administered a lethal dose of ketamine/xylazine cocktail either 24 h (sham, single blast, and triple blast groups) or 72 h following blast injury (triple blast day 3 group). Rats were euthanized following the operation and perfused with chilled PBS followed by 10% neutral buffered formalin or chilled PBS.

4.2.2 Neuropathology evaluation and immunohistochemistry

In brain samples from sacrificed rats were collected and fixed in 10% neutral buffered formalin. Tissues were processed with increasing ethanol series (70, 80, 95, and 100%), and they were treated with xylene and embedded in paraffin blocks. A Thermo HM355S microtome was used to section tissues at 5 μm thickness. Hematoxylin and eosin (H&E) staining was performed according to the standard protocol. For immunohistochemistry experiments, sections were labeled with anti-IBA-1 antibody (1:8000; Abcam, ab178847) and horseradish peroxidase-conjugated goat anti-rabbit secondary antibody (1:5000; Vector Labs, MP-745). Vector ImmPACT DAB (Vector Labs, SK-4105) was applied for 5 min, and hematoxylin counterstaining was performed. Digital images were acquired at 100X total magnification using an Olympus BX43 microscope equipped with LCmicro v2.2 software.

4.2.3 Assessment of BBB pathology with immunofluorescence microscopy

Brain tissues were removed and flash frozen in a slurry of ethanol and dry ice, and embedded in OCT. Brains were sectioned with a Leica cryo-microtome at 5 μm thickness. The midbrain region was primarily evaluated because the striatum and basal ganglia regions have been

correlated with BBB breakdown and permeability in AD and PD patients (10). Tissue sections were washed with PBS and fixed in methanol. Sections were blocked with 5% normal goat serum in PBS for 45 min at room temperature, and they were incubated with primary antibodies for 16–18 h at 4 °C. Primary antibodies included anti RECA-1 (Abcam ab9774, 1:400), anti-zona occludens-1 (ZO-1) (Invitrogen 61–7300, 1:100), anti-claudin-5 (Life Technologies 34–1600, 1:50), anti-CD13 (Abcam ab108382,1:750), anti-desmin (Abcam ab15200, 1:250), anti-platelet derived growth factor receptor β (PDGFR-β) (Abcam ab32570, 1:100), anti-Collagen IV (Millipore ab756p, 1:500), anti-glial fibrillary acidic protein (GFAP) (Millipore MAB360, 1:15,000) and anti-aquaporin-4 (AQP-4) (Millipore AB3594, 1:1000). Alexa Fluor 488 conjugated goat anti-mouse IgG, Alexa Fluor 488 conjugated goat anti-rabbit IgG, Alexa Fluor 568 conjugated goat anti-rat IgG, Alexa Fluor 568 conjugated goat anti-rabbit IgG or Alexa Fluor 687 conjugated donkey anti-mouse IgG (1:500) were used as secondary antibodies. All samples were mounted onto glass slides using DAPI containing Prolong anti-fade mounting media.

4.2.4 Image analysis

Digital images were acquired via a Zeiss Axio Scope A2 at 200X or 1000X total magnification and exposure times, which were maintained between cases, for each channel were set to avoid pixel saturation and maintained between cases. Five independent midbrain region images were captured from each animal. Quantitative analysis was completed using Zen Blue software. The surface area of each BBB component was measured within an immunofluorescence image. To minimize the possibility of evaluating vascular smooth muscle cells, we restricted evaluation to capillaries measuring less than 10 μm diameter. Percent area was calculated by measuring the density of claudin-5, ZO-1, collagen IV, PDGFR-β, desmin, CD13, or aquaporin-4. The fluorescent density of these antibodies was normalized to RECA-1 area, and average values per animal were presented in the graphs. Percent stained area values (%) were provided for GFAP and RECA-1 evaluation. Raw unsaturated images were used for all quantifications. Comparisons between experimental groups were based on average values.

4.2.5 Statistics

Statistical analyses were performed using GraphPad Prism, version 7.03 (GraphPad Software Incorporated, La Jolla, CA). All data were analyzed using the one-way ANOVA with Tukey post hoc test. Statistical significance was set at $p < 0.05$ (*$p < 0.05$; **$p < 0.01$; ***$p < 0.001$). All graphs were developed using GraphPad Prism, version 7.03. Error bars represent standard deviation (SD).

4.3 Results

4.3.1 Effect on acute neuropathology

We performed a post-blast clinical examination of all 16 animals, and only one animal in the repetitive blast group demonstrated ecchymotic hemorrhage within the pinna; the hemorrhagic focus measured 2 mm in diameter. Post-blast gross examination of animals did not exhibit skull fracture, brain hemorrhage or contusion, or any visible sign of damage to parenchymal organs (kidney, lung, heart, spleen, stomach, intestines, spinal cord and liver) (data not shown).

4.3.2 BBB capillaries after repetitive injury

Brain capillaries were identified with RECA-1, an antibody specific for rat endothelial cells. RECA-1 staining showed that capillaries of the BBB were uniform and widely distributed, and highlighted by diffuse cytoplasmic RECA-1 (red) expression in sham, single and repetitive blast injuries (Fig. 4.1A-D). Quantitatively, there was no significant change in vascular density in single and repetitive blast injuries compared to sham control (Fig. 4.1E).

Structurally, endothelial cells of brain capillaries form a restrictive paracellular barrier with intercellular tight junctions to ensure the BBB homeostasis (12, 13). The claudin family is an integral component of the tight junction proteins of endothelial cells. Claudin-5 exclusively contributes to BBB permeability and integrity (12). With immunofluorescence microscopy, these tight junctions were identified by a characteristic linear threadlike pattern along with endothelial cells (supp. Fig. 4.1A-B). A similar histological pattern was observed in single and repetitive blast injury and did not alter the claudin-5 structure (green) (supp. Fig. 4.1C–H). Quantitative analysis also confirmed that there was no significant change in claudin-5 protein expression in single and repetitive blast groups compared to the sham control (supp. Fig. 4.1I). In the BBB, claudins are

linked to the cytoskeletal system by the intercellular scaffolding proteins, zona occludens (ZO), which are essential for claudin assembly in the BBB (14). We identified distinct ZO-1 (green) protein expression closely associated with endothelial cells (red). The structural arrangement of ZO-1 displayed a delicate linear intercellular pattern (supp. Fig. 4.2A, B). A similar structural pattern was observed following the blast exposures (supp. Fig. 4.2C–H). Quantitative analysis showed that ZO-1 expression did not change in single and repetitive blast exposure (supp. Fig. 4.2I). The non-cellular basement membrane underlies the capillary endothelial cells of the BBB. It consists of major structural extracellular matrix proteins like type IV collagens and elastin and other specialized proteins like laminins, nidogen, and fibronectins (15). Type IV collagen is the most abundant protein in the basement membrane, and we evaluated the changes of this pan-basement membrane protein after single and multiple blast exposures (supp. Fig. 4.3A–H). Expression of collagen IV demonstrated no significant difference following blast exposure (supp. Fig. 4.3I).

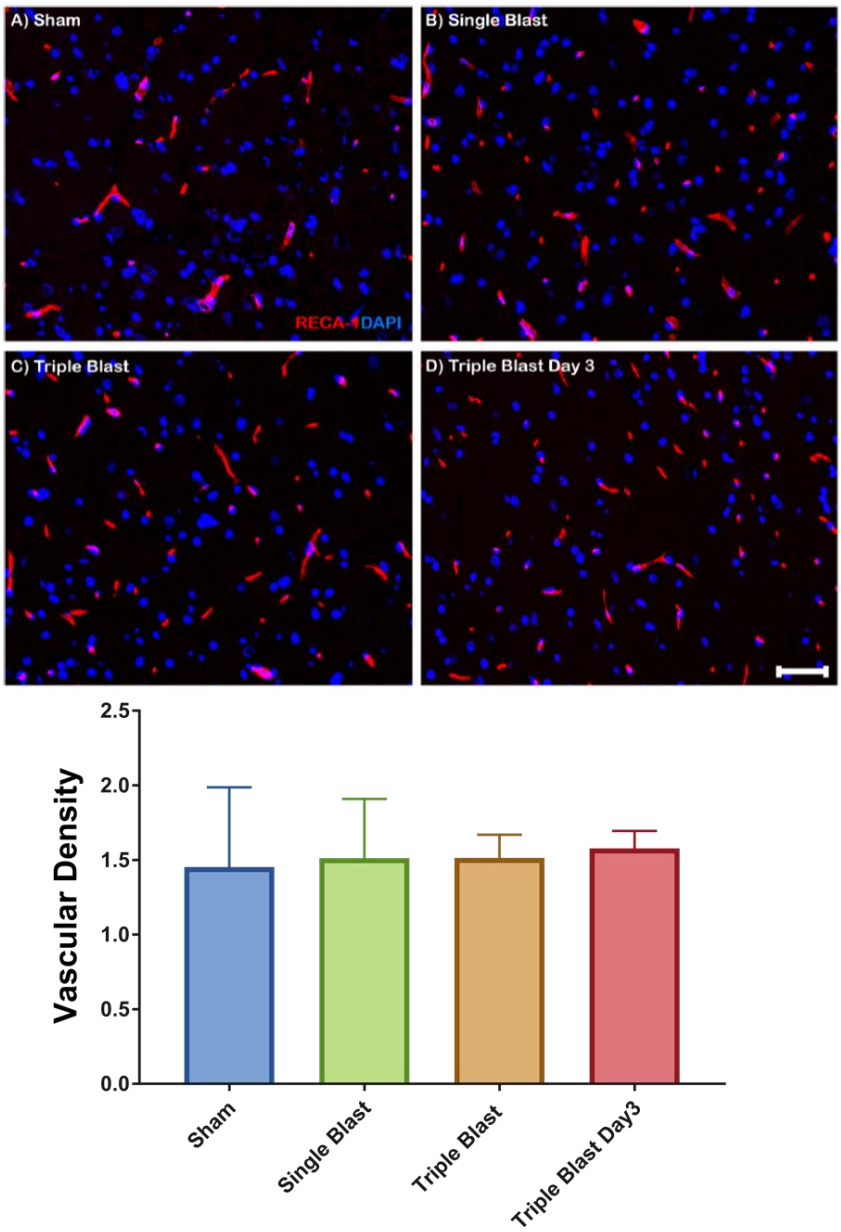

Figure 4.1. Vascular density in blast-induced traumatic brain injury. Representative immunofluorescence microscopy images of RECA-1 (red) costained with DAPI (blue) in sham (a), single blast (b), triple blast (c), and triple blast day 3 groups (d) (n = 4). e Quantitative analysis revealed a modest increase in RECA-1 expression pattern compared to the sham group, however the trend was not significant. Scale bar = 50 μm, *p < 0.05; **p < 0.01; ***p < 0.001, error bars show standard deviation (SD).

4.3.3 Repetitive blast injury is associated with increased CD13 and desmin-positive pericytes

Pericytes are located at the interface of capillary endothelial cells and are embedded within the basement membrane. Due to pericyte versatility and plasticity, we used different antibodies to identify different subpopulations of pericytes, including cell surface antigens like platelet derived growth factor receptor β (PDGFR-β) and CD13, and intermediate filament desmin (16). PDGFR-β is a well-characterized molecular marker of pericytes. Its activation is crucial for the proliferation and recruitment of pericytes (16). Although changes were not significant, (supp. Fig. 4.4), triple blast exposure slightly increased the PDGFR-β expression compared to the sham (1.17-fold, ns) and single blast (1.21-fold, ns) groups.

CD13 is a zinc-dependent membrane metalloprotease that has roles in signal transduction, differentiation, and tumor metastasis (17). Following a single blast injury, there was no significant change in the CD13 expression (green) compared to the sham control (Fig. 4.2A-D, I). As a response to the triple blast exposure, CD13 expression increased compared to the single blast and sham control, 1.47-fold ($p < 0.05$) and 1.52-fold ($p < 0.05$) (Fig. 4.2A–F). Following the 3-day post triple blast injury, CD13 demonstrated a recovery phenotype—these findings were similar to the sham control value (Fig. 4.2I).

We also evaluated the desmin-positive pericyte subtype (green) with immunofluorescence microscopy. Desmin is an intracellular filament protein and has a fundamental role in mechanical integrity (18). In the single and triple blast injury groups, the desmin-positive pericyte subpopulation increased 1.25-fold (not significant) and 1.60 fold ($p < 0.01$) in single and triple blast compared to the sham control, respectively (Fig. 4.3A–F, I). Moreover, the desmin-positive subpopulation was present 3 days following triple blast injury, which was quantified as 1.28-fold (not significant) increase compared to the sham control (Fig. 4.3G–I). Overall, changes in CD13 and desmin-positive pericytes were most prominent in the triple blast injury group, and a recovery phenotype observed 3 days post-repetitive injury (Figs. 4.2, 4.3 and supp. Fig. 4.4).

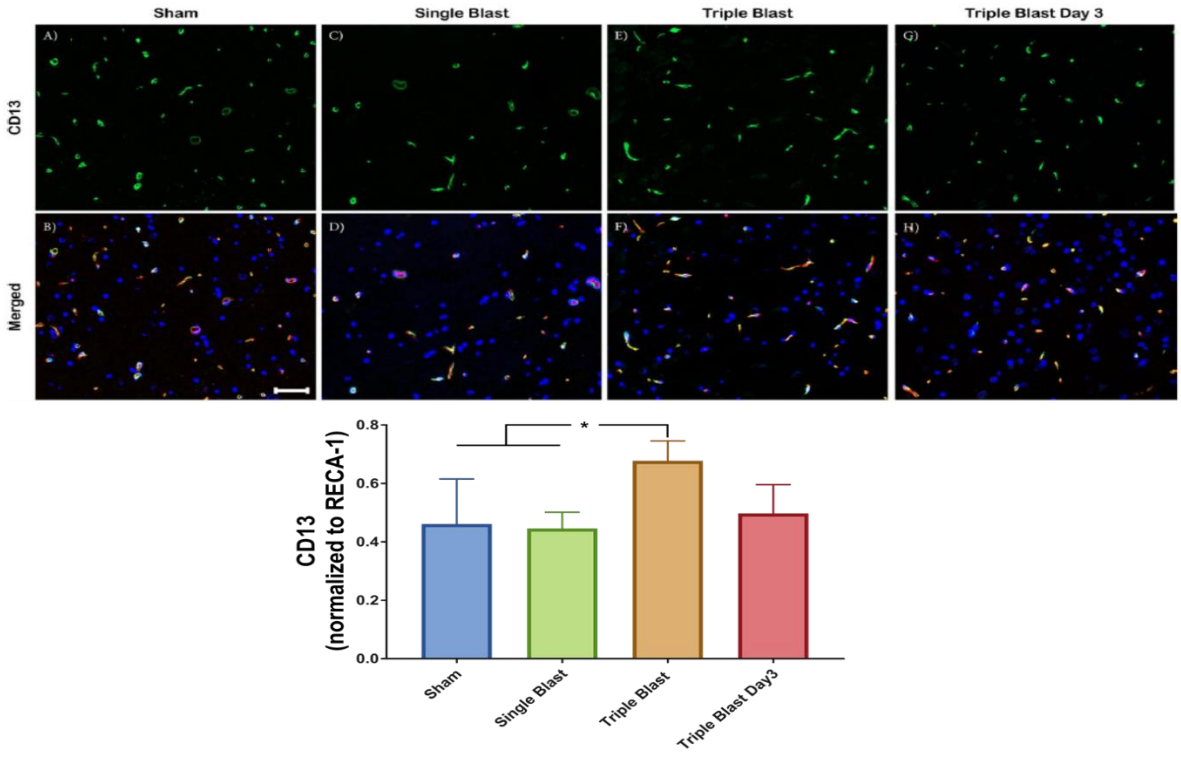

Figure 4.2. CD13-positive pericytes were elevated in repetitive mild blast-induced traumatic brain injury. Representative immunofluorescence microscopy images of CD13 (green), costained with RECA-1 (red) and DAPI (blue) in sham (a, b), single blast (c, d), triple blast (e, f) and triple blast day 3 groups (g, h) (n = 4). i Quantitative analysis revealed a significant increase in CD13-positive pericytes compared to the sham control and single blast injury. A recovery phenotype was observed 3 days after the repetitive injury. Scale bar = 50 μm, *p < 0.05; **p < 0.01; ***p < 0.001, Error bars show standard deviation (SD).

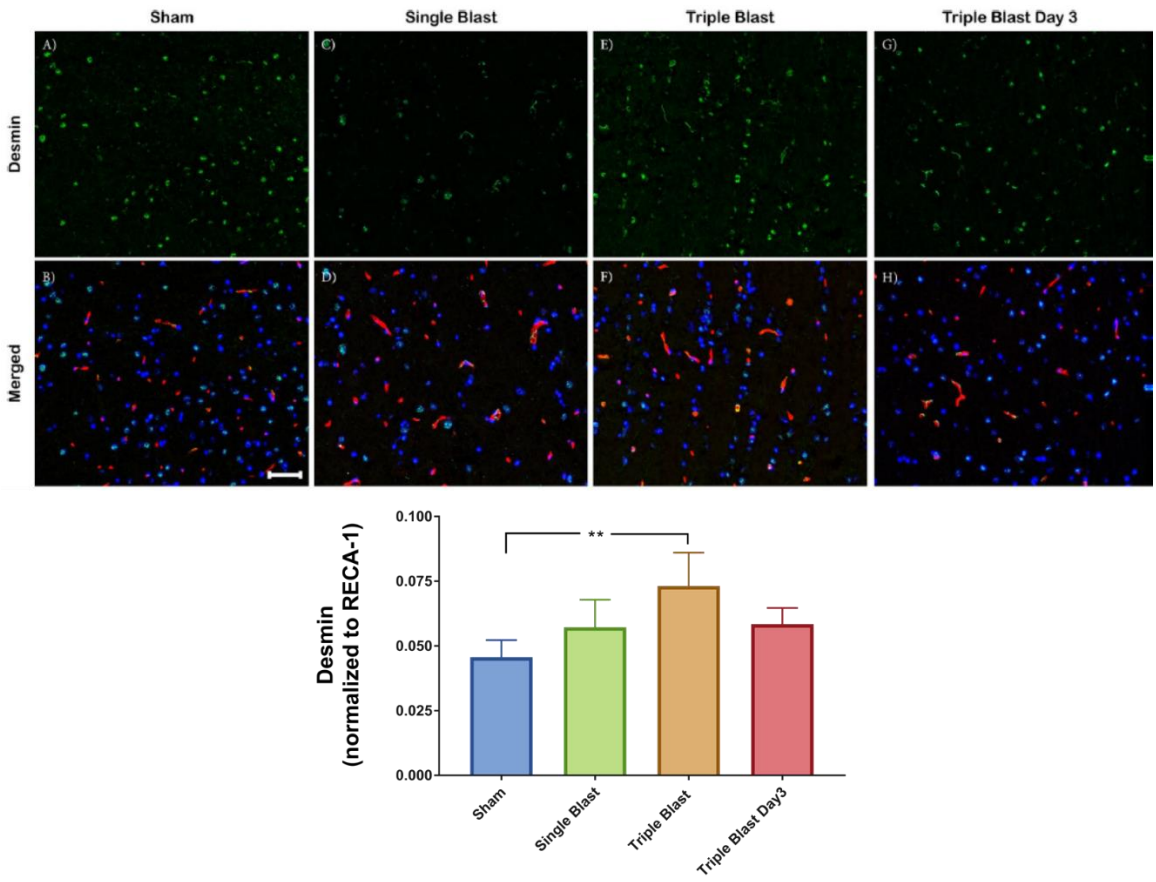

Figure 4.3. Increased desmin expression in repetitive mild blast-induced traumatic brain injury. Representative immunofluorescence microscopy images of desmin (green), costained with RECA-1 (red) and DAPI (blue) in sham (a, b), single blast (c, d), triple blast (e, f) and triple blast day 3 groups (g, h) (n = 4). i There was a 1.60-fold ($p < 0.01$) increase in desmin expression in the pericytes within the triple blast injury group. Scale bar = 50 μm, *$p < 0.05$; **$p < 0.01$; ***$p < 0.001$, error bars show standard deviation (SD).

4.3.4 Astrocytic end-feet coverage of the BBB following blast injury

Brain capillaries are covered circumferentially with astrocytic end-feet, and they contribute to BBB integrity (19). We evaluated the astrocytic end-feet coverage with aquaporin-4 (AQP-4), glial fibrillary acidic protein (GFAP), and RECA-1 after single and repetitive blast injuries (supp. Figs. 4.5 and 4.6). Yellow immunofluorescence staining indicates the co-staining of GFAP and AQP-4 (supp. Fig. 4.6D). Polarized astrocytic end-feet control solute and water diffusion in the BBB (20). An intermediate filament protein, GFAP, is exclusively expressed in reactive astrocytes and provides mechanical stability to astrocytic end-feet (21). In the sham control, AQP-4 water channel proteins were detected in the astrocyte endfeet that covered capillaries (supp. Fig. 4.6A–

D). We evaluated the AQP-4 (green) expression within the RECA-1 (red) area (supp. Fig. 4.5A–D). Quantitative analysis revealed a descending AQP-4 expression trend in the single blast (1.10-fold, not significant), triple blast (1.10-fold, not significant), and triple blast day 3 (1.16-fold, not significant) groups compared to sham control (supp. Fig. 4.5E).

Although AQP-4 expression did not change following the single or repetitive blast injuries, high magnification images showed astrocytic end-feet displacement in some vessels despite the presence of surrounding GFAP-positive astrocytic end-feet processes (supp. Fig. 4.6E–H, white arrow). Similarly, early signs of astrocytic end-feet displacement were detected after triple blast injuries (supp. Fig. 4.6I–P).

4.3.5 Assessment of neuroinflammation

Astrogliosis and microglial activation were identified with GFAP and Iba-1 expression, respectively (Fig. 4, supp. Fig. 4.7). In the single and repetitive blast groups, astrocytes displayed a reactive phenotype with pronounced GFAP expression and a hypertrophic phenotype with thickening of astrocytic endfeet (Fig. 4.4A–D). The amount of reactive and hypertrophic astrocytes was most prominent in the triple blast day 3 group. There was a 2.01-fold ($p < 0.01$) increased GFAP expression in triple blast day 3 group compared to the sham (Fig. 4.4E).

The elevated GFAP expression in triple blast day 3 group was also significantly different from the triple blast (1.59- fold, $p < 0.05$) group (Fig. 4.4E). There was an ascending trend in GFAP expression in single (1.37-fold) and triple blast (1.27-fold) groups compared to the sham control; however, they were not significant. Ionized calcium-binding adaptor molecule 1 (Iba-1) is expressed in microglia that participate in the regulation and function of microglia (21). In the sham control, resting microglia have highly ramified morphology with dense cell bodies and thin astrocytic processes (supp. Fig. 4.7A). In contrast to the sham control, elongated cells with densely stained short branches and enlarged cells with larger somata, and significantly thicker processes were identified in repetitive blast injury groups. This hypertrophic morphology was also observed with some retracted secondary processes (supp. Fig. 4.7C, D, black arrows). The bushy phenotype, which has numerous blunt and shrunken processes, was detected in the triple blast 24- and 72-h post-injury (supp. Fig. 4.7C, D, red arrows). Moreover, a couple of amoeboid microglia characterized by large rounded somata and no branched processes were also identified (supp. Fig. 4.7C, D, blue arrow).

In the single blast group, although ramified microglia phenotype was dominant, one to two hypertrophic and amoeboid figures were identified (supp. Fig. 4.7B).

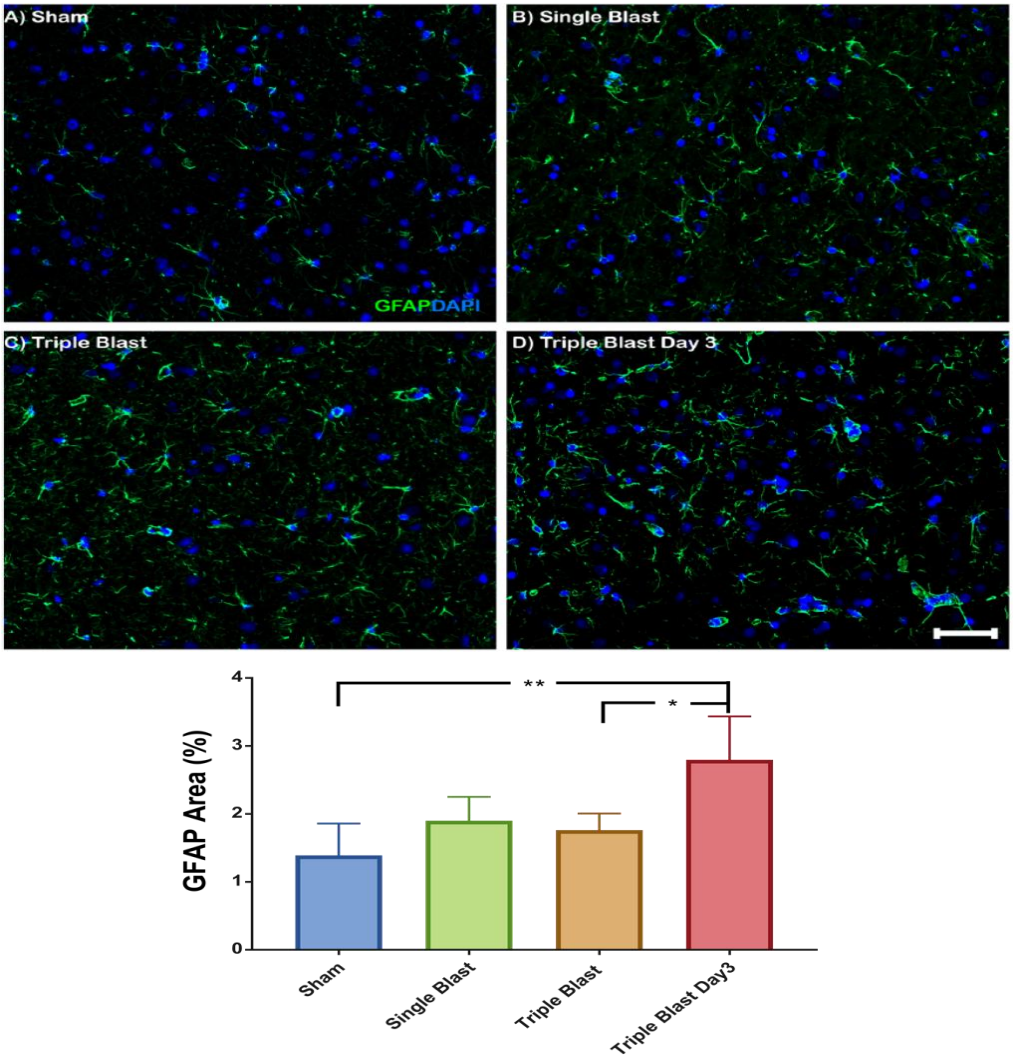

Figure 4.4. Astrogliosis is a key pathologic finding in repetitive blast-induced traumatic brain injury. Representative immunofluorescence microscopy images of GFAP (green), costained with DAPI (blue) in sham (a), single blast (b), triple blast (c) and triple blast day 3 groups (d) (n = 4). e Quantitative analysis showed increased GFAP expression as a long-term effect of repetitive blast injury. Scale bar = 50 μm, *p < 0.05; **p < 0.01; ***p < 0.001, error bars show standard deviation (SD).

4.4 Discussion

The BBB is a unique microvasculature network within the neuroparenchyma, which consists of nonfenestrated endothelial cells, a complex basement membrane network, heterogeneous pericytes, and astrocytic endfeet. This tightly regulated barrier hinders the entrance of macromolecules, ions, and harmful substances to the brain [16]. BBB breakdown is the hallmark of blast-induced traumatic brain injury. Although the extent of the BBB breakdown has been investigated by measuring the BBB permeability with different imaging modalities (5, 10, 22-24), the effect of bTBI on BBB dysfunction is poorly characterized.

Clinically, bTBI cases are classified as mild, moderate, and severe based on the severity of trauma. It has been reported that 85% of the cases are mild injury (25). Mild bTBI symptoms are generally transient, and neurocognitive impairment tests can be negative for those patients. Epidemiological studies have reported that mild singular blast exposure does not cause significant visible neuropathology. However, recurrence can demonstrate exacerbated pathological outcomes and behavioral abnormalities [33].

In this study, we used an open-ended shock tube model for blast wave generation to create a clinically relevant mild blast-induced traumatic brain injury model. Animals did not show any sign of distress or impairment, and blast waves did not impact survival. Our previous work did not demonstrate any identifiable behavioral deficits in rats following injury (10). We investigated the effect of the single blast and triple blast exposure on the BBB functional components using immunofluorescence microscopy. The integrity of the vasculature in the brain following blast injuries is clinically important due to the triggering neuroinflammatory response and eventual degeneration. Interestingly, the single and triple blast exposure did not affect the endothelial cell morphology or vascular density (Fig. 4.1).

Aberrant localization of tight junctions and their adaptor proteins have been demonstrated in BBB perturbations. Several groups have assessed the junctional complexes of the BBB in vitro and in vivo following blast exposure. Hue et al. demonstrated decreased ZO-1 and claudin-5 expression along with decreased transendothelial resistance in vitro. They also observed altered ZO-1 pathology from spindle-shape to more punctate morphology (22). In the animal model of single blast exposure, immunofluorescence and western blot analysis showed that occludin and ZO-1 were significantly increased (26). The study conducted by Kuriakose et al. reported

decreased occludin expression 15 min and 4 h after mild-blast injury. However, the recovery phenotype was observed 24 h after blast-injury (24).

Collagen IV is the most abundant basement membrane protein in the capillaries of the brain and crucial for the maintenance of the BBB. Following single and repetitive mild-blast injury, collagen IV expression remained the same in our study (supp. Fig. 4.3I). Changes in laminin expression after the single and repetitive blast were not evaluated due to the challenges in antibody optimization. Gama Sosa et al. reported abnormalities in collagen IV and laminin immunostaining following single and repetitive mild-blast (74.5 kPa) exposure (27). The collagen IV and laminin immunostaining in perfused-fixed tissue required a proteolytic epitope unmasking step with pepsin in healthy brains. However, antibody binding following blast exposure was achieved without proteolytic digestion, suggesting potential alterations in the basement membrane structure and tightness (27). Collagen IV has been closely associated with matrix metalloproteinase (MMP) activity in several diseases, including stroke (28). Elevated MMP activity was demonstrated in non-blast TBI and bTBI models with significant BBB permeability (29). Nonetheless, further molecular evaluation involving other basement membrane components is essential.

Pericytes have a critical role in BBB formation and homeostasis. The CNS harbors a heterogeneous population of pericytes, and those cells can be identified by their distinct morphology and notably different protein expression (30). The majority of healthy CNS vessels express PDGFR-β protein (31). Expression of other pericyte proteins is generally dependent upon the developmental stage or pathology. Due to the heterogeneous nature of pericytes in the BBB, it remains unclear if pericytes adopt a different phenotype or a subpopulation proliferates depending on the pathology. Because we detected changes only in desmin and CD13 proteins, but not in PDGFR-β, these preliminary findings suggest that an alteration in pericyte expression as a response to injury may be the result of the differentiation of pericyte subpopulations in the BBB in the absence of proliferation. Therefore, it still remains possible that smaller differences due to antibody sensitivity were not detected. Altogether, these data indicate the importance of pericytes and their plasticity in BBB functionality as a response to the repetitive bTBI.

Astrocytes in the CNS mediate the fluid exchange and signaling between the neuroparenchyma and the BBB. Astrocyte processes extend from the astrocytic body and are highly polarized to cover 99.7% of the BBB. The organization and distribution of the water channel protein aquaporin-4 (AQP-4) in the astrocytic end-feet is determined by the degree of polarity that

provides structural integrity to the BBB (32). Although AQP-4 expression did not change following the single or repetitive blast injuries, high magnification images showed mild astrocytic end-feet displacement in some vessels despite the presence of surrounding GFAP-positive astrocytic end-feet processes (supp. Fig. 4.6E–H, white arrow). Similarly, early signs of astrocytic end-feet displacement were detected after triple blast injuries (supp. Fig. 4.6I–P). Also, it has been shown that the failure of the polarization leads to the disruption of the basement membrane and eventually causes vessel and neurovascular unit disintegration in a multiple sclerosis model (33). Astrocytes are specialized cells in the CNS and one of the first responders to any insult. Typically, they preserve their domains and express scant GFAP protein. However, as a neuroinflammatory response to trauma, ischemia, or neurodegeneration, astrocytes have a hypertrophic phenotype with elevated GFAP expression (34). Similarly, our results revealed that blast injury entails molecular and phenotypic alterations of the astrocytes. The severity of reactive astrogliosis is closely associated with the frequency of blast exposure (Fig. 4.4E). Also, it has been shown that hypertrophic astrocytes contribute to detrimental neuronal plasticity, which may affect the BBB pathology (35).

Activation of microglia is crucial in acute and chronic neurodegeneration and detected after brain trauma (36). Microglial cells typically display ramified cytology that is characterized by round cell morphology with approximately 30 μm perimeter and 4–6 main branches with secondary and tertiary branches in health (36). In primary blast injury, microglia undergo substantial phenotypic changes, called activated or reactive microglia. Activated microglia present with a hypertrophic, bushy and/or amoeboid morphology, and they are often found in clusters (37, 38). Glial activation characterized by rounded cell bodies and fewer ramification associated with mild-blast injury has been demonstrated (23). These characteristics of microglia activation were identified in our preliminary findings following triple blast injury (supp. Fig. 4.7).

Overall, pathologic findings were most striking within desmin-positive pericytes, CD13-positive pericytes, and the neuroinflammatory response in the BBB following repetitive blast injury (Fig. 5a, b). Our group has previously shown diffuse acrolein increase in the brain after blast exposure. Future studies will determine if acrolein has an influence on the detailed BBB changes observed here, or if acrolein scavengers can mitigate such changes.

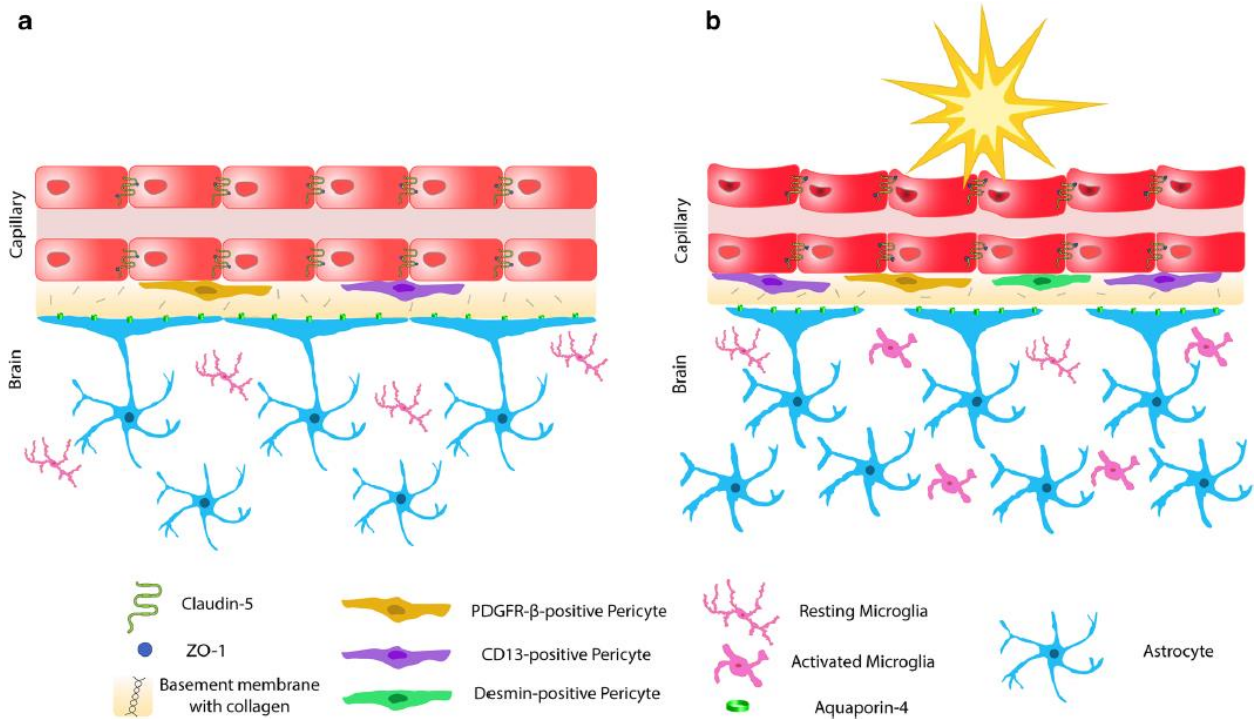

Figure 4.5. Overview of the blood–brain barrier (BBB) in health and following blast-induced traumatic brain injury. a Schematic representation of the brain capillaries consisting of tightly regulated endothelial cells (red), PDGFR-β (yellow) and CD13-positive (purple) pericytes embedded in collagen IV rich basement membrane (yellow–brown) with astrocytic end-feet (blue) containing aquaporin-4 water channel protein (green). Resting microglia in the neuroparenchyma are pink. b Following mild blast injury, there is an increase in desmin-positive (green) and CD13-positive (purple) pericytes. Astrocytic end-feet displacement is identified (astrocytic endfeet in blue and aquaporin-4 in green). GFAP expression elevates with a pronounced hypertrophic phenotype (blue). Microglia are activated and emerge with a hypertrophic, bushy and/or amoeboid morphology (pink).

4.5 Supplemental figures

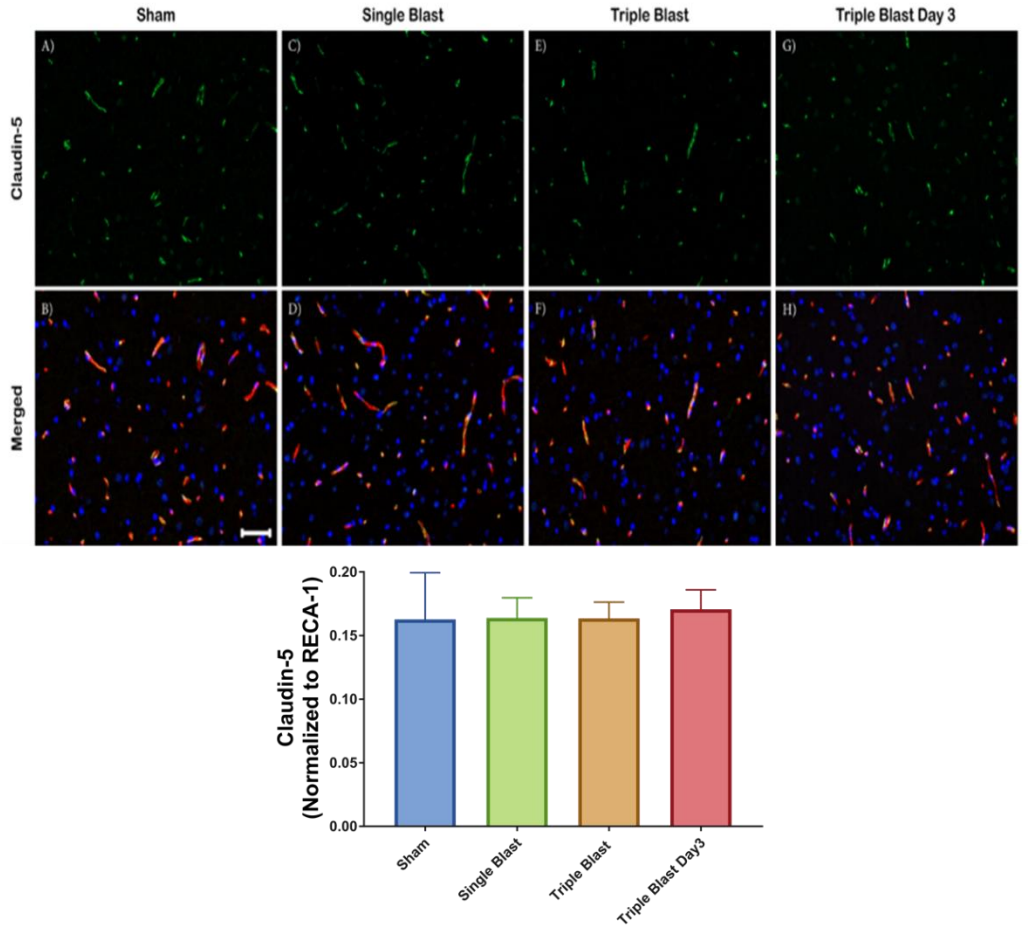

Supplemental Figure 4.1. BBB tight junctions following blast-induced traumatic brain injury. Representative immunofluorescence microscopy images of claudin-5 (green) costained with RECA-1 (red) and DAPI (blue) in sham (A-B), single blast (C-D), triple blast (E-F) and triple blast day 3 groups (G-H) (n=4). (I) There was no significant change in claudin-5 expression in the experimental groups compared to sham control. Scale bar=50 µm, * $p < 0.05$; ** $p < 0.01$; *** $p < 0.001$, error bars show standard deviation (SD).

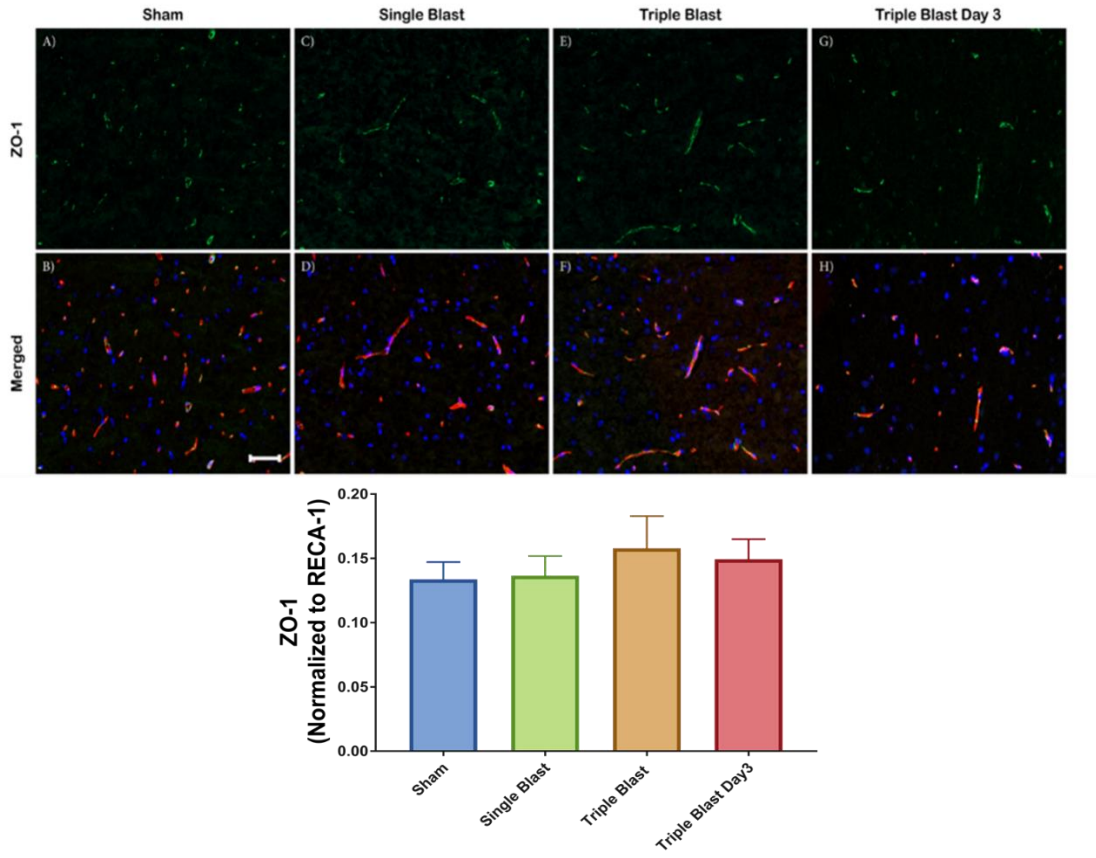

Supplemental Figure 4.2. ZO-1 expression in repetitive blast-induced traumatic brain injury. Representative immunofluorescence microscopy images of ZO-1 (green) costained with RECA-1 (red) and DAPI (blue) in sham (A-B), single blast (C-D), triple blast (E-F) and triple blast day 3 groups (G-H) (n=4). (I) There is no significant change in ZO-1 expression compared to sham control. Scale bar=50 µm, * $p < 0.05$; ** $p < 0.01$; *** $p < 0.001$, error bars show standard deviation (SD).

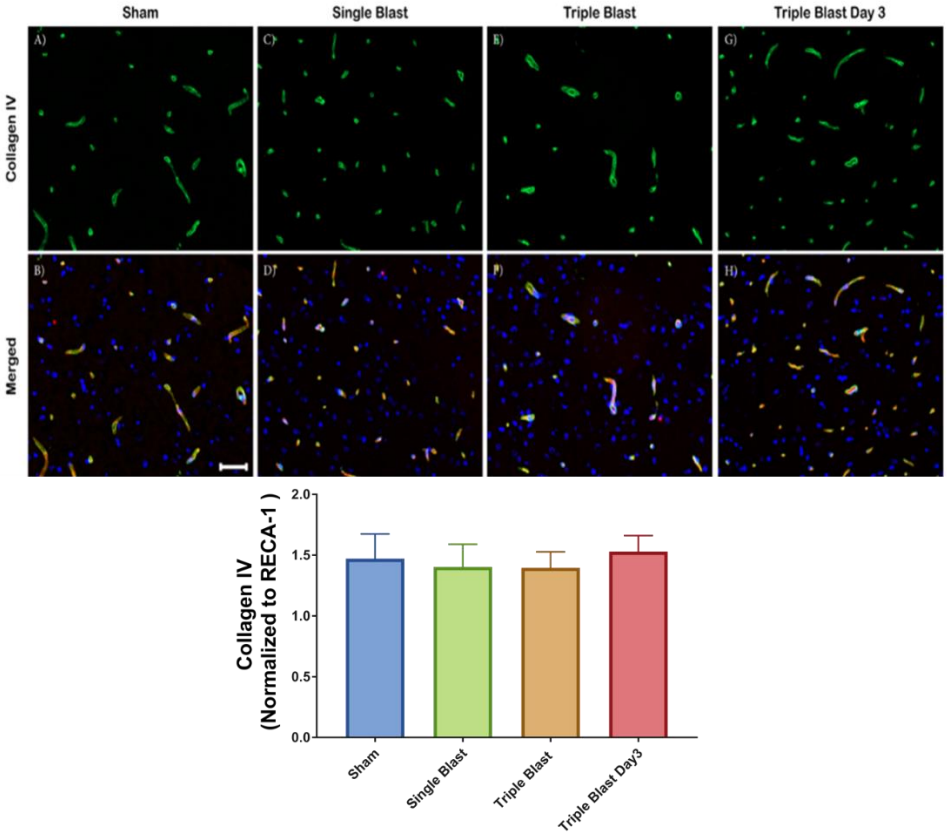

Supplemental Figure 4.3. Basement membrane of the BBB following blast-induced traumatic brain injury. Representative immunofluorescence microscopy images of collagen IV (green) costained with RECA-1 (red) and DAPI (blue) in sham (A-B), single blast (C-D), triple blast (E-F) and triple blast day 3 groups (G-H) (n=4). (I) While not significant, collagen IV expression in single blast and triple blast injury was modestly diminished compared to sham control. Three days following repetitive injury, recovery of collagen IV expression was identified. Scale bar=50 µm, * $p < 0.05$; ** $p < 0.01$; *** $p < 0.001$, error bars show standard deviation (SD).

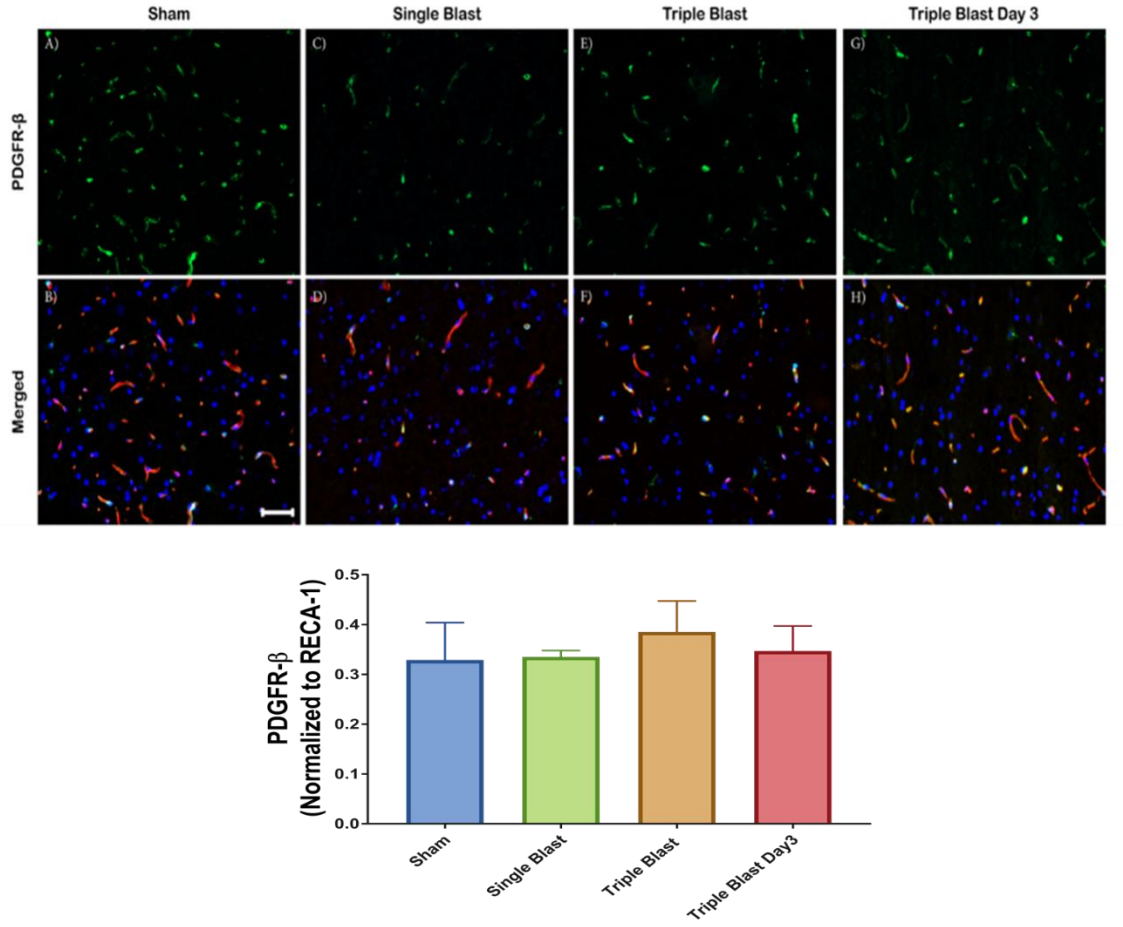

Supplemental Figure 4.4. PDGFR-β expression in blast-induced traumatic brain injury. Representative immunofluorescence microscopy images of PDGFR-β (green) costained with RECA-1 (red) and DAPI (blue) in sham (A-B), single blast (C-D), triple blast (E-F) and triple blast day 3 groups (G-H) (n=4). (I) Quantitative analysis revealed that PDGFR-β expression was slightly elevated in the triple blast group. A rescue phenotype was observed three days following bTBI. Scale bar=50 μm, * $p < 0.05$; ** $p < 0.01$; *** $p < 0.001$, error bars show standard deviation (SD).

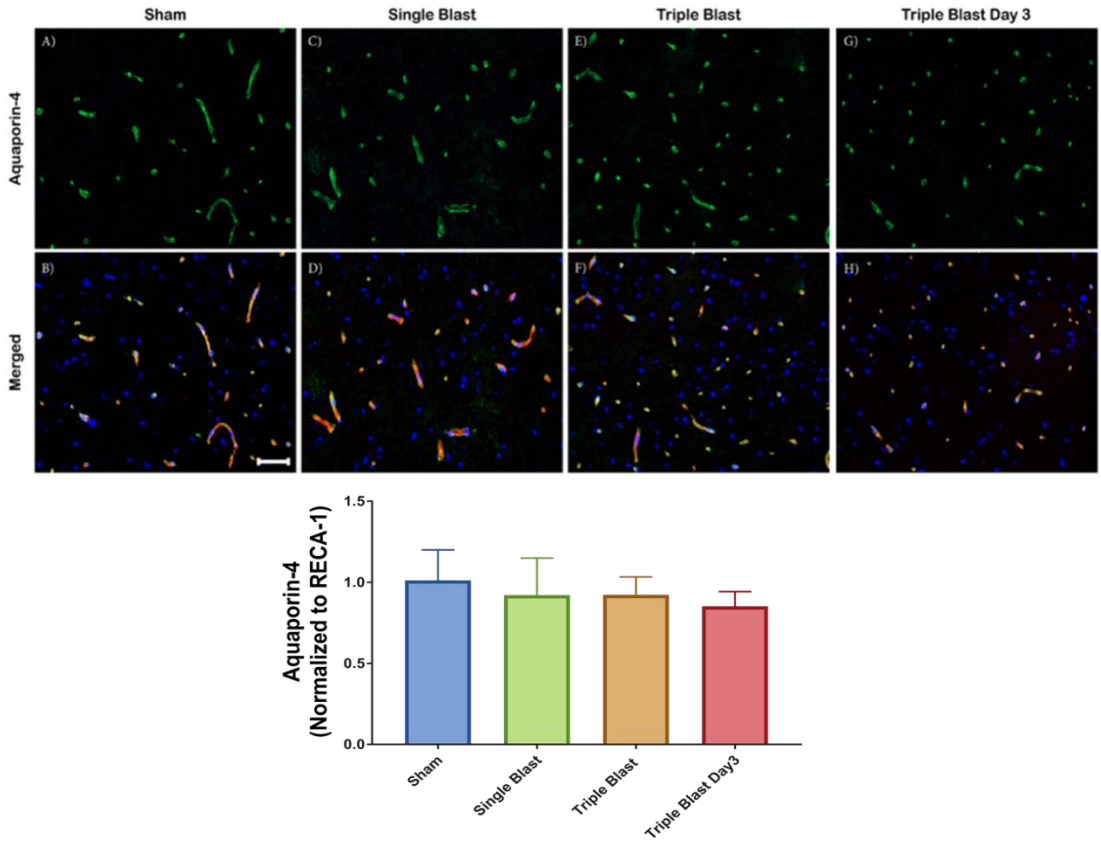

Supplemental Figure 4.5. Aquaporin-4 expression in blast-induced traumatic brain injury. Representative immunofluorescence microscopy images of AQP4 (green) costained with RECA-1 (green) and DAPI (blue) in sham (A-B), single blast (C-D), triple blast (E-F) and triple blast day 3 groups (G-H) (n=4). (I) Quantitative analysis revealed a descending AQP-4 expression trend in the single blast (1.10-fold, not significant), triple blast (1.10-fold, not significant), and triple blast day 3 (1.16-fold, not significant) groups compared to sham control. Scale bar=50 μm, * $p < 0.05$; ** $p < 0.01$; *** $p < 0.001$, error bars show standard deviation (SD).

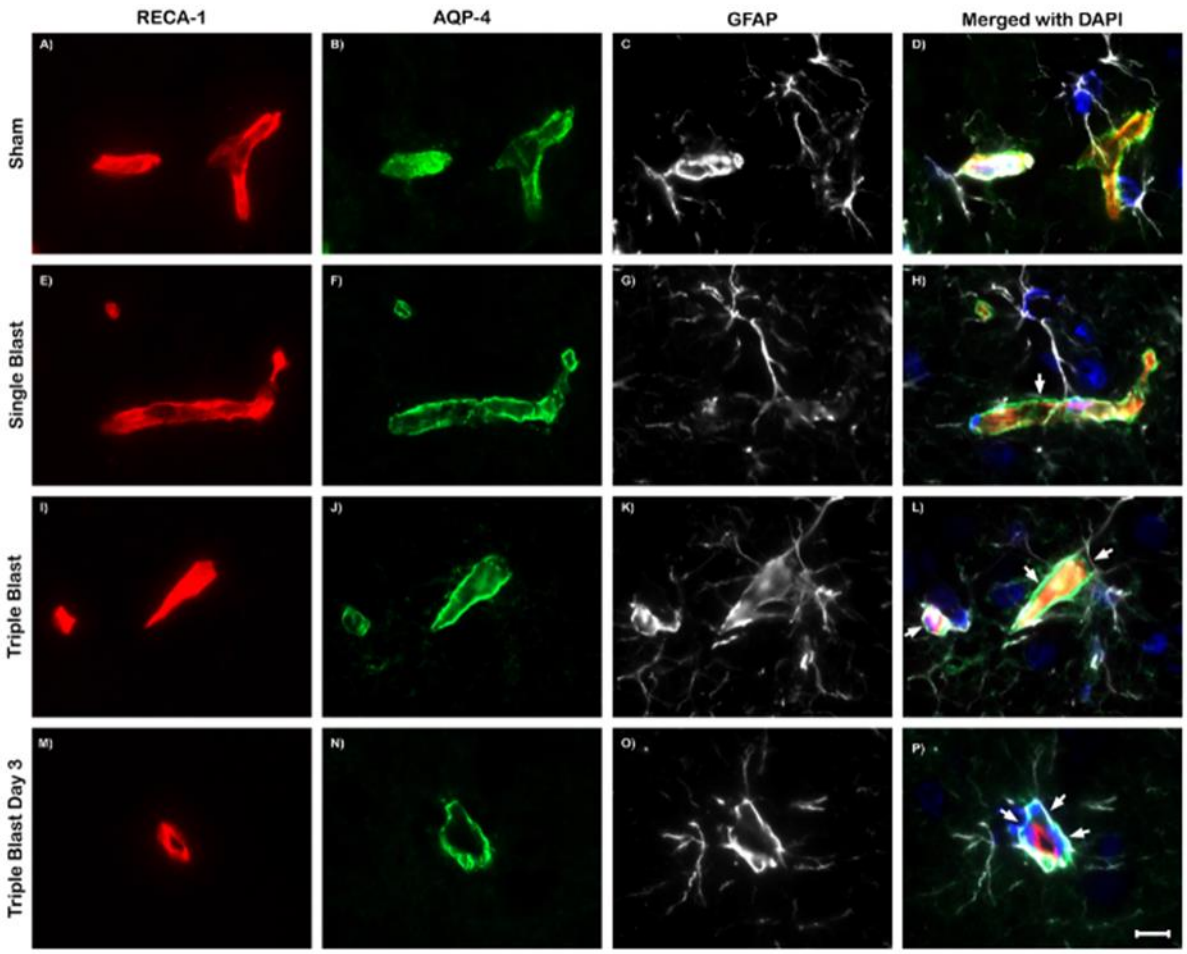

Supplemental Figure 4.6. Astrocyte coverage of the BBB following blast-induced traumatic brain injury. Representative immunofluorescent microscopy images of brain capillaries (red) were costained with RECA-1 (red), aquaporin-4 (green), GFAP (white) and nuclei (DAPI). Scale bar=10 μm. White arrows demonstrate astrocytic displacement. Vessels in A-H are presented in longitudinal section, and I-P are presented in cross-section.

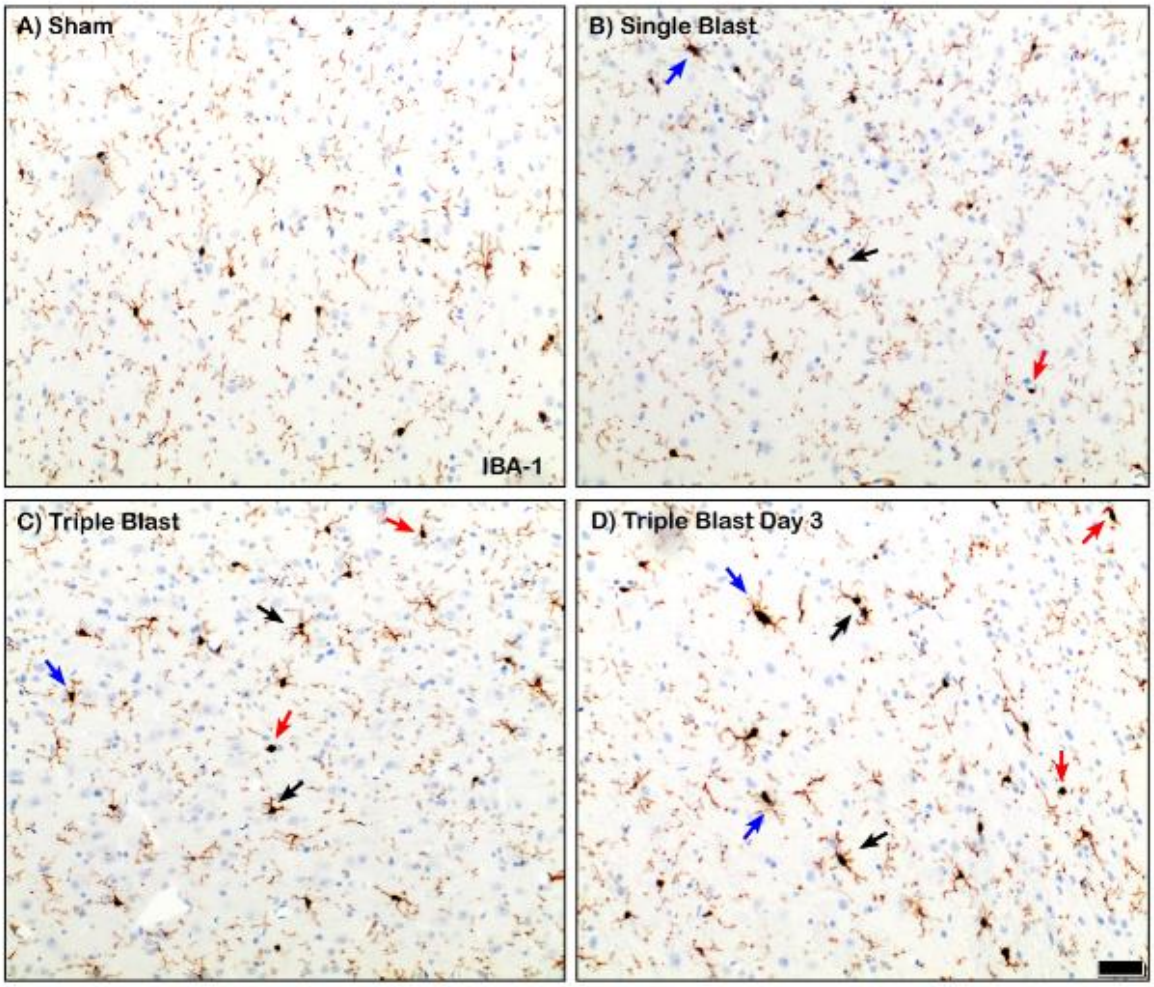

Supplemental Figure 4.7. Microglial activation in repetitive blast injury. Representative immunohistochemistry images of IBA-1 (brown) in sham (A), single blast (B), triple blast (C), and triple blast day 3 groups. (A) In the sham control, microglia are predominantly ramified. (B-D) Hypertrophic (black arrows), bushy (blue arrows), and amoeboid (red arrows) morphology can be seen in response to single and repetitive blast injuries. Scale bar=50 µm.

4.6 Acknowledgements

Much of this work is published with permission to reprint. Seth Herr is a co-author and contributed collaboratively to data collection, study design, and manuscript writing. Thank you Mr. Victor Bernal-Crespo at the Purdue University Histology Research Laboratory for the assistance, a core facility of the NIH-funded Indiana Clinical and Translational Science Institute.

Alexandra M. Dieterly is supported by the Purdue Research Foundation.

This was supported in part by the Indiana Clinical and Translational Sciences Institute, funded in part by Award Number UL1TR001108 from the National Institutes of Health, National Center for Advancing Translational Sciences, Clinical and Translational Sciences Award. The content is solely the responsibility of the authors and does not necessarily represent the official views of the National Institutes of Health.

4.7 References

1. Rosenfeld JV, McFarlane AC, Bragge P, Armonda RA, Grimes JB, Ling GS. Blast-related traumatic brain injury. Lancet Neurol. 2013;12(9):882-93.

2. Katherine H. Taber PD, Deborah L. Warden MD, Robin A. Hurley MD. Blast-Related Traumatic Brain Injury: What Is Known? The Journal of Neuropsychiatry and Clinical Neurosciences. 2006;18(2):141-5.

3. Abdul-Muneer PM, Schuetz H, Wang F, Skotak M, Jones J, Gorantla S, et al. Induction of oxidative and nitrosative damage leads to cerebrovascular inflammation in an animal model of mild traumatic brain injury induced by primary blast. Free Radic Biol Med. 2013;60:282-91.

4. Ahmed FA, Kamnaksh A, Kovesdi E, Long JB, Agoston DV. Long-term consequences of single and multiple mild blast exposure on select physiological parameters and blood-based biomarkers. Electrophoresis. 2013;34(15):2229-33.

5. James S. Meabon, Bertrand R. Huber, Donna J. Cross, Todd L. Richards, Satoshi Minoshima, Kathleen F. Pagulayan, et al. Repetitive blast exposure in mice and combat veterans causes persistent cerebellar dysfunction. Science. 2016;8(321).

6. Magnuson J, Leonessa F, Ling GSF. Neuropathology of Explosive Blast Traumatic Brain Injury. Current Neurology and Neuroscience Reports. 2012;12(5):570-9.

7. Acosta SA, Tajiri N, de la Pena I, Bastawrous M, Sanberg PR, Kaneko Y, et al. Alpha-synuclein as a pathological link between chronic traumatic brain injury and Parkinson's disease. J Cell Physiol. 2015;230(5):1024-32.

8. Forrester JV, McMenamin PG, Dando SJ. CNS infection and immune privilege. Nature Reviews Neuroscience. 2018;19(11):655-71.

9. Newcombe EA, Camats-Perna J, Silva ML, Valmas N, Huat TJ, Medeiros R. Inflammation: the link between comorbidities, genetics, and Alzheimer’s disease. Journal of Neuroinflammation. 2018;15(1):276.

10. Walls MK, Race N, Zheng L, Vega-Alvarez SM, Acosta G, Park J, et al. Structural and biochemical abnormalities in the absence of acute deficits in mild primary blast-induced head trauma. J Neurosurg. 2016;124(3):675-86.

11. Sweeney MD, Sagare AP, Zlokovic BV. Blood–brain barrier breakdown in Alzheimer disease and other neurodegenerative disorders. Nature Reviews Neurology. 2018;14(3):133-50.

12. Nitta T, Hata M, Gotoh S, Seo Y, Sasaki H, Hashimoto N, et al. Size-selective loosening of the blood-brain barrier in claudin-5–deficient mice. Journal of Cell Biology. 2003;161(3):653-60.

13. Abbott NJ, Patabendige AAK, Dolman DEM, Yusof SR, Begley DJ. Structure and function of the blood–brain barrier. Neurobiology of Disease. 2010;37(1):13-25.

14. Umeda K, Ikenouchi J, Katahira-Tayama S, Furuse K, Sasaki H, Nakayama M, et al. ZO-1 and ZO-2 independently determine where claudins are polymerized in tight-junction strand formation. Cell. 2006;126(4):741-54.

15. Engelhardt B, Sorokin L. The blood-brain and the blood-cerebrospinal fluid barriers: function and dysfunction. Seminars in immunopathology. 2009;31(4):497-511.

16. Sweeney MD, Ayyadurai S, Zlokovic BV. Pericytes of the neurovascular unit: key functions and signaling pathways. Nature Neuroscience. 2016;19(6):771-83.

17. Kunz J, Krause D, Kremer M, Dermietzel R. The 140-kDa protein of blood-brain barrier-associated pericytes is identical to aminopeptidase N. J Neurochem. 1994;62(6):2375-86.

18. Paulin D, Li Z. Desmin: a major intermediate filament protein essential for the structural integrity and function of muscle. Experimental Cell Research. 2004;301(1):1-7.

19. Kubotera H, Ikeshima-Kataoka H, Hatashita Y, Allegra Mascaro AL, Pavone FS, Inoue T. Astrocytic endfeet re-cover blood vessels after removal by laser ablation. Scientific Reports. 2019;9(1):1263.

20. Obermeier B, Daneman R, Ransohoff RM. Development, maintenance and disruption of the blood-brain barrier. Nature Medicine. 2013;19(12):1584-96.

21. Eng LF, Ghirnikar RS, Lee YL. Glial fibrillary acidic protein: GFAP-thirty-one years (1969-2000). Neurochem Res. 2000;25(9-10):1439-51.

22. Hue CD, Cho FS, Cao S, Nicholls RE, Vogel Iii EW, Sibindi C, et al. Time Course and Size of Blood-Brain Barrier Opening in a Mouse Model of Blast-Induced Traumatic Brain Injury. J Neurotrauma. 2016;33(13):1202-11.

23. Readnower RD, Chavko M, Adeeb S, Conroy MD, Pauly JR, McCarron RM, et al. Increase in blood-brain barrier permeability, oxidative stress, and activated microglia in a rat model of blast-induced traumatic brain injury. Journal of neuroscience research. 2010;88(16):3530-9.

24. Kuriakose M, Rama Rao KV, Younger D, Chandra N. Temporal and Spatial Effects of Blast Overpressure on Blood-Brain Barrier Permeability in Traumatic Brain Injury. Scientific Reports. 2018;8(1):8681.

25. Masel BE, Bell RS, Brossart S, Grill RJ, Hayes RL, Levin HS, et al. Galveston Brain Injury Conference 2010: clinical and experimental aspects of blast injury. J Neurotrauma. 2012;29(12):2143-71.

26. Lucke-Wold BP, Logsdon AF, Smith KE, Turner RC, Alkon DL, Tan Z, et al. Bryostatin-1 Restores Blood Brain Barrier Integrity following Blast-Induced Traumatic Brain Injury. Molecular neurobiology. 2015;52(3):1119-34.

27. Gama Sosa MA, De Gasperi R, Janssen PL, Yuk FJ, Anazodo PC, Pricop PE, et al. Selective vulnerability of the cerebral vasculature to blast injury in a rat model of mild traumatic brain injury. Acta neuropathologica communications. 2014;2:67.

28. Baeten KM, Akassoglou K. Extracellular matrix and matrix receptors in blood-brain barrier formation and stroke. Developmental neurobiology. 2011;71(11):1018-39.

29. Higashida T, Kreipke CW, Rafols JA, Peng C, Schafer S, Schafer P, et al. The role of hypoxia-inducible factor-1α, aquaporin-4, and matrix metalloproteinase-9 in blood-brain barrier disruption and brain edema after traumatic brain injury. J Neurosurg. 2011;114(1):92-101.

30. Brown LS, Foster CG, Courtney J-M, King NE, Howells DW, Sutherland BA. Pericytes and Neurovascular Function in the Healthy and Diseased Brain. Frontiers in Cellular Neuroscience. 2019;13(282).

31. Armulik A, Genové G, Mäe M, Nisancioglu MH, Wallgard E, Niaudet C, et al. Pericytes regulate the blood–brain barrier. Nature. 2010;468(7323):557-61.

32. Mathiisen TM, Lehre KP, Danbolt NC, Ottersen OP. The perivascular astroglial sheath provides a complete covering of the brain microvessels: An electron microscopic 3D reconstruction. Glia. 2010;58(9):1094-103.

33. Wolburg-Buchholz K, Mack AF, Steiner E, Pfeiffer F, Engelhardt B, Wolburg H. Loss of astrocyte polarity marks blood-brain barrier impairment during experimental autoimmune encephalomyelitis. Acta neuropathologica. 2009;118(2):219-33.

34. Sofroniew MV, Vinters HV. Astrocytes: biology and pathology. Acta neuropathologica. 2010;119(1):7-35.

35. Robinson C, Apgar C, Shapiro LA. Astrocyte Hypertrophy Contributes to Aberrant Neurogenesis after Traumatic Brain Injury. Neural plasticity. 2016;2016:1347987.

36. Graeber MB, Streit WJ. Microglia: biology and pathology. Acta neuropathologica. 2010;119(1):89-105.

37. Beynon SB, Walker FR. Microglial activation in the injured and healthy brain: what are we really talking about? Practical and theoretical issues associated with the measurement of changes in microglial morphology. Neuroscience. 2012;225:162-71.

38. Wyatt-Johnson SK, Herr SA, Brewster AL. Status Epilepticus Triggers Time-Dependent Alterations in Microglia Abundance and Morphological Phenotypes in the Hippocampus. Front Neurol. 2017;8:700.

CHAPTER 5. TARGETED DELIVERY OF ACROLEIN SCAVENGER HYDRALAZINE IN SPINAL CORD INJURY USING FOLATE-LIGAND-DRUG CONJUGATION

5.1 Introduction

Spinal cord contusion injury (SCI) results in many complications, both behaviorally and cellularly. Most notably are hyperalgesia, locomotor impairment, cell death and spinal tissue degeneration (1, 2). While many factors contribute to these pathologies, much research has implicated neurotoxic and reactive aldehydes, such as acrolein (3-7). Acrolein accumulates rapidly, peaking at 48 hours post injury, and persisting at significant levels for up to two weeks. As a result of lipid peroxidation, acrolein forms rapidly and causes continued destruction to cell membranes and lipid-rich myelin (8). Due to the high reactivity of acrolein, it can crosslink and damage lipids as well as proteins and DNA, leading to cellular stress and death (8, 9). When acrolein is injected into the spine at physiologically relevant concentrations, cell death and tissue degeneration is observed (7). Further, studies have successfully attempted to clear acrolein after injury using various aldehyde scavenging techniques. If acrolein is cleared after injury significantly less tissue destruction, decreased hyperalgesia, and restoration of locomotor function is observed (6, 10, 11). Thus, acrolein is a critical instigator of the pathogenesis of spinal cord injury that when removed, can greatly improve outcomes.

While the formation of acrolein is ubiquitous among cells, those involved in the immune response have been shown to generate excessive levels of reactive oxygen species (ROS) in SCI (12). This high ROS production is accompanied by acrolein generation through lipid peroxidation, but also through myeloperoxidase. Myeloperoxidase is abundant in immune cells such as neutrophils and macrophages and produces acrolein as an enzymatic metabolite (13-15). These macrophages accumulate in high numbers in SCI, through the breakdown of the blood brain barrier and peripheral recruitment, resulting in injury site accumulation and proliferation. Spinal cord resident macrophages, or microglia, will also undergo chemotaxis (although to a much lesser extent) and proliferation at the site of injury (16, 17). As a result, a hallmark outcome of spinal cord injury is localized, diffuse, and significantly high levels of inflammation (12, 17). This inflammation, (specifically number of macrophages/microglia), increases until peak levels at 7 days post injury (dpi), before slowly declining (17). Thus, the localization of immune cells in

injury regions of tissue may provide a key targeting opportunity for therapeutics such as acrolein scavengers.

To scavenge the significant levels of acrolein in SCI, our group has shown that administration of hydralazine, an FDA approved medication for the treatment of hypertension, is effective (6). However, SCI patients often suffer from blood pressure dysregulation and hypotension (18). Thus while safe for human use and an effective acrolein scavenger, hydralazine's ability to lower blood pressure is a major hurdle when considering its application for SCI patients.

Folate, or vitamin B9, is uptaken by folate receptors 1 and 2 (FOLR), which are significantly upregulated on activated macrophages (19). Given this, various drugs can be attached to folate as a targeted delivery system to sites of inflammation (19). Therefore, when considering together 1) the damaging effects of acrolein and the benefits of its removal, 2) the effectiveness of hydralazine at lowering acrolein, its safe use in humans but side effect of lowering blood pressure, 3) the abundant inflammation present in spinal cord injury, and 4) the ability of folate-targeting to deliver drugs only to the site of injury, we therefore hypothesize that hydralazine conjugated to folate (F-HDZ) will benefit SCI by removing acrolein without effecting blood pressure. In this study we aimed to first test if targeted drugs will be uptaken by folate-positive cells specifically in the SCI area, and next determine if F-HDZ will work to clear acrolein without an effect on blood pressure.

5.2 Materials and methods

5.2.1 Animals and diet

Young male Sprague Dawley rats were used in accordance to approved Purdue Animal Care and Use Committee protocols. Rats were first placed on a special low folate diet for 2 - 3 weeks before use, to lower serum folate concentrations to physiologically relevant levels. This is done to avoid unwanted competition with our folate-drugs, since standard rat chow contains an unnecessarily high level of folate. At the time of experimental use, rats had grown to approximately 200 – 240 grams.

5.2.2 Drugs

Folate conjugated drugs were synthesized and purified in house. These include Near Infra-Red dye conjugated to Folate (F-NIR) and Hydralazine conjugated to folate (F-HDZ). NIR dye only (unconjugated) was also synthesized in house. Hydralazine hydrochloride (HDZ) was purchased (Sigma H1753-5G).

5.2.3 Injury model

Rats were given standard, clinically relevant spinal cord injuries as previously described(6). Briefly, rats were anesthetized using an intraperitoneal injection of a ketamine-xylazine cocktail. A T10 laminectomy was done followed by a moderate level contusion injury with an infinite horizon drop impactor at a moderate setting (200 kDyne). Approximately 30 minutes – 1 hour post injury, rats were given NSAID Ketoprofen (10mg/kg subcutaneously, for 2 dpi) followed by 3mL saline (subcutaneously). Rats were grouped according to study. For F-NIR dye drug uptake studies, rats were grouped as sham (laminectomy with no injury to the spinal cord) receiving F-NIR, injury receiving F-NIR, or injury receiving NIR dye only. For testing blood pressure and acrolein levels, rats were grouped to receive either hydralazine (5mg/kg intravenous), F-HDZ (5mg/kg intravenous), injury only (sham injection), or healthy age matched controls.

5.2.4 Blood pressure recording

Rats were acclimated to blood pressure setup and room during the two week period prior to experiments. Rats blood pressure measurements were recorded by a single, blind investigator, using KentScientific CODA tail cuff system. Rats were acclimated until consistent baseline levels could be recorded. After injury, rats received daily IV injections of drug according to the described group. Approximately 30 min – 1 hour after injection, on both 4 dpi and 7 dpi, blood pressure measurements were taken. Investigator would record 5 – 10 measurements every session for each rat, which were later averaged. All diastolic and systolic measurements were normalized to each individual rats baseline (preinjury) recordings before final statistics.

5.2.5 Perfusion and tissue collection

For F-NIR studies, rats received a single injection on day 7, and were perfused 24 hours later on day 8. For blood pressure and acrolein level studies, on day 8 after receiving a final drug injection in the morning, rats were sacrificed later in the afternoon. Intracardial perfusion was done using oxygenated Krebs solution or chilled 1xPBS, after heavy ketamine/xylazine anesthesia. Rats spinal cords were dissected and immediately placed in 4% formalin/PBS solution for 2 days, followed by 30% sucrose/PBS solution for 3 days. Cords were then frozen in OTC cubes using an isopentane/dry ice slurry, and cryo-sliced into transverse sections (Thermo HM 525NX) at 25 um thickness. Sections were then stored in 0.01% Sodium Azide and PBS at 4°C until biochemical analysis.

5.2.6 Immunohistochemistry

Spinal sections were immunostained overnight with anti-acrolein-lysine (StressMarq) followed by biotinylated secondary antibodies (Vector Laboratories), incubated in ABC avidin/biotin complex solution (Thermo Scientific™, #32020) and developed using the DAB Peroxidase (HRP) Substrate Kit, 3,3′-diaminobenzidine (Pierce™ DAB Substrate Kit). Sections were dried on a slide warmer and dehydrated in ascending series of ethanol/water solutions, and mounted with Paraclear (Polysciences) and Toluene. Images were taken using a standard light microscope (Olympus). Quantification was done using standard techniques for measuring DAB intensity on ImageJ software (20).

5.2.7 Fluorescent and NIR Microscopy

For fluorescence staining, sections were immunostained overnight with anti-IBA1 (Abcam), followed by incubation in TexasRed secondary (JacksonImmuno). Sections were then mounted on glass slides and cover slipped using ProLong Gold Antifade Mounting media. Images were taken using a microscope with TexasRed filters and a special NIR filter (Nikon TiS).

Alternatively, sections were washed in 3% PBST for 20 min, followed by 1xPBS for 5 min, and directly mounted (no co-staining) and cover slipped (ProLong Gold Antifade media). Sections were then scanned using a red filter and a NIR filter (AZURE Sapphire).

Fluorescence intensity was quantified using standard techniques and ImageJ as done prior (21).

5.2.8 Statistics

All data are presented as mean and standard deviation error bars. Tukey One way ANOVA or Student's t test were used for statistical assessment where necessary (JMP 13 Software). The statistical significance threshold was set at $p < 0.05$.

5.3 Results

5.3.1 Validation of spinal cord injury site targeting

In order to validate targeted delivery of drugs in our model, F-NIR dye was injected into rats on 7 dpi, 24 hours before sacrifice on day 8. F-NIR will allow for the observation or tracking of folate-conjugated drugs to the injured spinal tissue site, where we hypothesize they will accumulate. In Fig. 5.1, transverse cord sections were mounted and scanned. Rostral sections are from regions approximately 0.25 inches from the T10 injury site (Fig. 5.1A). In Fig. 5.1B, sections are from the injury epicenter (epi) of the same rat. Interestingly, CNS tissues are known to have endogenous red autofluorescence (22), which was exploited here to represent gross tissue structure. F-NIR dye is shown in green. As analyzed in Fig. 5.1C, epicenter tissue uptakes significantly more dye than rostral regions, indicating successful drug targeting ($p<0.03$, $n=7$, students T-test). Sham rats show some signal bordering the sections, likely from inflammation of the dura (supp. Fig. 5.1A). The SCI epicenter is characterized by low perfusion, the formation of cysts and scar tissues. To further validate the mechanism of folate delivery rather than cellular affinity for the NIR drug, or the possibility of NIR drugs becoming trapped in the epicenter, some rats were similarly given NIR dye only (unconjugated dye) injections and examined. Rats given this show no green signal in injured cord sections (supp. Fig. 5.1B, blue arrow).

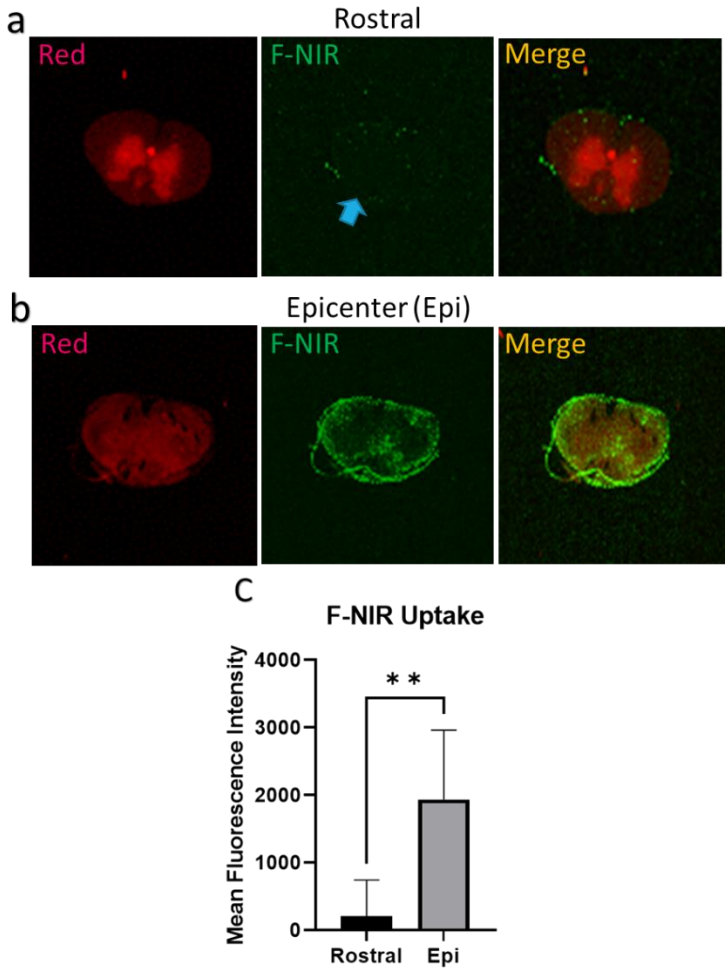

Figure 5.1. Uptake of F-NIR in the injured region of the spinal cord. Drug was administered to a group of rats on 7 dpi, and tissue collected 24 hours later. A-B) Red shows autofluorescence to reveal tissue structure, Green shows F-NIR signal. Merge reveals an overlay of the two colors. Representative sections shown are different regions of the spinal cord from the same rat. A) Rostral sections of the injured spinal cord, blue arrow points to tissue location. B) Lesion site of the spinal cord, or Epicenter (EPI). C) Quantification of F-NIR signal intensity in Rostral compared to epicenter. Little signal is found in rostral sections, and significantly more is seen in Epi ($p < 0.01$, $n = 7$ per group). Statistics done with students T-test.

5.3.2 Validation of targeted drug uptake by IBA1 positive cells

Macrophages will significantly upregulate the folate receptor when activated. Further, when activated, microglia undergo morphological changes from resting (ramified) to more activated stages such as hypertrophic and bushy, or fully activated amoeboid stage (20, 23). At the amoeboid stage, microglia are difficult to differentiate from activated macrophages (24). To confirm cellular intake of folate conjugated drugs in our model of SCI is by IBA1 positive

macrophage/microglia uptake, we performed immunofluorescence staining of F-NIR injected tissue with IBA1. In Fig. 5.2, F-NIR is now shown as a blue color, this was artificially changed from green to enhance clarity. The IBA1 positive staining is in red. In Fig. 5.2A, sham rats show more arborized, ramified microglia with no F-NIR observed. In Fig. 5.2B, microglia in rostral sections of injury rats become bushy, with minimal F-NIR co-staining. In Fig. 5.2C, IBA1 cells abundantly have amoeboid morphologies and high F-NIR signal.

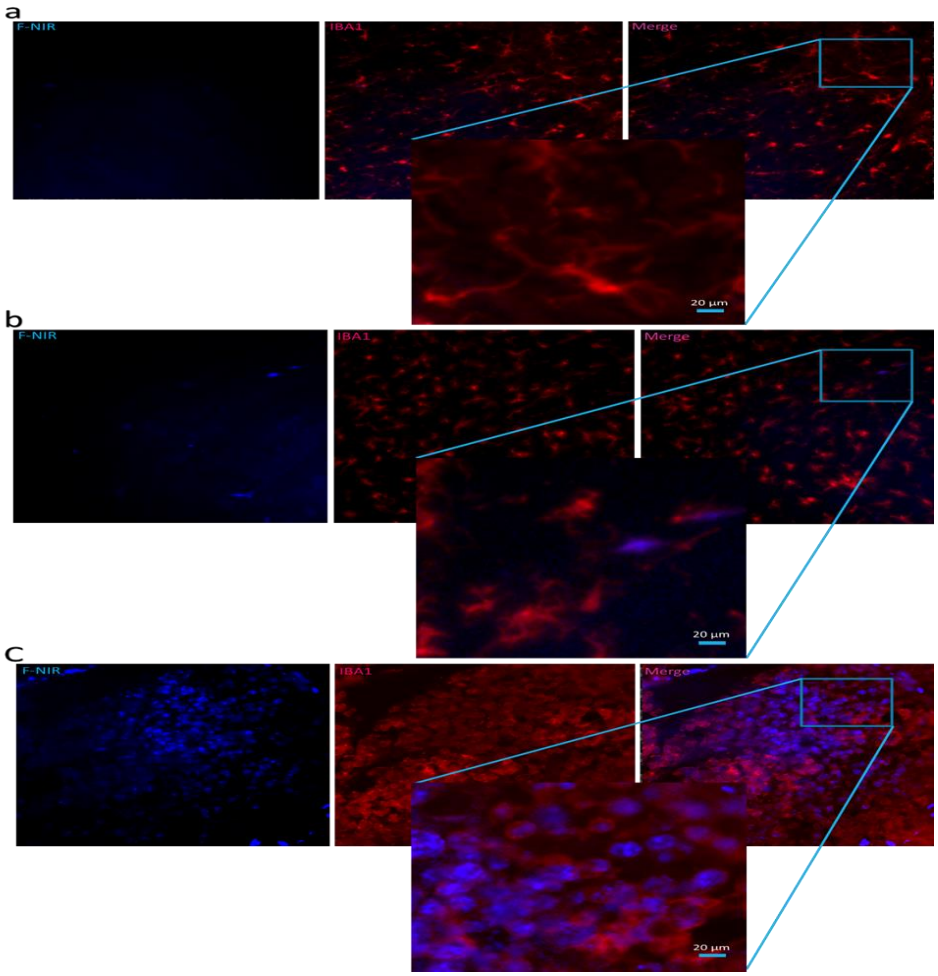

Figure 5.2. Histological examination of rats injected with F-NIR. Drug was administered to a group of rats on 7 dpi, and tissue collected 24 hours later. A-C) Blue indicates F-NIR drug signal, and red indicates IBA1 macrophages/microglia. Merge reveals an overlay of the two colors. A) Sham rats show no obvious F-NIR drug uptake, and ramified microglia. A zoom in box of the merged image reveals microglia in the ramified state. B and C) Representative images shown are different regions of the spinal cord from the same rat. B) Rostral sections reveal minimal F-NIR dye uptake. Zoom in box of the merged image reveals microglia at this distance appear to be in the bushy stage. The minimal F-NIR signal is seen merging with IBA1 red color. C) Epicenter sections indicate high F-NIR signal. In the zoom in box of the merge image, microglia/macrophages appear to be abundant and in the amoeboid state, and overly with the F-NIR blue signal. Scale bar = 20 µm.

5.3.3 Structure of folate-hydralazine

Hydralazine is an effective acrolein scavenger, and FDA approved medication for lowering blood pressure. In Fig. 5.3, our F-HDZ molecule was made with a cleavable linker conjugating hydralazine to folate. This conjugation will allow for targeting of hydralazine to the injured area. Once uptaken by the folate receptor of macrophages, hydralazine will become activated and released from the linker, thus free to remove acrolein. This linker and release system has been used previously and its stability *in-vivo* validated (25).

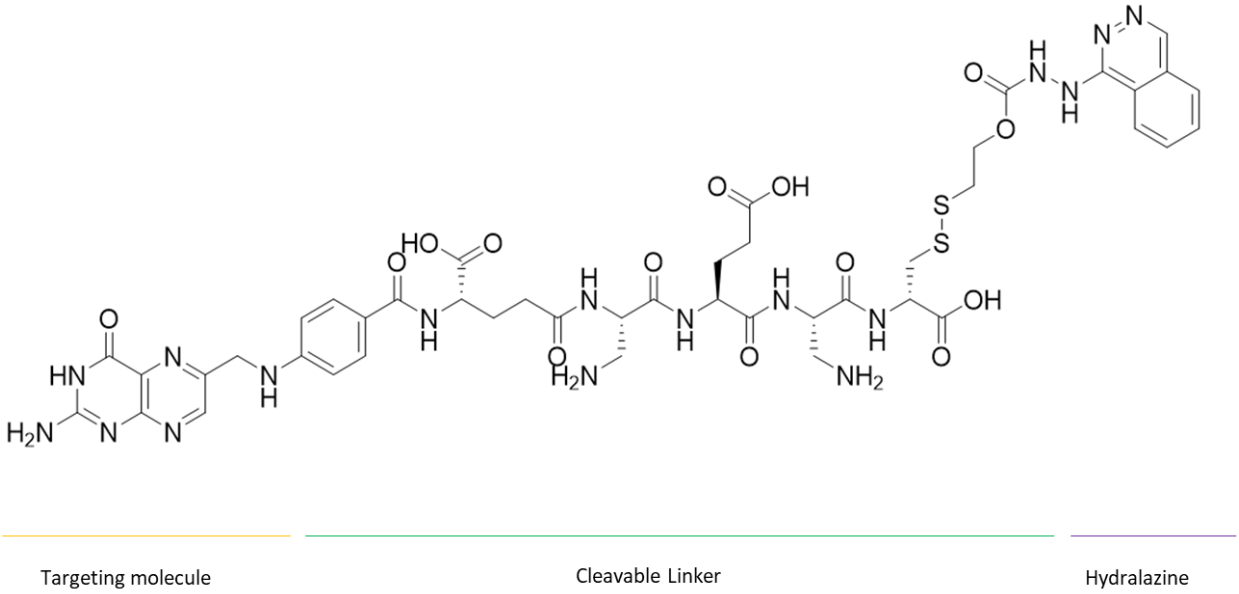

Figure 5.3. Proposed confirmational chemical structure of our novel F-HDZ drug. Targeting molecule folate is on the left (yellow underline). The cleavable linker (green underline) attaches the targeting molecule to hydralazine (purple underline). Once inside a cell, the linker will release activated hydralazine.

5.3.4 Evaluation of acrolein levels

In Fig. 5.4 acrolein levels are measured to determine if F-HDZ still functions as an acrolein scavenger. Representative scans of the transvers cord sections are shown with brown color indicating Acrolein-adduct positive staining (Fig. 5.4A). In Fig. 5.4B, quantification of the images is graphed. Compared with control, injury rats shown significantly elevated acrolein ($n=6$, $p<0.001$). In this group, HDZ rats show significant increase of acrolein from control, although not as elevated as the injury only ($n=4$, $p<0.05$). F-HDZ rats do not show significant elevation of acrolein from control, and show a significant decrease from injury group ($n=5$, $p<0.01$).

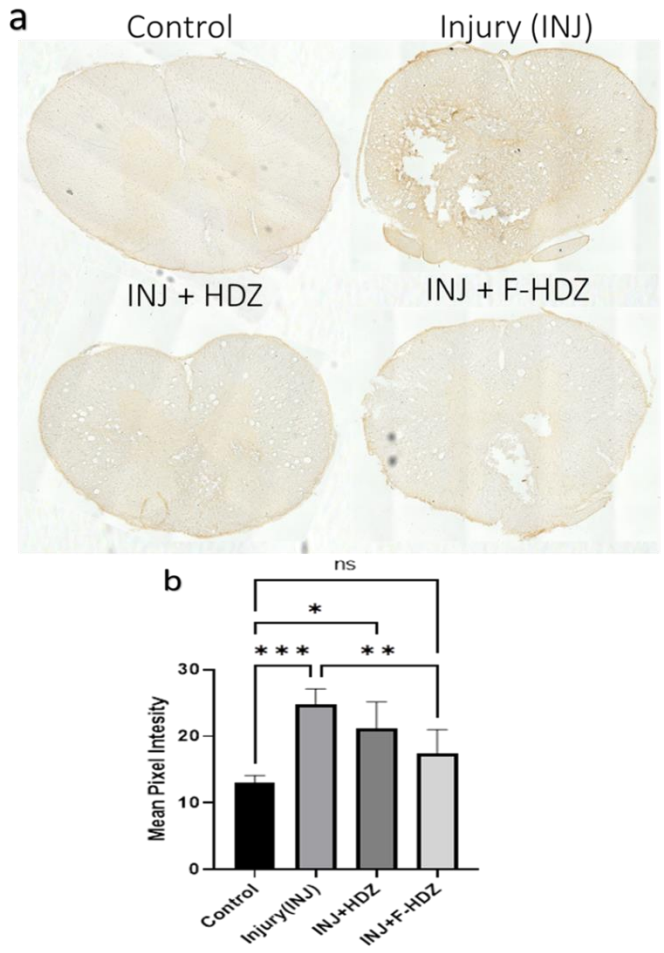

Figure 5.4. Acrolein-adducts in the spinal cord epicenter after F-HDZ administration. Rats were given Vehicle, HDZ or F-HDZ daily for 8 dpi, and tissue collected in the afternoon after last administration (morning) on day 8. A) Immunohistochemistry of transverse sections of the spinal cord show acrolein-adducts in brown color, for each group: Control, Injury (INJ), Injury given hydralazine (INJ + HDZ), and injury given hydralazine conjugated to folate (INJ + F-HDZ). B) Quantification of acrolein-adduct staining. The INJ group show significant elevation from control groups. Although not as significant as the INJ group, INJ + HDZ shows a significant elevation from control. There is no statistical difference from the control group and the INJ + F-HDZ, and significant difference between the control and INJ + F-HDZ. N = 3-6 per group. *$p<0.05$, **$p<0.01$, ***$p<0.001$, ns=no significance. Statistics done with Tukey's One Way ANOVA.

5.3.5 Effects of drugs on blood pressure of injured rats

Rats blood pressure was measured on 4 and 7 dpi, to determine if the F-HDZ still has a potent effect of lowering blood pressure. On day 4 in Fig. 5.5A, both diastolic and systolic measures showed a significant decrease of blood pressure for HDZ rats, when compared to control ($n=4$, $p<0.05$). Interestingly, F-HDZ rats not only did not show an effect of lower blood pressure,

but were also significantly elevated when compared to the HDZ rats (n=4, p<0.01). Individuals with spinal cord injury are known to have many homeostatic imbalances, often suffering from hypotension. This was seen here, with injury only rats having lower levels of blood pressure, although not significant. However, in Fig. 5.5B on 7 dpi, injury rats have a significantly lower level of blood pressure when compared with control (n=4, p<0.05). Further, 7 day HDZ rats show more significant decrease from control (n=4, p<0.01). Finally, F-HDZ rats had no change in blood pressure when compared with control, similar to the 4 dpi tests.

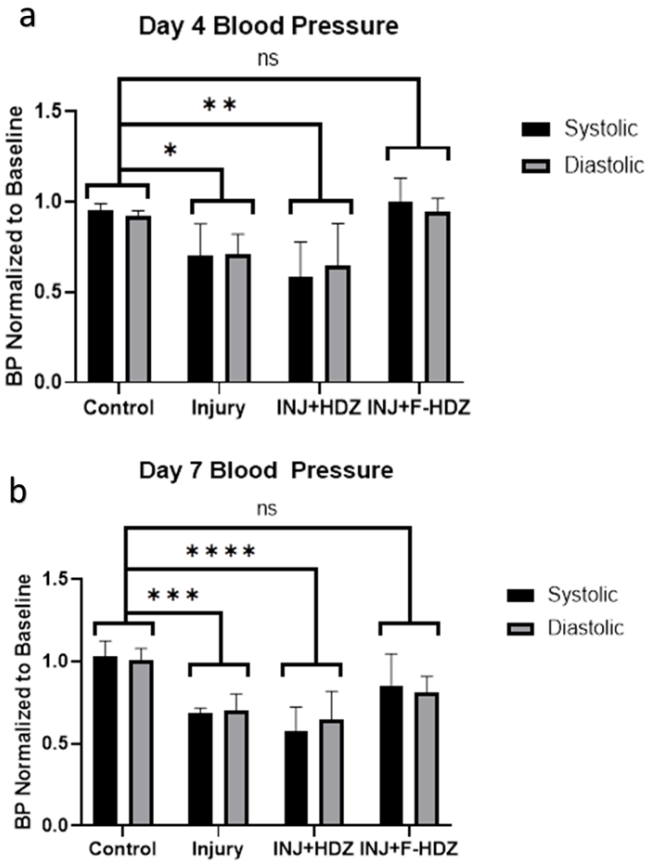

Figure 5.5. Novel drug conjugate F-HDZ does not effect blood pressure. Blood pressure (BP) was measured twice during an 8 day timeframe for Control, Injury, Injury given hydralazine (INJ + HDZ), and injury given hydralazine conjugated to folate (INJ + F-HDZ). Rats were habituated to tail cuff setup prior to surgery, and baseline values recorded. Measurements were taken 30 min – 1 hour after drug administration. All systolic (black bar) and diastolic (grey bar) is graphed as a ratio to baseline values. A) On 4 dpi, injury shows a significant decrease in BP values from control, and INJ + HDZ a greater difference from control. The INJ + F-HDZ group shows now difference from control rats. B) On 7 dpi, the same trend of BP is observed with injury showing a significant decrease in BP values from control, and INJ + HDZ a greater difference from control. The INJ + F-HDZ group shows now difference from control rats. N = 3-4 per group. *p<0.05, **p<0.01, ***p<0.001, ****p<0.0001, ns=no significance. Statistics done with Tukey's One Way ANOVA.

5.4 Discussion

Here, we aimed to validate if drug targeting is a viable option for our spinal cord injury model. This was accomplished in both Figs. 5.1 and 5.2, where F-NIR drug was injected into injured rats. The NIR signal was subsequently observed specifically in the T10 injured area, and less so rostral to this site, indicating the drug is targeted to the injury site and not acting elsewhere. Spinal cord injury is hallmarked by high levels of inflammation, including activated microglia and infiltrating macrophages (17). These cells are likely the mechanism for targeted drug uptake, and here IBA1 positive cells were found readily uptaking a F-NIR dye (Fig. 5.2). Although inflammation is present in rostral sections, it gradually decreases away from the epicenter in both numbers and active states of microglia/macrophage. For instance, in the sections we examined at 0.25 inches rostral, microglia were present but not fully activated; instead they expressed more bushy or reactive states and did not readily uptake F-NIR (Figs. 5.1 and 5.2B). Further, in sections of the spinal cord away from the epicenter it's unlikely for infiltrating macrophages to be observed. A recent study of T10 contusion injury in mice found infiltrating macrophages on 4 dpi will infiltrate as far away as 2 mm from the injury area. However, infiltrating macrophages quickly migrated toward the epicenter area, and are only found approximately 1.25 mm away at 7 dpi and 0.6 mm at 14 dpi (16). This reflects our findings, explaining why F-NIR uptake is observed in the epicenter region and not rostral areas. This finding is further supported by other models of neurotrauma showing folate positive cells at the injury site. For instance, one study showed the ability to target folate positive microglia/macrophages in a model of inflammatory experimental autoimmune encephalomyelitis (EAE) (26). After brain injection of EAE inducing proinflammatory compounds, FOLR positive immune cells were present around the injection site. Thus, the results of our study support prior findings of targeting success in models of CNS trauma.

The presence of activated immune cells in the injured spinal cord has been the subject of much debate, although much research has now shown they are crucial for proper recovery. While macrophages contribute to acrolein production and other increases of ROS, they also play many beneficial roles in SCI such as clearing of debris or release of growth factors such as brain-derived neurotrophic factor (12, 27). Using macrophagic IRF8-deficient chimeric mice to remove the ability of infiltrating macrophages migrate into T10 contusion injured tissue, tissue pathology was significantly worsened in these mice (16). Given their benefits to SCI pathology, efforts have been devoted to polarize microglia/macrophages towards anti-inflammatory states (28). However,

potent macrophage polarizing, anti-inflammatory drugs already exist for use in humans, including NSAIDS and corticosteroids (29). However, these are not currently used in the treatment of SCI patients. In fact, large clinical trials using corticosteroids in humans worsened outcomes of traumatic brain injury patents and significantly increased death (30). Thus, dramatic repolarizing, or removal, of microglia/macrophages in SCI will likely worsen injury. However, their presence in the injury site allows for an opportunity to remove key elements of neurotoxicity SCI, such as acrolein, which is a negative consequence of both microglia/macrophage abundance and widespread lipid peroxidation in cord tissue (4, 5, 15).

Neurotoxic aldehydes such as acrolein form in abundance after SCI. Like inflammation, acrolein levels are highest in the epicenter but can diffuse away from this site (3). Hydralazine is effective in removing acrolein in SCI as well as other disease models hallmarked by oxidative stress including alcoholic liver diseases, EAE, and Parkinson's disease (6, 31-33). Here, hydralazine lowered acrolein, although not significantly (Fig. 5.4 B). This could be due to low *n* (n=4 for this group), or differences in route of administration (previously done by intraperitoneally). However, the F-HDZ did lower acrolein levels significantly (Fig. 5.4 B). The effectiveness of F-HDZ can likely be attributed to several aspects. First, the folate receptor will continually recycle and endocytose more folate-conjugated drug (34). This allows for concentrations of the folate-drug to reach high levels in injury tissue: and much higher levels when compared to injections of unconjugated drugs such as hydralazine. Next, the linker of F-HDZ will release the activated hydralazine molecule (25). While acrolein is present and produced by macrophages and myeloperoxidase, it is also produced in other cells and fatty regions such as myelin. The high accumulation of HDZ in macrophages will likely lead to permeation out of the cells to scavenge acrolein elsewhere in cord tissue. However, more studies are warranted to confirm this theory.

Relevantly, spinal cord injury patients often suffer an array of homeostatic imbalance, cardiac and circulatory issues and low blood pressure (18, 35). This is a major cause of concern when considering clinical use of HDZ in SCI patients, which would likely further complicate cardiovascular and blood pressure homeostasis. The mechanism of hydralazine lowering blood pressure involves binding action on smooth muscle cells of blood vessels (36). Here, targeted F-HDZ will only be released in the injury site, after uptake by folate receptor positive cells. Thus, we hypothesized that after injection, F-HDZ will not have an effect on blood pressure. In

accordance with this theory, in Fig. 5.5A,B, low blood pressure in injury only rats was observed. We expected that hydralazine will lower blood pressure further below that of injured rats, and this was mostly observed as well. We also theorized that F-HDZ will show levels comparable to that of injury only rats, but above that of HDZ rats. Instead, our F-HDZ group was elevated above the injury groups and similar to controls, on both 4 and 7 dpi, although not significantly higher than injury. This apparent restoration of blood pressure could be a beneficial result of acrolein scavenging. Our prior studies have shown reduction of cyst formation and protection/restoration of tissue at the injury site after hydralazine administration (6). By promoting neuronal survival and restoring tissue structure, F-HDZ could help to improve the homeostatic imbalance of spinal cord injury. However, this mechanism was not examined in detail here.

Our goal was to determine if folate conjugation acts to target drugs to the SCI area, if F-HDZ functions as an acrolein scavenger, and if F-HDZ will lower blood pressure. Our findings indicate that F-HDZ is a promising therapeutic for SCI, however, the current study is not without limitations. While the F-HDZ drug did not lower blood pressure, its novelty suggests it could have other side effects, or unknown long-term side effects. Although, no side effects were observed here and other folate-conjugated drugs are currently progressing through later-stage clinical trials in humans with promising results. Also, acrolein is known to positively correlate with levels of inflammation and therefore F-HDZ by lowering acrolein could reduce folate receptor positive inflammatory cells, limiting drug targeting abilities in injured tissue over time. To help address these potential limitations, future studies will examine longer timepoints to quantify changes in inflammation and include behavioral tasks such as pain and locomotion. Longer timepoints will also allow us to continue monitoring for any side effects that may develop. Finally, F-HDZ will also be tested in other pathologies hallmarked by increases in acrolein, such as Parkinson's, traumatic brain injury, and multiple sclerosis.

5.5 Supplemental figures

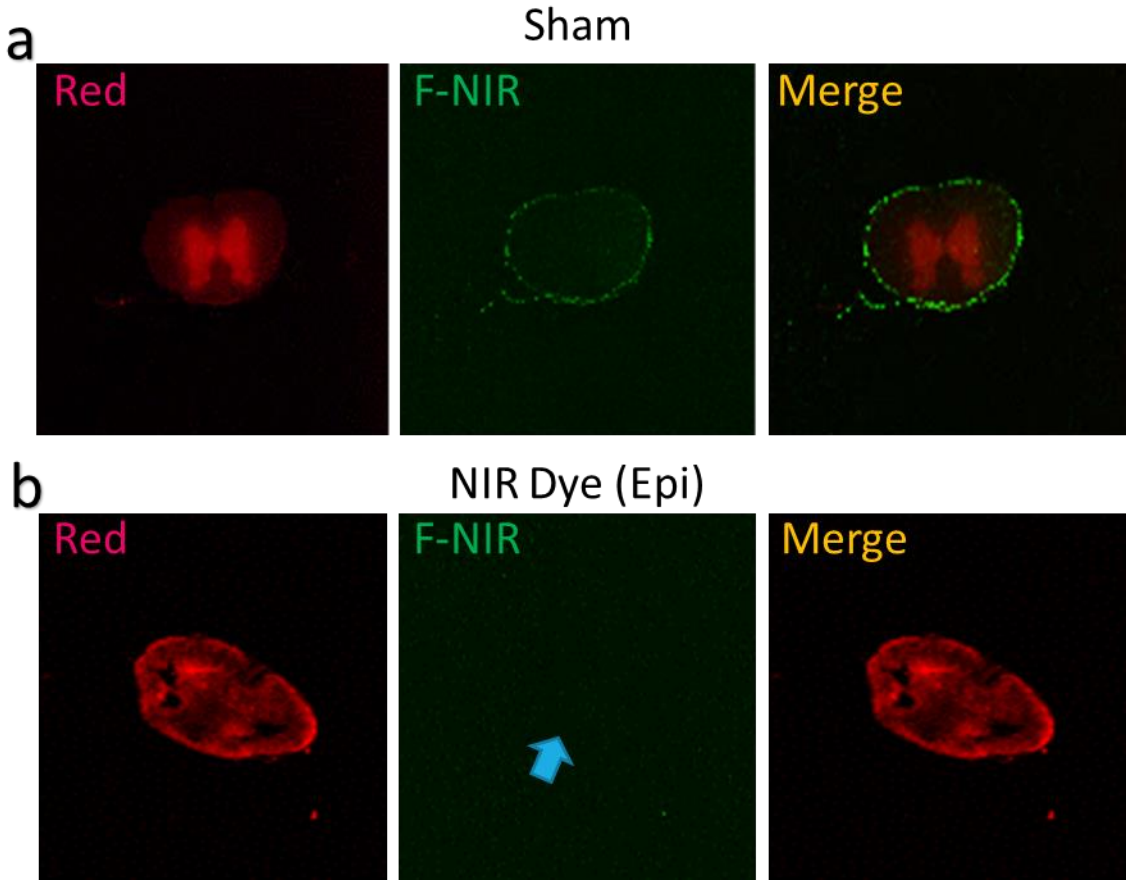

Supplemental Figure 5.1. Uptake of F-NIR in sham rats or unconjugated NIR dye uptake in the epicenter (Epi) of injured rats. Drugs were administered to groups of rats on 7 dpi, and tissue collected 24 hours later. A-B) Red shows autofluorescence to reveal tissue structure, Green shows F-NIR signal. Merge reveals an overlay of the two colors. A) Spinal region T10 sections of the sham surgery rat. F-NIR boarders the tissue, but is not observed penetrating. This is likely due surrounding inflammation and inflammation of the dura from the laminectomy. B) Lesion site of the spinal cord, or Epicenter (EPI), of an injured rat. Unconjugated dye (NIR Dye) is not observed in the spinal cord, indicating targeted delivery of the dye to injured tissue requires folate-conjugation. Blue arrow points to tissue location.

5.6 References

1. Lipinski MM, Wu J, Faden AI, Sarkar C. Function and Mechanisms of Autophagy in Brain and Spinal Cord Trauma. Antioxid Redox Signal. 2015;23(6):565-77.

2. Shiao R, Lee-Kubli CA. Neuropathic Pain After Spinal Cord Injury: Challenges and Research Perspectives. Neurotherapeutics. 2018;15(3):635-53.

3. Burcham PC. Acrolein and Human Disease: Untangling the Knotty Exposure Scenarios Accompanying Several Diverse Disorders. Chem Res Toxicol. 2017;30(1):145-61.

4. Luo J, Shi R. Acrolein induces axolemmal disruption, oxidative stress, and mitochondrial impairment in spinal cord tissue. Neurochem Int. 2004;44(7):475-86.

5. Hamann K, Durkes A, Ouyang H, Uchida K, Pond A, Shi R. Critical role of acrolein in secondary injury following ex vivo spinal cord trauma. J Neurochem. 2008;107(3):712-21.

6. Park J, Zheng L, Marquis A, Walls M, Duerstock B, Pond A, et al. Neuroprotective role of hydralazine in rat spinal cord injury-attenuation of acrolein-mediated damage. J Neurochem. 2014;129(2):339-49.

7. Gianaris A, Liu NK, Wang XF, Oakes E, Brenia J, Gianaris T, et al. Unilateral microinjection of acrolein into thoracic spinal cord produces acute and chronic injury and functional deficits. Neuroscience. 2016;326:84-94.

8. Uchida K, Kanematsu M, Morimitsu Y, Osawa T, Noguchi N, Niki E. Acrolein is a product of lipid peroxidation reaction. Formation of free acrolein and its conjugate with lysine residues in oxidized low density lipoproteins. J Biol Chem. 1998;273(26):16058-66.

9. Luo J, Shi R. Acrolein induces oxidative stress in brain mitochondria. Neurochem Int. 2005;46(3):243-52.

10. Tian R, Shi R. Dimercaprol is an acrolein scavenger that mitigates acrolein-mediated PC-12 cells toxicity and reduces acrolein in rat following spinal cord injury. J Neurochem. 2017;141(5):708-20.

11. Chen Z, Park J, Butler B, Acosta G, Vega-Alvarez S, Zheng L, et al. Mitigation of sensory and motor deficits by acrolein scavenger phenelzine in a rat model of spinal cord contusive injury. J Neurochem. 2016;138(2):328-38.

12. Trivedi A, Olivas AD, Noble-Haeusslein LJ. Inflammation and Spinal Cord Injury: Infiltrating Leukocytes as Determinants of Injury and Repair Processes. Clinical neuroscience research. 2006;6(5):283-92.

13. Melissa M. Anderson, Stanley L. Hazen, Fong F. Hsu, Heinecke JW. Human Neutrophils Employ the Myeloperoxidase–Hydrogen Peroxide–Chloride System to Convert Hydroxy-amino Acids into Glycolaldehyde, 2-Hydroxypropanal, and Acrolein. J Clin Invest. 1996;99(3).

14. Shaeib F, Khan SN, Thakur M, Kohan-Ghadr HR, Drewlo S, Saed GM, et al. The Impact of Myeloperoxidase and Activated Macrophages on Metaphase II Mouse Oocyte Quality. PLoS One. 2016;11(3):e0151160.

15. Gross S, Gammon ST, Moss BL, Rauch D, Harding J, Heinecke JW, et al. Bioluminescence imaging of myeloperoxidase activity in vivo. Nature Medicine. 2009;15(4):455-61.

16. Kobayakawa K, Ohkawa Y, Yoshizaki S, Tamaru T, Saito T, Kijima K, et al. Macrophage centripetal migration drives spontaneous healing process after spinal cord injury. Science Advances. 2019;5(5):eaav5086.

17. Beck KD, Nguyen HX, Galvan MD, Salazar DL, Woodruff TM, Anderson AJ. Quantitative analysis of cellular inflammation after traumatic spinal cord injury: evidence for a multiphasic inflammatory response in the acute to chronic environment. Brain : a journal of neurology. 2010;133(Pt 2):433-47.

18. Claydon VE, Steeves JD, Krassioukov A. Orthostatic hypotension following spinal cord injury: understanding clinical pathophysiology. Spinal Cord. 2006;44(6):341-51.

19. Xia W, Hilgenbrink AR, Matteson EL, Lockwood MB, Cheng J-X, Low PS. A functional folate receptor is induced during macrophage activation and can be used to target drugs to activated macrophages. Blood. 2009;113(2):438-46.

20. Wyatt-Johnson SK, Herr SA, Brewster AL. Status Epilepticus Triggers Time-Dependent Alterations in Microglia Abundance and Morphological Phenotypes in the Hippocampus. Front Neurol. 2017;8:700.

21. Walls MK, Race N, Zheng L, Vega-Alvarez SM, Acosta G, Park J, et al. Structural and biochemical abnormalities in the absence of acute deficits in mild primary blast-induced head trauma. J Neurosurg. 2016;124(3):675-86.

22. Cindy Laramore JC. Triple-Labeling Whole-Mount In Situ Hybridization Method for Analysis of Overlapping Gene Expression in Brain Tissue with High Level of Autofluorescence. Journal of Cytology and Histology. 2015;s3.

23. Graeber MB, Streit WJ. Microglia: biology and pathology. Acta neuropathologica. 2010;119(1):89-105.

24. Haage V, Semtner M, Vidal RO, Hernandez DP, Pong WW, Chen Z, et al. Comprehensive gene expression meta-analysis identifies signature genes that distinguish microglia from peripheral monocytes/macrophages in health and glioma. Acta neuropathologica communications. 2019;7(1):20.

25. Srinivasarao M, Low PS. Ligand-Targeted Drug Delivery. Chemical Reviews. 2017;117(19):12133-64.

26. Elo P, Li XG, Liljenbäck H, Helin S, Teuho J, Koskensalo K, et al. Folate receptor-targeted positron emission tomography of experimental autoimmune encephalomyelitis in rats. J Neuroinflammation. 2019;16(1):252.

27. Weishaupt N, Blesch A, Fouad K. BDNF: The career of a multifaceted neurotrophin in spinal cord injury. Experimental neurology. 2012;238(2):254-64.

28. Akhmetzyanova E, Kletenkov K, Mukhamedshina Y, Rizvanov A. Different Approaches to Modulation of Microglia Phenotypes After Spinal Cord Injury. Frontiers in Systems Neuroscience. 2019;13(37).

29. Desgeorges T, Caratti G, Mounier R, Tuckermann J, Chazaud B. Glucocorticoids Shape Macrophage Phenotype for Tissue Repair. Frontiers in Immunology. 2019;10(1591).
30. Alderson P, Roberts I. Corticosteroids for acute traumatic brain injury. The Cochrane database of systematic reviews. 2005;2005(1):Cd000196.

31. Chen WY, Zhang J, Ghare S, Barve S, McClain C, Joshi-Barve S. Acrolein Is a Pathogenic Mediator of Alcoholic Liver Disease and the Scavenger Hydralazine Is Protective in Mice. Cellular and molecular gastroenterology and hepatology. 2016;2(5):685-700.

32. Leung G, Sun W, Zheng L, Brookes S, Tully M, Shi R. Anti-acrolein treatment improves behavioral outcome and alleviates myelin damage in experimental autoimmune encephalomyelitis mouse. Neuroscience. 2011;173:150-5.

33. Ambaw A, Zheng L, Tambe MA, Strathearn KE, Acosta G, Hubers SA, et al. Acrolein-mediated neuronal cell death and alpha-synuclein aggregation: Implications for Parkinson's disease. Mol Cell Neurosci. 2018;88:70-82.

34. Paulos CM, Reddy JA, Leamon CP, Turk MJ, Low PS. Ligand binding and kinetics of folate receptor recycling in vivo: impact on receptor-mediated drug delivery. Molecular pharmacology. 2004;66(6):1406-14.

35. Furlan JC, Fehlings MG. Cardiovascular complications after acute spinal cord injury: pathophysiology, diagnosis, and management. Neurosurgical Focus FOC. 2008;25(5):E13.

36. EBEIGBE AB, ALOAMAKA CP. Mechanism of hydralazine-induced relaxation of arterial smooth muscle. Cardiovascular Research. 1985;19(7):400-5.

CHAPTER 6. CONCLUSIONS

6.1 Conclusions and future directions

The overall goal of this dissertation is to investigate the role of acrolein in neurotrauma and linked disorders. In Parkinson's, we found acrolein removal promotes cellular and behavioral outcomes in our rodent model and in-vitro. In blast traumatic brain injury, a relatively newer and understudied injury, the mechanisms of disease are not as clear. Using this model we therefore performed studies on the detailed structural changes that may occur. In spinal cord injury, acrolein clearance has been investigated more extensively, and the benefits of removal established. Therefore to further enhance our acrolein scavenging capabilities in SCI, we employed novel means for acrolein clearance. This work is focused on areas of neurotrauma and related neurodegeneration such as PD, and is divided into several related chapters.

Neurotrauma significantly increases the likelihood of developing debilitating neurodegenerative conditions, such as Parkinson's disease (PD). In chapter 2 we examine PD in detail, which is hallmarked by oxidative stress, acrolein increase, and cell death of critical dopaminergic cells. Given this link of PD and neurotrauma, and the known involvement of reactive aldehydes in PD, we used two FDA approved medications for heavy metal toxicity (Dimercaprol, DP), or for hypertension (Hydralazine, HZA), in a 6-OHDA model of PD. These medications are both shown to be effective acrolein scavengers. Dimercaprol and HZA are safe for use in humans and may have an accelerated path to use for PD patients. We find in chapter 2 that both these drugs show significant benefits on cellular and behavioral outcomes in our PD model and in-vitro. These promising results will be followed by future studies that could reveal further their benefits. For instance, both iron and copper accumulation are implicated in PD and can accelerate dopamine oxidation (1, 2). Therefore, DP may offer neuroprotective benefits beyond acrolein scavenging, making it a uniquely attractive PD treatment. Also, studies on alpha-synuclein aggregation may reveal additional benefits of aldehyde scavenging and a likely link of acrolein leading to PD after a neurotrauma incident. Already our data and others indicates that acrolein can promote PD hallmark protein alpha-synuclein aggregation (3, 4). Thus, DP and HZA may help inhibit the aggregation of this protein.

Relevantly, our group has shown that acrolein in blast traumatic brain injury (bTBI) can lead to increased PD markers, such as alpha-synuclein aggregation in the brain (4). The increased likelihood of developing of PD after bTBI is also found in human studies as mentioned in chapter 1. Blast TBI is a newer model, given its recent prevalence in modern warfare and ease of creating improvised explosive devices. This model is further understudied given the difficulty of creating a reproducible blast wave in a lab setting. Our lab has this model established and have shown pathologies including blood brain barrier (BBB) leakage in rats receiving a bTBI and injected with Evans Blue labeled albumin (5). Permeability of the BBB is heavily linked to neurodegenerative diseases such as PD, and a possible link to development of PD as well as a therapeutic target for intervention. However, the detailed BBB structural changes after a bTBI have never been done in detail. We conducted such study in chapter 4, and found several significant changes in BBB structure after bTBI. Interestingly, these changes appear related to the frequency of blast (single vs triple), and the time of pathological analysis after injury (1 or 3 days). Our findings of the BBB changes after bTBI will allow us to better apply treatments that target these changes. We have shown prior that acrolein significantly elevates after bTBI, and thus acrolein scavengers could potentially reverse the structural changes found here and the increased likelihood of developing PD. Interestingly, blast is the leading cause of SCI in warfare (above firearm, vehicle crash, and other) (6). Furthermore, new models of blast SCI are being developed, and show that a blast wave alone can damage spinal tissue (7). While our lab does not yet have this model, blast SCI could be a helpful tool for investigating this clinically relevant injury.

Spinal cord injury is hallmarked by a surge of aldehydes, and prior work demonstrates the benefits of acrolein removal on cord tissue and behavioral outcomes. While DP and HDZ are effective acrolein scavengers, they have side effects, or other biological targets given their FDA approval for other conditions. For instance, HDZ is an approved medication for hypertension. Given this, we investigate in chapter 3 an alternative and possibly more effective mechanism for acrolein removal: ALDH2. This enzyme is a powerful acrolein scavenger and its activity is doubled by small molecule Alda-1, which has no known side effects. Chapter 3 suggests that ALDH2 is important for cell survival from aldehydes, yet, its expression is lower after SCI, which may be due to high levels of acrolein post injury that can damage the enzyme. Further, chapter 3 suggests Alda-1 is a promising tool for removing acrolein after injury, and that mutant ALDH2*2 transgenic mice can help reveal the importance of ALDH2 in a clinically relevant manner. This

promising data sets the groundwork for many more investigations involving ALDH2, ALDH2*2 mice, and the benefits Alda-1.

As mentioned, HDZ is an effective and the most commonly used acrolein scavenger in research. However, the known effect of lowering blood pressure is concerning for HDZ, especially in SCI. This is because individuals with SCI are already likely to suffer from hypotension, making it difficult to justify giving them HDZ, despite the many known benefits of HDZ on SCI recovery (8, 9). Therefore in chapter 5 we use a molecular targeting system to create a new hydralazine molecule: folate-conjugated to hydralazine (F-HDZ). We show for the first time that this targeting system is capable of delivering payloads directly to injured tissue in our SCI model. Further, we show that F-HDZ still acts as an effective acrolein scavenger, and finally, that it does not lower blood pressure.

Taken together, this dissertation furthers our understanding of acrolein in neurotrauma and related neurodegeneration such as PD. We investigate further the pathological changes that occur after injury and open the door to application of novel acrolein scavengers. In future studies, successful aldehyde scavengers can be selected to combat acrolein in other neurological conditions known to have elevated acrolein such as multiple sclerosis and concussion injury (10-12).

6.2 References

1. Montes S, Rivera-Mancia S, Diaz-Ruiz A, Tristan-Lopez L, Rios C. Copper and copper proteins in Parkinson's disease. Oxidative medicine and cellular longevity. 2014;2014:147251.

2. Dichtl S, Haschka D, Nairz M, Seifert M, Volani C, Lutz O, et al. Dopamine promotes cellular iron accumulation and oxidative stress responses in macrophages. Biochemical pharmacology. 2018;148:193-201.

3. Ambaw A, Zheng L, Tambe MA, Strathearn KE, Acosta G, Hubers SA, et al. Acrolein-mediated neuronal cell death and alpha-synuclein aggregation: Implications for Parkinson's disease. Mol Cell Neurosci. 2018;88:70-82.

4. Acosta SA, Tajiri N, de la Pena I, Bastawrous M, Sanberg PR, Kaneko Y, et al. Alpha-synuclein as a pathological link between chronic traumatic brain injury and Parkinson's disease. J Cell Physiol. 2015;230(5):1024-32.

5. Walls MK, Race N, Zheng L, Vega-Alvarez SM, Acosta G, Park J, et al. Structural and biochemical abnormalities in the absence of acute deficits in mild primary blast-induced head trauma. J Neurosurg. 2016;124(3):675-86.

6. Szuflita NS, Neal CJ, Rosner MK, Frankowski RF, Grossman RG. Spine Injuries Sustained by U.S. Military Personnel in Combat are Different From Non-Combat Spine Injuries. Military medicine. 2016;181(10):1314-23.

7. del Mar N, von Buttlar X, Yu AS, Guley NH, Reiner A, Honig MG. A novel closed-body model of spinal cord injury caused by high-pressure air blasts produces extensive axonal injury and motor impairments. Experimental neurology. 2015;271:53-71.

8. Claydon VE, Steeves JD, Krassioukov A. Orthostatic hypotension following spinal cord injury: understanding clinical pathophysiology. Spinal Cord. 2006;44(6):341-51.

9. Park J, Zheng L, Marquis A, Walls M, Duerstock B, Pond A, et al. Neuroprotective role of hydralazine in rat spinal cord injury-attenuation of acrolein-mediated damage. J Neurochem. 2014;129(2):339-49.

10. Chen CH, Ferreira JC, Gross ER, Mochly-Rosen D. Targeting aldehyde dehydrogenase 2: new therapeutic opportunities. Physiol Rev. 2014;94(1):1-34.

11. Leung G, Sun W, Zheng L, Brookes S, Tully M, Shi R. Anti-acrolein treatment improves behavioral outcome and alleviates myelin damage in experimental autoimmune encephalomyelitis mouse. Neuroscience. 2011;173:150-5.

12. Burcham PC. Acrolein and Human Disease: Untangling the Knotty Exposure Scenarios Accompanying Several Diverse Disorders. Chem Res Toxicol. 2017;30(1):145-61.